CZECH TECHNICAL UNIVERSITY IN PRAGUE

FACULTY OF MECHANICAL ENGINEERING

DEPARTMENT OF MECHANICS, BIOMECHANICS AND MECHATRONICS

ELECTRICAL RESISTANCE MEASUREMENT FOR STRUCTURAL HEALTH MONITORING OF COMPOSITE MATERIALS

by

Ing. Nikola Schmidová

Doctoral Study Programme: Mechanical Engineering

Study Field: Mechanics of Rigid and Deformable Bodies and Environment

Supervisor: prof. Ing. Milan Růžička, CSc.

Supervisor specialist: Ing. Karel Doubrava, Ph.D.

A thesis submitted to

the Faculty of Mechanical Engineering, Czech Technical University in Prague,

in partial fulfilment of the requirements for the degree of doctor.

Prague December 2023

Declaration

I hereby declare that I am the sole author of this dissertation thesis and that I have not used any sources other than those listed in the bibliography and identified as references.

….....

Ing. Nikola Schmidová

Prague, December 2023

Acknowledgements

I would like to first of all thank the thesis supervisor prof. Ing. Milan Růžička, CSc. for his professional guidance and valuable advice throughout the study and work on the topic. Furthermore, I would like to thank all my colleagues from the Department of Elasticity at the Faculty of Mechanical Engineering, CTU in Prague, who supported me with their advice and comments during the work on the topic. Last but not least, I would like to thank my colleagues from industrial companies and research organizations, with whom I had the opportunity to cooperate during the work on the topic and who inspired me with their work in solving technical problems.

This thesis could not have been done without the support of my family. I thank them for their understanding, the many concessions they had to make, and most importantly for their supply of positive energy.

Annotation

The dissertation deals with the topic of monitoring of long-fiber composite material structures using the method of measuring changes in electrical resistance. It deals with two approaches. The first approach is based on measuring of the electrical resistance change directly on long-fiber carbon composites. These measurements allow the detection of deformation and damage within the material. The second approach employs the use of sensors made of carbon fiber tows that exhibit piezoresistive behavior.

Novel findings on the use of carbon fiber sensors for detecting barely visible impact damage (BVID) are presented. Additionally, thermography has been validated for visualizing sensor damage and localization of damage along the sensor length.

This work includes a comparative analysis of existing methods for determining the electrical resistivity of composites. It also assesses the impact of these methods on predicting delamination size through finite element (FE) simulations. The influence of temperature and the positioning of electrical contacts on delamination detection are quantified using FE simulations. Finally, the dissertation introduces a new technique for fabricating electrical contacts on the inner surface of composite profiles and the results of damage detection of both approaches on components fabricated by the winding technology are also presented.

Keywords: SHM; piezo-resistive sensor; carbon fiber sensor; impact damage; BVID; polymer composites; sensor embedment; NDT; active thermography; electrical resistance; Structural Health Monitoring; damage detection; Composites.

Anotace

Disertační práce Monitorování a lokalizace poškození kompozitních materiálů pomocí měření změny elektrického odporu se zabývá tématem monitorování konstrukcí z dlouhovláknových kompozitních materiálů pomocí metody měření změny elektrického odporu. Konktrétně se zabývá dvěma přístupy. První přístup spočívá v měření změny elektrického odporu přímo na dlouhovláknových uhlíkových kompozitech. Z naměřených hodnot elektrického odporu lze detekovat deformaci i poškození materiálu. Druhá metoda spočívá v použití senzorů vyrobených ze svazků uhlíkových vláken, které vykazují piezorezistivní chování.

V práci jsou prezentovány nové výsledky ohledně možnosti využití senzorů z uhlíkových vláken pro detekci BVID impaktu. Byla validována termografická metoda pro vizualizaci poškození senzoru a lokalizaci poškození po délce senzoru.

Jsou prezentovány výsledky porovnání několika používaných metod pro stanovení rezistivity kompozitu. V práci byl dále stanoven vliv použití konkrétních metod na predikci velikosti delaminace pomocí numerické simulace metodou konečných prvků. Pomocí konečně prvkových simulací je kvantifikován vliv teploty a vzdálenosti el. kontaktů na detekci delaminace. V práci jsou uvedeny také výsledky použití nové metody výroby el. kontaktů na vnitřním povrchu kompozitního profilu a výsledky detekce poškození obou metod na komponentách vyrobených technologií navíjení.

Klíčová slova: SHM; piezorezistivní senzor; senzor z uhlíkových vláken; impaktní poškození; BVID; polymerní kompozity; integrace senzoru; NDT; aktivní termografie; elektrický odpor; monitorování zdraví konstrukce; detekce poškození; kompozity.

Contents

Nomenclature

Abbreviation	Description
3PB	Three-point bending test
4PB	Four-point bending
2T	Two-terminal (measurement method)
4T	Four-terminal (measurement method)
4W	Four-wire (electrical resistance measurement method)
BVID	Barely visible impact damage
CBM	Condition based maintenance
CF	Carbon fiber
CFRTP	Carbon fiber reinforced thermoplastic
CFRP	Carbon fiber reinforced polymer
CF-PPS	Carbon fiber, polypropylene sulphide matrix
CNT	Carbon nanotube
CW	Crack-wire sensor
DCB	Double-cantilever beam
DFOS	Distributed fiber optics sensing
ER	Electrical resistance
ERCM	Electrical resistance change measurement
ERT	Electric resistance tomography
FE	Finite element
NDT	Non-destructive testing
SHM	Structure health monitoring

Symbol	Description	Units
R	resistivity	[Ω]
r	radius	[m]
ρ_x	resistivity (the index indicates the measurement direction)	[Ωm]
l	length	[m]
A	cross-section	[m^2]
ε	strain	[-]
ν	Poisson's ratio	[-]
k	strain sensitivity	[-]
U	voltage	[V]
w	width	[m]
t	thickness	[m]

1 Introduction

Carbon Fiber Reinforced Polymer (CFRP) composites are nowadays widely used for structural components across the aircraft, automotive, and manufacturing industries. These materials are also employed in civil infrastructure for the construction and reinforcement of bridges and roofs. In all these applications, a high level of safety has to be ensured. CFRP composites excel by their high strength, rigidity, low density, damping properties, and fatigue resistance. However, a notable drawback is their tendency to exhibit minimal signs of damage before failure, unlike conventional materials such as steel, aluminum alloys, or concrete.

Traditionally, parts are controlled by naked eye during scheduled maintenance checks. However, during these inspections, damage to composite parts can be easily overlooked. Therefore, efficient in-situ assessment of a components damage state and accurate prediction of its remaining service life are necessary.

Greater use of NDT techniques to monitoring damage state of CFRP components can be suggested. However, conventional NDT techniques like C-scan, X-ray, thermography, and eddy current testing are time-consuming and typically require taking the component out of service. Additionally, with increasing pressure on cost savings, the aircraft industry is shifting towards Structural Health Monitoring (SHM) and Condition-Based Maintenance. Several SHM techniques are already under investigation. The SHM approaches are spreading in other industries as well.

One of the potential SHM methods for composite structures is the Electric Resistance (ER) measuring method. There is a wide range of approaches, which utilize measurement of electrical resistance. These can be broadly categorized into two groups.

The first group exploits the electrical properties of the material of the primary structure itself. This includes composite materials with carbon fibers or carbon particles, and non-conductive fiber composites with conductive particles in the resin, such as Carbon Nanotubes (CNTs) or carbon black.

The second group involves integrating sensors into the composites. The measurement of electrical resistance of these sensors are used for strain and damage sensing. Among these sensors we can include sensors made from carbon fibers and tows, CNTs, buckypaper, and other novel materials.

This research focuses on the self-sensing capabilities of carbon fiber composites without the addition of conductive particles because the usage of nanoparticles requires extra demands on save handling, which is not easy to withstand during manufacturing. The second area of interest is the use of carbon fiber tows as sensors. Their robustness makes them suitable for standard composite manufacturing processes. Additionally, Carbon Fiber sensors (CF sensors) made from carbon fiber tows can be easily tailored for specific sensing applications.

Both approaches under investigation are relatively cost-effective in terms of preparation, and the sensing equipment required is more accessible compared to measurement units used for optical fibers or acoustic emission. Crucially, both approaches utilize the structural material itself for sensing.

The sensing ability of carbon fibers have been documented in the literature. In this work are presented experiments dealing with new possible utilization of sensors made of carbon fiber tow. The investigated area is impact damage. Influence of the material type, cyclic loading, temperature, and size of impact energy on impact damage detection using carbon fiber tow as a sensor is discussed.

Previous experimental studies have proved that coupling between the damage and loading state of CFRP composites and their electrical resistance exists. This phenomenon is attributed to the unique composition of CFRPs, which consist of electrically conductive and piezoresistive carbon fiber tows, and an insulating polymer matrix, typically epoxy. The possibility of damage monitoring in these composites has been demonstrated through numerous experiments. Although a lot of work have been done on describing coupling between the measured electrical resistance and the material state, a lot of information is missing to be able to perform electrical resistance method in industrial applications.

The method based on electrical resistance measurement has wide range of potential applicability. On the other hand, there are many influences which can affect the method, such as temperature, fiber orientation, stacking sequence, and electrical contact configuration.

It is essential to identify and quantify the influences on the measured electrical resistance of CFRP composites more precisely. Understanding these limitations will help further development and application of this method. In this work, we specifically explore how electrical contact configuration, temperature, and material resistivity impact delamination detection using the electrical resistance method.

The findings, based on experimental verification at the component level, along with recommendations for future research, are summarized at the conclusion of the thesis.

The next section outlines the structure of this thesis, providing a roadmap for readers and a brief description of each chapter for easier navigation through the text.

1.1 Thesis layout

In Chapter 2, the electrical properties of carbon fiber tows and CFRP composites are described. This chapter also covers configurations of the ER measurement method and provides a brief overview of published results in strain, fatigue, and damage monitoring using the ER measurement method.

Chapter 3 defines the aims and objectives of the thesis.

Chapters 4, 5, and 6 summarize all the author's results and findings based on experimental investigations. Chapter 4 presents findings on the use of carbon fiber sensors for impact damage detection and strain sensing. In chapter 5 are described results of the experimental campaign and Finite Element (FE) analysis for delamination detection using the ER measurement method. Chapter 6 summarizes findings regarding the application of both methods on filament wound profiles.

Conclusions and suggestions for further work are presented in Chapter 7.

2 State of the art

There are many approaches being investigated for the goal of Structural Health Monitoring (SHM) of composite materials. Several SHM techniques have been tested during full-scale fatigue tests and in-flight tests, such as Acoustic Emission (AE), Acousto-ultrasonic (AU) (Ultrasonic Guided Waves - UGW), Comparative Vacuum Monitoring (CVM), and Crack Wires (CW). These methods are the most matured, but there are also other promising SHM methods such as Fiber Bragg sensors (FBG), high-definition distributed strain sensing using optical fibers based on Optical Frequency Domain Reflectometry (OFDR) [1], or methods based on Eddy Current. Fatigue Damage Sensors, Strain Gauges and Crack Propagation Gauges are also used for SHM monitoring [2]. Mechanochromatic composites, which exhibit a change of color under stress or damage have been also investigated [3]. Other new approaches are continually published, self-reporting constructions are of great interest in all industrial sectors. An overview of SHM methods is given in Table 1.

In this work we focus on two specific approaches: carbon fiber roving for damage detection and the measurement of the electrical resistance response of the whole CFRP composite [4]. It is believed that a better understanding of both phenomena is beneficial, and both approaches can enrich each other.

The author has decided to focus on these two monitoring approaches due to the following reasons:

- They utilize the intrinsic bearing material of the structure.
- The methods can be tailored to specific applications, which are known to be challenging to monitor by other methods (e.g., impact damage, delamination of complex shaped structures, as shown in Fig. 1, monitoring of structures that are difficult to reach, or which are covered).
- The equipment and materials required for these methods are available and relatively inexpensive, a factor often decisive for practical applications.

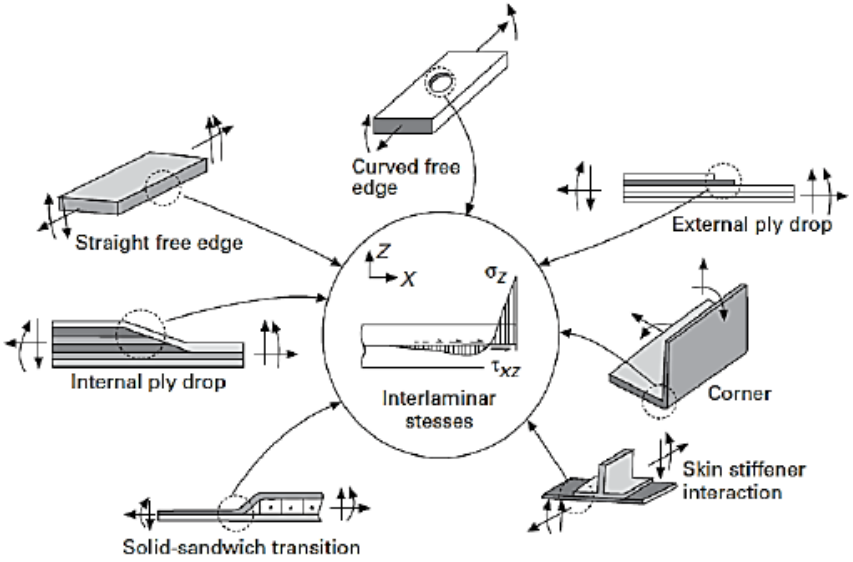

Fig. 1 Delamination at material and material discontinuities [5].

Table 1 SMH methods - overview

	Abbreviation	Delamination detection	Impact Detection	Strain Measurement	Rupture/ Crack detection	Fatigue	Debonding	Advantages	Disadvantages
Electrical resistance measurement	(ER)	●	●	●	●	●	●	See Table 3	See Table 3
Ultrasonic Guided Waves	(UGW)	●	●		●			- already used for metal parts - already tested on composites during flight tests - quite precise location of damage	- needs sophisticated signal processing and high data volumes management - temperature dependent - wave propagation is anisotropic - actuators has to be attached to the structure
Electromechanical Impedance	(EMI)				●		●	- could be complementary to UGW (same sensors) - already evaluated on full-scale airplane segment	- strong temperature dependency
Eddy Current	(EC)				●			- widely used for NDT	- very low depth of penetration - crack is expected directly under the sensor
Acoustic Emission	(AE)	●	●		●			- effectively cover wide area (sound-wave propagation is quite efficient) - quickly identify suspected problem area	- must run continuously, produce huge amount of data, difficult to recognize sensor failure, prone to false positive alarm - only general location within the structure - detailed inspection with alternative technique is necessary
Fiber Bragg Grating	(FBG)	●		●	●		●	- no electromagnetic interference - can be embedded in material	- need complex device for optical signals (expensive)
Strain Gauges	(SG)			●	●			- spot measuring of strain	- inappropriate for damage monitoring - possibility of crack can be indicated
Crack Propagation Gauges	(CPG)				●			- hot spot monitoring of crack growth	
Fatigue Damage Sensor	(FDS)					●		- accurate record of accumulative fatigue damage	- structure is not examined directly, but via attached coupon
Comparative Vacuum Monitoring	(CVM)	●			●			- no electromagnetic interference	- hot spot monitoring of crack growth - Sensitive to temperature and atm. Pressure
Crack wire	(CW)				●			- simple conductive/resistive principle	- specialized sensor for tail strike indication (Airbus A380)

2.1 Structural and mechanical properties of CFRP composites

In this thesis will be investigated long fiber CFRP composites and in this section, the structure of long-fiber CFRP composites is described, and their main mechanical properties are briefly discussed.

2.1.1 CFRP structures and mechanical properties

For the purposes of this research, only long-fiber CFRP composites with an epoxy resin matrix will be considered. Two types of carbon fibers may be used, ex-PITCH[1] (high-modulus) and ex-PAN[2] (high-strength fibers can be used. Unless specified otherwise, references to 'carbon fibers' in this text will imply ex-PAN fibers. Whenever ex-PITCH carbon fibers are discussed, they will be explicitly mentioned.

There are number of CFRP structures, which can be used. A CFRP composite can be prepared using either unidirectional layers or woven layers. When unidirectional layers are stacked only in two perpendicular directions, we refer to the resulting material as cross-ply laminates. Unidirectional layers can also be stacked in various other sequences. In this text, CFRP composites made of woven layers will be referred to as woven CFRP composites.

The mechanical properties of CFRPs are influenced by both the stacking sequence and the type of woven CFRP. Composites with unidirectional fibers exhibit the highest tensile strength when aligned parallel to the fiber direction, and the lowest tensile strength when the alignment is perpendicular to the fiber direction.

2.1.2 Damage and failure mechanism of CFRP

Damage and failure mechanisms in composite structures are closely linked to the method of production, such as pultrusion, filament winding, and manual or automated lay-up. Additionally, the type of loading on the composite structure significantly influences these mechanisms. Several fundamental damage modes are identified, including fiber breakage, fiber pull-out, fiber kinking, transverse matrix cracking, and delamination.

Among these, delamination is notably the most degrading and serious type of damage in composites produced by lay-up methods. It significantly reduces the strength of the material during subsequent loading [6].

[1] ex-PITCH – carbon fibers which are generally produced from petroleum asphaltene or coal tar [86]
[2] ex-PAN – carbon fibers, which are produced from polyacrylonitrile (PAN, CH_2-CH-CN) [86]

2.2 Theoretical background

This chapter describes the theoretical relationships and mathematical formulas that will be used to discuss the electrical properties of carbon fibers and carbon fiber composites.

2.2.1 Strain sensing – piezoresistivity

A carbon fiber can be represented as a cylinder of radius *r*, resistivity ρ and length *l*. We will discuss piezoresistivity of such cylinder. An electrical resistance of such specimen is calculated as follows:

$$R = \rho \cdot \frac{l}{A}, \tag{1}$$

where cross-section *A* is defined

$$A = \pi \cdot r^2 , \tag{2}$$

than

$$R = \rho \cdot \frac{l}{\pi \cdot r^2} . \tag{3}$$

According to [7] the total differential of $R = f(\rho, L, r)$ can be expressed as follows:

$$dR = \frac{\delta R}{\delta \rho} d\rho + \frac{\delta R}{\delta L} dL + \frac{\delta R}{\delta r} dr. \tag{4}$$

Using equation (3) in eq. (4) we can write the relative change of resistance as:

$$\frac{dR}{R} = \frac{1}{\rho} d\rho + \frac{1}{L} dL - \frac{2}{r} dr. \tag{5}$$

We can use equation for longitudinal strain: $\frac{dL}{L} = \epsilon_L$ and Poisson ratio $\nu = -\frac{\frac{dr}{r}}{\frac{dl}{L}}$ in eq. (5) and write:

$$\frac{dR}{R} = \frac{d\rho}{\rho} + \varepsilon_L(1 + 2\nu). \tag{6}$$

In eq. (6) the term $\frac{d\rho}{\rho}$ represents the piezoresistive effect (material effect – microstructural effect [8]) and the term $\varepsilon_L(1 + 2\nu)$ represents the geometrical effect.

According to [7] it is possible to simplify the eq. (6) as follows:

$$\frac{dR}{R} = k \cdot \varepsilon . \tag{7}$$

The strain sensitivity *k* than includes effect of piezoresistivity and effect of change of geometry caused by applied strain.

In case of using carbon fibers for sensing it is noted in [7], that strain sensitivity *k* is dependent on effective Poisson's ratio, which depends on the Poisson's ratio of the sensors fiber (can be influenced by the coating or impregnating) and Poisson's ratio of the structure on which is the sensor installed or integrated ($-\varepsilon_y/\varepsilon_x$).

The strain sensitivity *k* represents both longitudinal and transversal strain sensitivity:

$$\frac{dR}{R} = k_l \cdot \varepsilon_l + k_t \cdot \varepsilon_t. \tag{8}$$

More information can be found in [9].

2.2.2 Description of the electrical resistivity of CFRP

CFRP composite plates are usually prepared by laminating individual layers of lamina at different angles of the fibers to the longitudinal axis. The electrical resistivity ρ of CFR composite of each lamina depends on the direction of measurement and the direction of the carbon fibers.

In unidirectional CFR composite plates, we can distinguish three perpendicular measurement directions and three distinct resistivities (ρ_x, ρ_y, ρ_z).

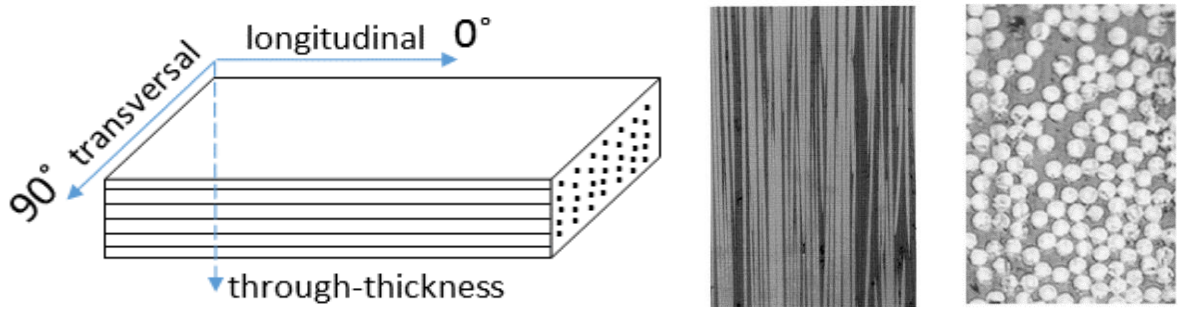

(a) (b) (c)

Fig. 2 Measurement direction for electrical resistivity of unidirectional CFR composite plate in section a), contact of align carbon fibers in transversal direction (b) [10], fiber-fiber contact in through-thickness direction (c) [11]

2.3 Electrical properties of carbon fibers and influences of embedment

Several sensors have been investigated that utilize the properties of carbon particles and fibers of varying sizes. These sensors include those made of carbon fibers and tows, sensors made of CNTs [12], sensors made of buckypaper and other new materials [13]. This work focuses on sensors made of carbon fiber tows, which consist of thousands of carbon fibers.

2.3.1 Electrical properties of carbon fibers

Carbon fibers are electrically conductive and also show piezoresistivity [7], [14], [15], [16]. In [16], a broad range of carbon fibers (PAN-fibers, graphite fibers, low modulus, high modulus) was investigated, and their piezoresistive behavior was determined. It is important to note, that each type of carbon fiber shows different piezoresistive behavior, as shown in Fig. 3. The carbon fibers vary also in resistivity, as seen in Fig. 4. References [17] and [16] demonstrate that piezoresistivity in carbon and graphite fibers is determined by various parameters, such as type of microstructure and microstructure parameters (crystallite size and interplanar distance). The studies also reveals that high modulus graphite fibers exhibit negative piezoresistivity, while carbon fibers with relatively small crystallite size and higher tensile strain exhibit positive piezoresistive effect.

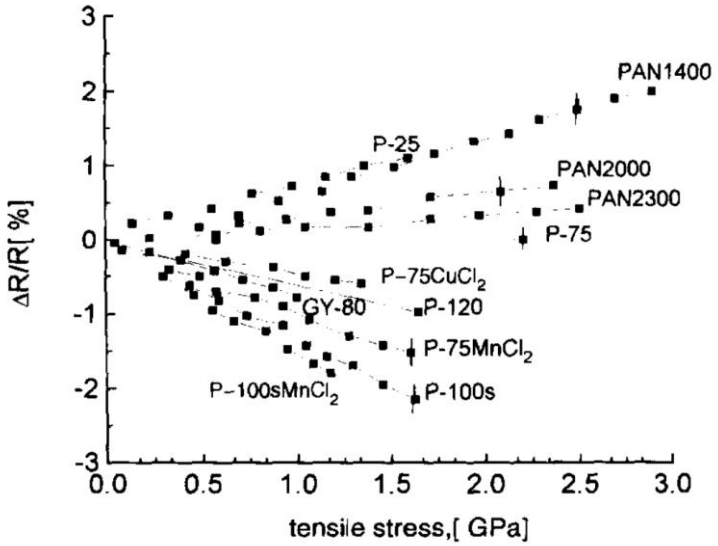

Fig. 3 Changes in relative resistance of carbon and graphite fibers as a function of stress (figure was published in [16])

According to [14], most of the reversible resistance change in 10E-Torayca T300 PAN based carbon fiber under elastic deformation is caused by the dimensional changes (see section 2.2.1). However, a part of the reversible resistance change is attributed to micromechanical changes. The strain sensitivity *k* for this type of fiber was determined to be between 1.8-2.3.

For sensing applications, it is important whether there is linear relationship between applied strain and measured electrical resistance. In [17], Owston stated that based on experimental measurements conducted on several types of fibers, those fiber which are least straight when unloaded show less linear dependency between applied strain and measured electrical resistance change.

A strain limit can be set for sensing applications. According to [16] PAN based fiber show linear dependency up to fracture, Pitch based fibers showed non-linear dependency. No hysteresis of piezoresistive behavior was observed for investigated fibers.

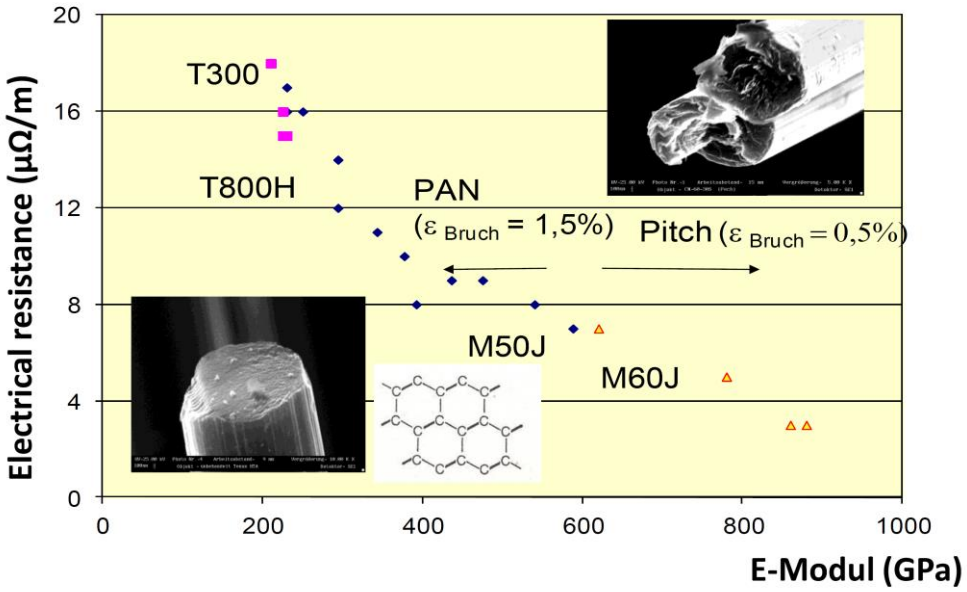

Fig. 4 Electrical resistance of ex-PAN and ex-PITCH carbon fibers [18]

2.3.2 Influence of embedment of carbon fibers on its sensing properties

If fibers are embedded, they cannot change dimensions freely. The piezoresistive behavior of the fibers, defined by equation (6), can be affected by the surrounding material. Residual stresses can also affect the piezoresistive behavior of the carbon fiber if the carbon fiber is incorporated in the composite material [15]. In [19], on comparative study of single carbon fibers (TohoTenax HM35 sized and unsized) was demonstrated, that the gauge factor for integrated fibers were lower likely due to epoxy shrinkage during curing (part of carbon fibers were not integrated in the structure and same carbon fibers were integrated in the epoxy resin).

The piezoresistivity of integrated carbon fibers can be influenced not only by residual stresses, but also by the lack of straightness of the carbon fiber [19].

2.4 Sensing properties of carbon fiber rovings

For practical applications it is difficult to manipulate with individual carbon fibers (diameter 7-8 µm). In literature we can find many applications when carbon fiber rovings (tows) are used for strain sensing. Carbon fiber roving can contain varying amounts of carbon fibers (1K=1.000 filaments, 3K=3.000 filaments, 12K=12.000 filaments). The conduction of such a bundle of carbon fibers is more complex and so can be the stress distribution in the carbon fiber roving [20], [21].

There is a question about techniques for contacting carbon fiber rovings. Ideally, all filaments of the roving should be electrically connected to lead wires. Otherwise through thickness/transversal conduction pattern will have influence on the contact resistivity of the sensor (see Fig. 5). This is especially important for thicker rovings. The individual fibers of the carbon fiber tow touch each other

and the contact between individual fibers can change during loading, which may affect the measured electrical resistivity [15]. The sensing ability of the sensors can be influenced by pre-stress applied during manufacturing, due to increased straightening of the filaments and an increase in the number of fiber-fiber contacts. This influence was investigated in [22].

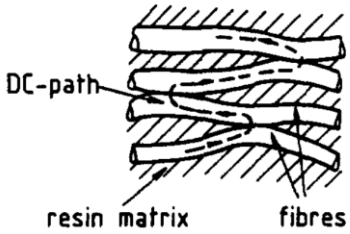

Fig. 5 Schematic related to transverse resistivity from [23].

Various techniques can be used for preparing electrical contacts, including the use of clips, metal splices, conductive paints, conductive adhesives, or deposition of nickel (electroplated coating) [24]. Conductive carbon cement was also used for electric contact preparation [25]. The process for depositing nickel is described in [26].

Several authors have investigated the use of carbon fiber tows for strain sensing [27], [28], [22], [20], [24], [29], [30], [25], [31]. The methods for preparing the sensors differ slightly in each paper. Sensors made of carbon fiber tows are also called differently in the research community. Some authors called them Carbon Fiber Yarn (CFY) sensor, they speak about carbon roving for strain sensors or continuous carbon fiber as a long-gauge sensory agent and others.

Horoschenkoff [7] published several papers regarding measuring with carbon fiber tows. In [7], he provides a detailed description of the preparation of a carbon fiber sensor (CF sensor). The sensor is prepared in three steps:

1) Pre-curing - this step should lead to align all filaments of the roving and resolves the problem with waviness of the individual filaments. The sensor also become stiffer for further manipulation.
2) Preparing of electrical connections – nickel electroplating is suggested for preparing the reliable electrical contacts.
3) Embedding of the sensor on the structure or in the structure – the sensor can be embedded directly in the composite layup, or a GFRP patch can be used.

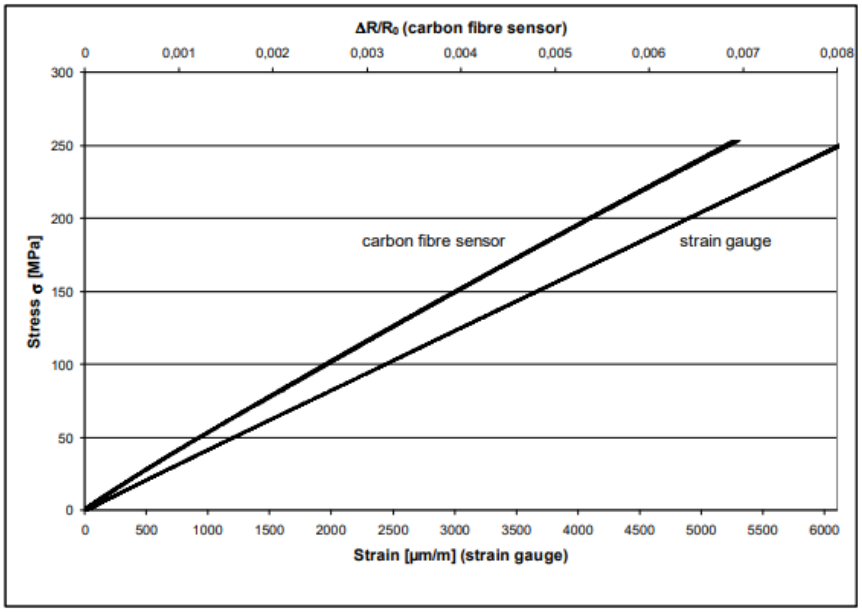

Fig. 6 Electrical resistance of ex-PAN carbon fiber tows under tensile loading – 10 load cycles at a strain level of 6,000 µm/m for the 0° laminate with tabs [27].

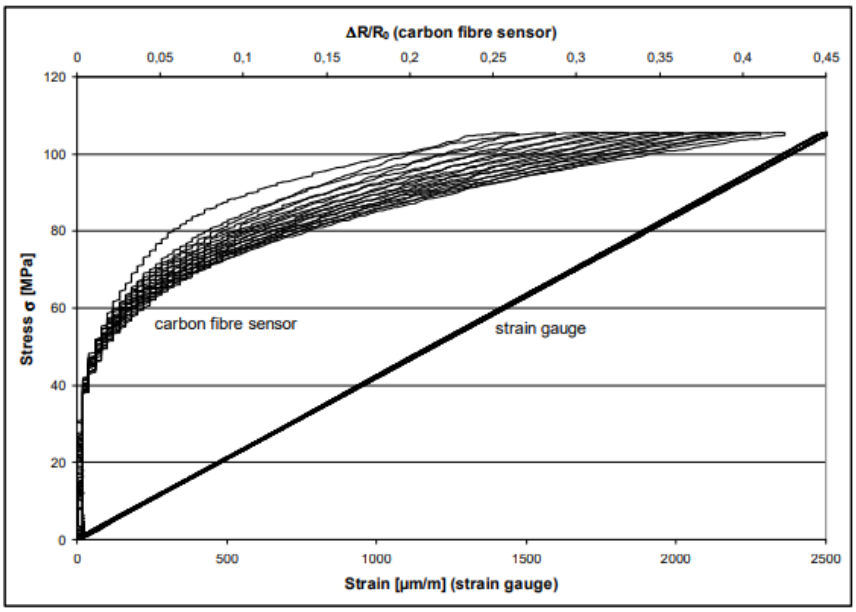

Fig. 7 Electrical resistance of ex-PITCH carbon fiber tows under tensile loading - 10 load cycles at a strain level of 2,500 µm/m for the 0° laminate with tabs [27]

Horoschenkoff used 1K Toray T300 carbon fiber tow for his experiments. The same material was employed in the examination of individual carbon fibers [14]. According to research presented in [27], ex-PAN carbon fiber tows exhibit linear dependency between measured electrical resistance and applied tensile strain up to 6000 µm/m (= 0,6 %), as shown in Fig. 6. In contrast, ex-PITCH fibers do not show linear dependence between applied strain and measured electrical resistance [32], as illustrated in Fig. 7. Additionally, the same research group described transverse sensitivity of the CF sensor in [9].

Carbon fibers can also be used for damage detection. Horoschenkoff and his team succesfully demonstrated microcrack detection in glass fiber reinforced polymer composites using an integrated CF sensor [33]. In [7] Horoschenkoff additionally showcased the use of carbon fibers as heating elements

in CFRP composites and show potential application for impact damage detection, although detailed data on such experiments are not provided.

The application of carbon fibers for strain sensing of larger structure was been shown on practical applications. Horoschenkoff and his team conducted practical measurements using CF sensor, integrating the sensors into an x-ray table [34] and for monitoring deformation of a car roof [35].

In [36] the use of sensors made of carbon fibers tows for strain monitoring of windmill blades is described. In this application, the sensors were stitched to the glass fabric and were not pre-cured. The contacting of the sensors was realized by clamping carbon fiber tow between thin copper plates.

For practical applications, it is also necessary to consider the influence of temperature change and humidity on the measurements. Influence of the temperature on the sensing ability was described in [28], [37].

Results of measurement of influence of humidity were presented in [37], where Forintos stated, that the influence of humidity on the sensor made of 24 K carbon fiber tow Sigrafil C T24-5.0/270-E100 (SGL Carbon Group, Germany) is an order of magnitude smaller than the influence of temperature.

Changes in the measured signal from a CF sensor can also be caused by cyclic loading. The effect of cyclic loading was described in [38] for several load cycles (Fig. 8) and in [27] for 10 load cycles (Fig. 6, Fig. 7 and Fig. 8).

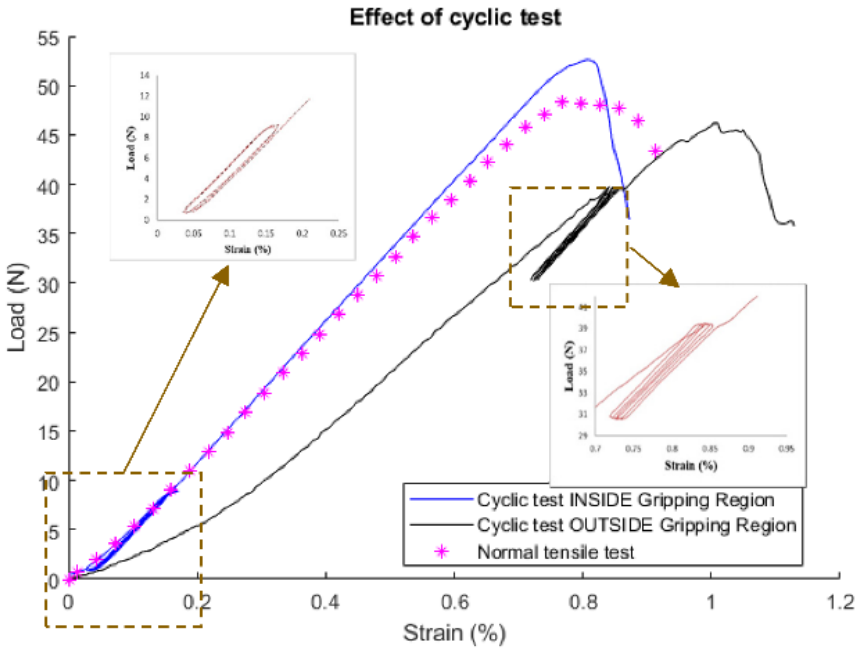

Fig. 8 Cyclic test of CF sensor presented in [38]

Individual carbon fiber sensors can be arranged in mesches [7] or denser in grids [39], [40], as shown in Fig. 9 and Fig. 10. The crosssections of the fibers or the sensors in the grid can be separated by

insulating fibers or sheets. When the network becomes denser, it transitions to sheets of carbon fiber fabric. Measuremnents are no longer conducted on individual fiber tows, but on the number of tows.

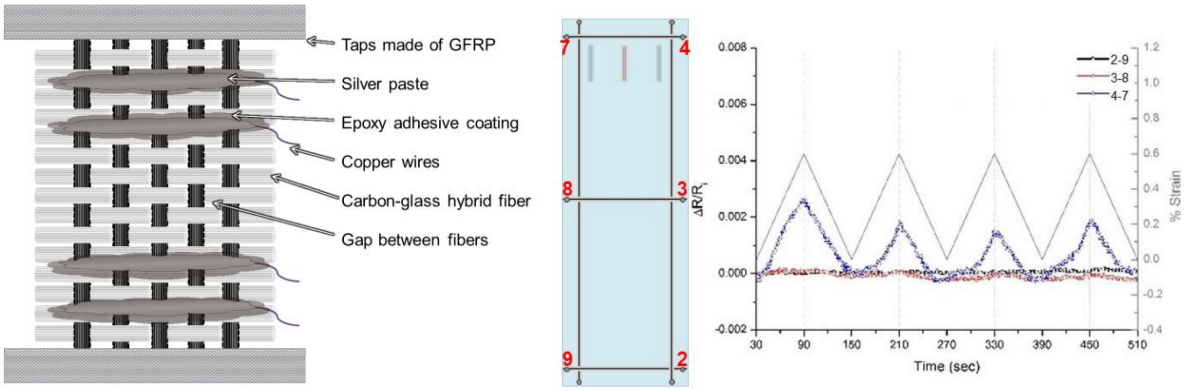

Fig. 9 A schematic of specimen made of multiple carbon fiber tows and glass fibers [39] (left), Specimen description of a specimen with carbon fiber grid sensor and its electromechanical response of multiple electrical channels [39] (right).

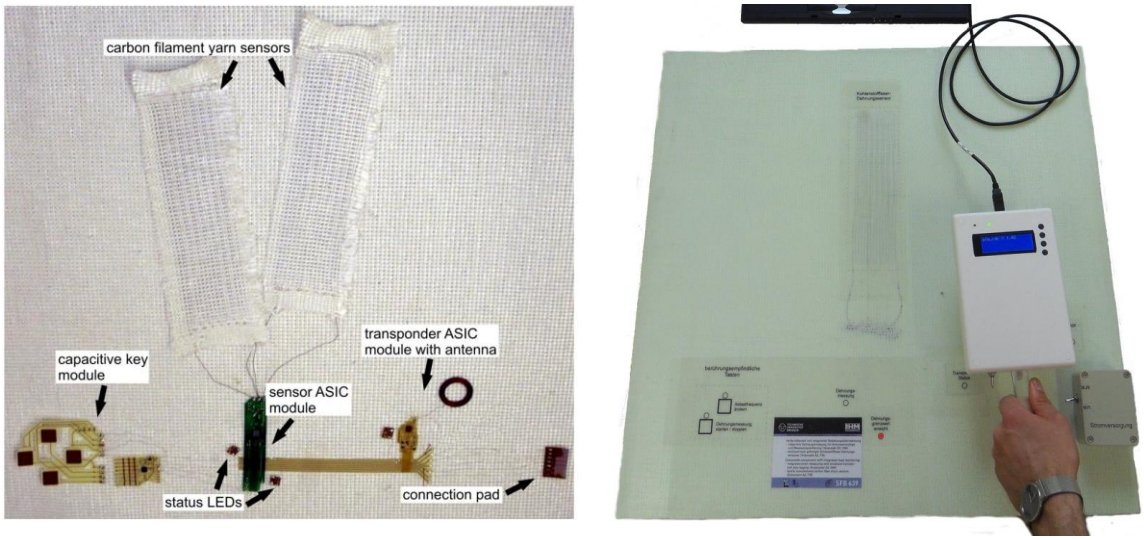

Fig. 10 Sensor network modules and carbon filament yarn strain sensors on knitted fabric before stacking and curing (left), demonstrator setup: composite component with embedded sensor network and laptop with hand reader for the read-out of the stored data (right). [40]

The advantages and disadvantages of the method based on usage of sensors made of carbon fiber tows are summarized in Table 2.

Table 2 Carbon Fiber Sensor (CF sensor) - overview

	advantages	disadvantages
Carbon Fiber Sensor (CF sensors)	- in-situ monitoring	- electric current has to be supplied to the sensor - possible problem with electromagnetic coupling
	- CF sensor can be manufactured in defined length and shape	- signal is integrated along the fiber length – configuration of the measurement has to be adjusted to the specific application
	- small diameter of the sensor	- CF sensor must be integrated during manufacturing or installed to the surface
	- measurement device is not too expensive	- resistance is temperature dependent - temp. compensation needed (additional temperature measurement or unloaded sensor measurement at the same temperature – "dummy sensor")
		- reliable electrical contacts must be prepared
		- calibration of each sensor should be performed
	- electrical resistance of CF sensor is loading state dependent	
	- is electrical resistance fatigue dependent? – not described	
	- electrical resistance is damage dependent	

2.5 Electrical properties of CFRP composites

The ER measurement method has been primarily applied to CFRP composites made from ex-PAN fibers with a thermoset polymer matrix. Research has also been conducted on composites with added particles, such as nanoparticles or carbon black in glass fiber reinforced polymer composites. However, only long-fiber composites made of carbon fibers are in the scope of this research.

Although CFRP composites consist of electrically conductive carbon fibers and an electrically non-conductive epoxy, they exhibit electrical conductivity in all three dimensions. This conductivity is due to the contact between carbon fibers, similar to what has been observed in carbon fiber sensors. The fibers come into contact during the fabrication process [11], as illustrated in Fig. 11. The way of fabrication nevertheless influences the volume fraction of carbon fibers and thereby affecting the material's conductivity [11], [41] . The conductivity is further influenced by the orientation of the fibers [42] and the stacking sequence [11]. Different conductivities in the longitudinal and through thickness directions lead to a non-uniform current distribution in the thickness direction [43], which can also impact determination of electrical resistivity, especially when the electrical contacts are placed on the surface of thicker specimens.

The temperature dependency of measured electrical resistance [42] is well known, as shown in Fig. 12 and must be compensated during the measurements or the measurement has to be done under consistent conditions.

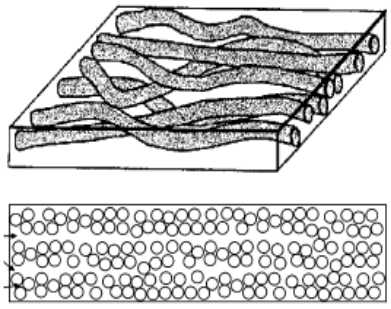

Fig. 11 Schematic model of carbon fiber network in CFRP composite [11]

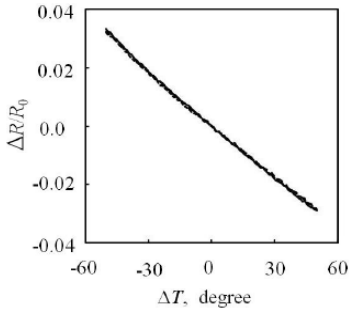

Fig. 12 Temperature change effect of electrical resistance change ration of quasi-isotropic CFRP laminate [42]

The ability of the material to sense deformation is based on the piezoresistive behavior of carbon fibers. The electrical resistance response to loading and damage will be described in more detail later in further text.

2.6 Electric resistance measurement method in general

Simple instrumentation for electrical resistance measurement has a great potential in the field of fiber composite materials. It is possible to measure directly on composites made of carbon fibers as mentioned above. Electrical resistance measurement can also be applied for nonconductive composites that are doped with conductive particles or equipped with sensors from conductive fibers. In all these applications similar problems must be solved, such as the fabrication of electrical contacts or the configuration of these contacts.

It is necessary to quantify all influences on measured resistance, in order to differentiate changes caused by temperature, loading, fatigue and various types of damage (such as delamination and, fiber breakage).

Describing of limits is crucial for the further development and practical application of the method. Clearly, for the practical use of the electrical resistance measurement method, adjusting of the method will be necessary according to loading, environmental influences, dimensions of the examined component, and the type of damage that needs to be detected. It is also important to find a method to identify any potential damage to the electrical contacts and wiring. The author suggests periodic inspections of the system under consistent loading states (e.g., structure without payload) and at the same working conditions (temperature, humidity, etc.) to verify the calibration control system. Changes due to humidity could also be mitigated by applying protective coatings, which are already used in the automotive and aerospace industries.

Table 3 Electrical resistance (ER) measurement method - overview

	advantages	disadvantages
Electrical resistance measurement method	- in-situ monitoring	- electric current has to be supplied to the material - possible problem with electromagnetic coupling
	- no additional sensors needed - information direct from the structure	- signal is structure dependent (dependent on stacking sequence and type of material, manufacturing)
	- measurement device is not too expensive	- signal is dependent on configuration of electrical contacts
		- signal is dependent on orientation of the material (electrical anisotropy of the CFRP composite)
		- resistance is temperature dependent - temp. compensation needed (additional temperature measurement or measurement always at the same temperature) - resistance is dependent also on humidity
		- reliable electrical contacts must be prepared
	- electrical resistance is loading state dependent	
	- electrical resistance is fatigue dependent	
	- electrical resistance is damage dependent	

Evaluation of measured data must be adjusted for each case.

Repeatability of the measurement? Reliability of the measurement?

2.6.1 Electric resistance measurement method on CFRP

Carbon fibers used for fabrication of CFRP composites have high electric conductivity. Most commonly used epoxy matrix and other types of matrices are insulators. For that fact long-fiber CFRP composites show strong anisotropic electrical resistance.

Published experimental works have proven that coupling between damage and loading state of the material and measured resistance by CFRP composites can be observed [44], [45], [46]. Some of the published work deals with impact and delamination detection, some focuses on damage accumulation during fatigue [41], [42].

Because of above mentioned facts the damage detection by means of electric resistance measuring method is a complex task. Nevertheless, this method shows also important advantages. Electrical resistance measurement method does not require expensive equipment, it could be done automatically without an operator and on inaccessible places. The method uses carbon fibers itself as sensors. Pros and cons of ER measurement method on composite materials are summarized in Table 3.

2.6.2 Variants of electrical resistance measurement configurations according to its purpose

Electrical resistance measurements in the frame of our topic are done for two purposes.

First one is **to determine electrical resistivity of the material**. These values could be used in finite element analysis.

The second purpose is **to monitor damage of the material or structure**, the measured values are dependent on the configuration of electrical contacts and are not property of the material.

Specimens for determination of electrical resistivity can be prepared special for this purpose, but it is more difficult to determine relationship between loading (temperature, damage) and measured electrical resistance. Chung in [47] stated that: ”The two-probe method is not reliable, even if the contact resistance is small. This is because both the contact resistance and specimen volume resistance can change as the degree of the stimulus is varied. As a consequence, the observed change in resistance upon variation in the stimulus degree may be due to a combination of change in contact resistance and a change in the volume resistance. In general, the contact resistance and volume fraction may change in the same direction or in opposite direction in response to the same stimulus.”

Further in [47] is advised not to place contacts on the surface receiving load, but to use embedded electrical contacts. Further it is advised to use four-probe method.

2.6.3 Methods for electrical resistivity determination

The electrical resistivity of the material can be determined by two measurement configurations: two-probe method (Fig. 14) and four probe method (Fig. 15). Pitfalls of these two methods are summarized also in [47].

2.6.3.1 Two-probe method

In case of two probe method – only two electrical contacts are used, current and voltage electrodes are not separated. The contact resistance (R_c) of the electrodes is included in the measured electrical resistance (R_m). The contact resistance consists of several parts:

- electrical resistance of the contact itself (for instance the conductive ink or epoxy),
- electrical resistance of the interface between the contact material and the specimen [47],
- electrical resistance of the measured material due to low resistivity in the through thickness material., see Fig. 13. This part can be eliminated, when the electrical contacts are prepared on the edges of the material, see Fig. 23.

If the contact resistance R_c could not be neglected, the resistivity of the material can be determined by multiple measurements on several specimens with different length. This approach was adopted also in [41]. All the electrodes used for electrical resistance determination must be of the same quality [47], because for the electrical resistance determination it is assumed that the R_c is the same for all specimens.

The resistance/resistivity of the material is determinate according to the transmission line method based on at least three specimens of different length [47].

The measured value R_m is equal to

$$R_m = \frac{\sigma \cdot l}{A} + R_c \ , \tag{9}$$

where σ is resistivity of the material, A is cross-section of the measured specimen, l is length of the specimen and R_c is contact resistance. In case we plot R_m versus l, we should obtain linear dependency between measured values of R_m and the l values. The cross-section of the obtained strait line and the y-axis is the value of contact resistance. Here we describe contact resistance as one value, but it can be written as

$$R_c = 2 \cdot R_{ci} \ , \tag{10}$$

where R_c is sum of contact resistances (R_{ci}) on both ends of the measured specimen.

2.6.3.2 Four-probe method[3]

When the four-terminal (4T) electrical measurement method is used (Fig. 15), electrical resistance of lead wires, electrical contacts, and electrical resistance due to imperfect bonding is eliminated. On the other hand, preparing 4 contacts instead of two is more demanding. But only one such specimen should be sufficient for electrical resistivity determination [47].

The calculated electrical resistance is also dependent on the distance between current and voltage contacts in the case of 4T method [48], when current terminals are placed on the surface and not on the edges.

[3] *In the text we use abbreviation 4T for four-terminal method. An abbreviation 4W refer to four-wire measurement method, when two or four terminals are used. The usage of four wires reduces the influence of resistance of the connecting wires. In all further measurements the resistance of connecting wires was reduced by using four wires although two-terminal (2T) configuration of electrodes was used.*

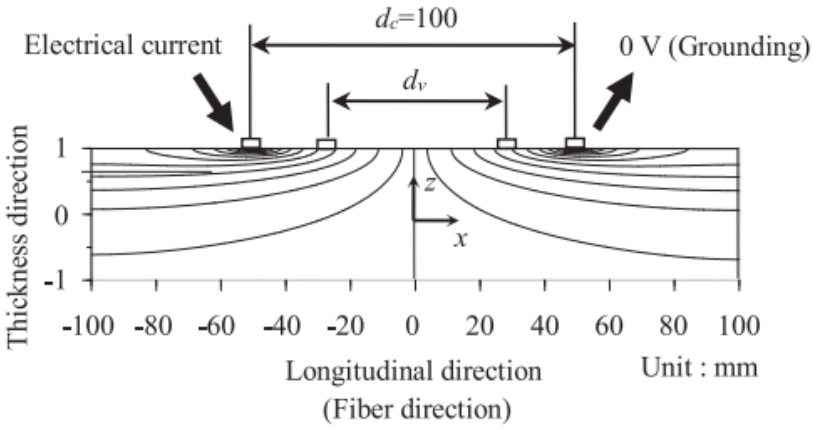

Fig. 13 Contour plot of electrical potential in the unidirectional CFRP laminate. The Figure is copied from [48].

2.6.4 Methods for damage detection using electrical voltage/potential measurement

The four-terminal method can be also used without counting electrical resistance from measured electrical current and voltage.

Only voltage can be compared for damaged/deformed states. In this case the method can be called the voltage change method (Fig. 16). In the case of electrical potential change method, the same contact for current ground and minus voltage contact is used (Fig. 17). This means that electrical resistance of the ground (minus voltage contact) is involved in the measurement. Detailed information about the electric potential method can be found in [49].

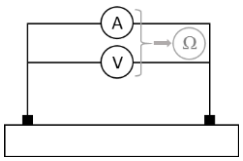

Fig. 14 Two-terminal measuring method.

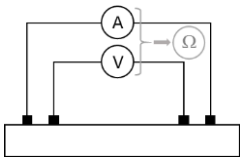

Fig. 15 Four-terminal measuring method.

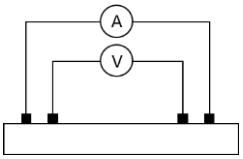

Fig. 16 Voltage change method.

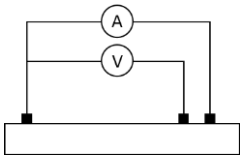

Fig. 17 Potential change method.

For plate type specimens multi probe methods have been also used (Fig. 18, Fig. 19, Fig. 20). When electrical contacts are situated around the specimen edge, measurement method is frequently called Electrical Resistance Tomography (ERT) [50].

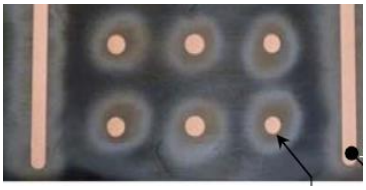

Fig. 18 Specimen with multi probes [51]

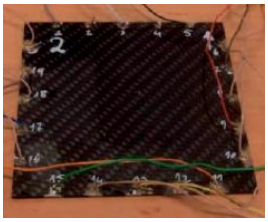

Fig. 19 Plate type specimen for electrical resistance tomography [50]

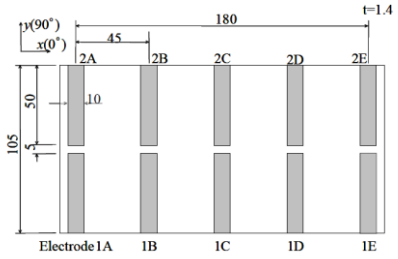

Fig. 20 Specimen with stripe electrical contacts [52]

2.6.5 Impedance measurement

Besides resistance measurement via direct current (DC), it is possible to measure impedance via alternating current (AC). When measuring via AC we get information also about dependency of electrical impedance and phase angle on AC frequency. Dependency of these values on stacking sequence and loading can be found in [53], dependency of impedance and phase angle on damage of CFRP composite is presented in [54]. Advantage of impedance measurement could be found in measuring two quantities instead of one.

According to results in [53] change in electrical impedance depending on loading is the greatest for low frequencies ($[0]_2$, $[90]_8$ and [90,0,90] laminates). Bigger change in phase angle was observed for higher AC frequencies.

Impedance measurement can bring more information about damage, but the measurement and evaluating is more time demanding and measurement equipment more expensive than equipment for DC resistance measurement. From practical point of view, we try to find simple, relatively cheap and time undemanding method, so we will focus on DC resistance measurement.

2.6.6 Electrical resistance measurement configuration – determination of electrical resistivities, determination of response to loading

As mentioned in section 2.2.2 CFRP composites are conductive in all three dimensions thus, electrical resistance or voltage change can be measured in longitudinal (fiber), transversal and through-thickness direction, see. Fig. 21.

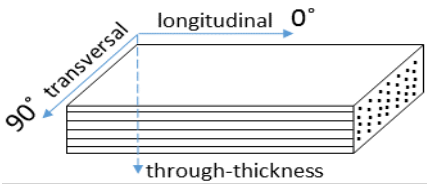

Fig. 21 Possible direction of ER measurement.

It is necessary to determinate electrical resistivities of investigated composite material in order to be able to predict possible damage detection using finite element analysis.

For sensing electrical resistivity of the composite material different configurations of electrical contacts were used, see Fig. 22 and Fig. 23. When using configuration according to Fig. 23 we must consider contact resistance as described in [41]. The technology used for contact preparation can strongly affect

the measured values of electrical resistivities and also the response of measured electrical resistivity to applied strain as described in [55] and [48]. The size and distance of electrical contacts, 2-terminal vs. 4 terminal measurement [49] also must be taken into consideration.

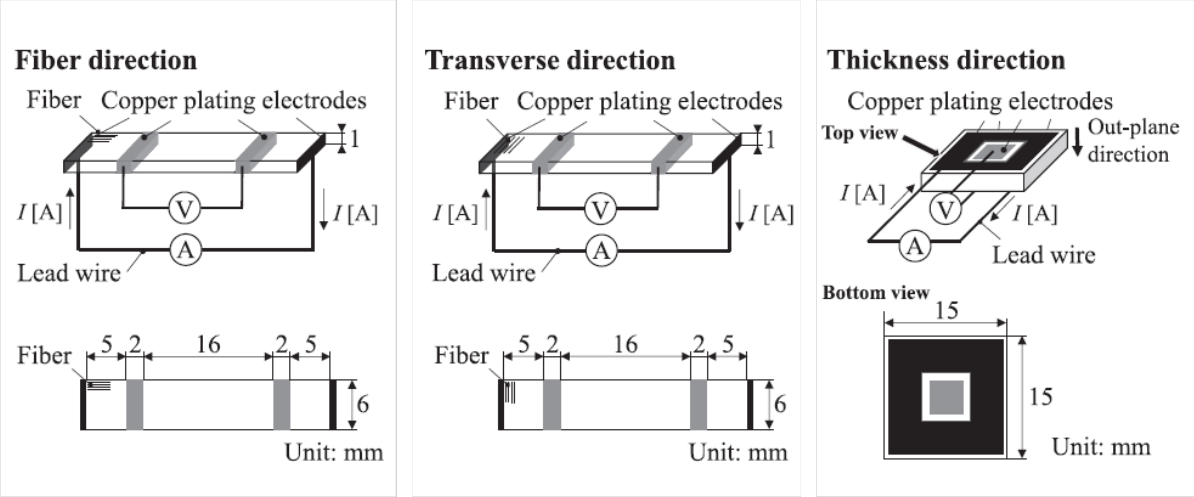

Fig. 22 Specimen configuration used to measure electrical conductivity [56].

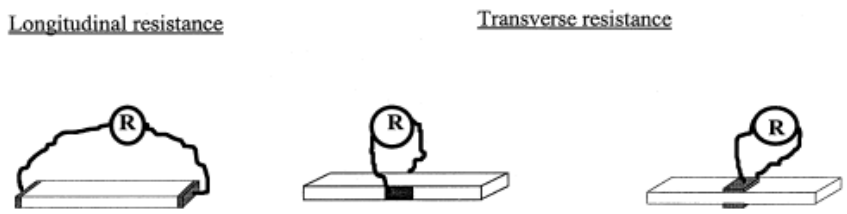

Fig. 23 Electrodes configuration for resistance measurement [41].

Number of different electrical contact configurations are also used for electrical resistance measurement, which serve for damage detection, see Fig. 24 and Fig. 25. When measuring oblique resistance or evaluate measurement using only electrodes on one surface, measured values depend on distance between current and voltage electrodes [61] and on current injection pattern [62], see Fig. 24 and Fig. 25.

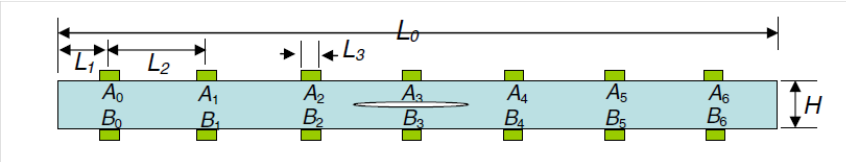

Fig. 24 Electrode configuration for determining dependence of voltage and resistance percentage change on distance between current and voltage contacts [57].

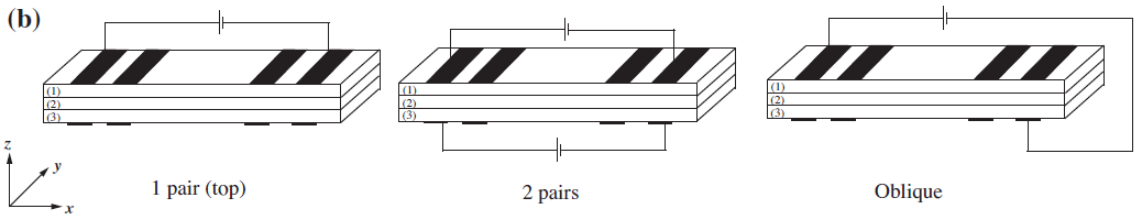

Fig. 25 Current injection pattern for 4T electric resistance measurement [58]

2.6.7 Electrical contact preparation

The combination of used conductive material and electrical contact configuration can affect the measured electrical resistivity of the material. Electrical contacts can be prepared by using several manufacturing methods: using conductive epoxy, using conductive ink, electroplating of nickel or other materials. Before applying the conductive layer, the surface of the composite material is often prepared by sanding, degreasing, or etching. This can also affect the electrical contact quality and further measurement [55].

2.6.8 Electrical resistance response of CFRP composites to loading

Electrical resistance response to the loading is different for each type of loading, type of material and the configuration of electrical contacts. These influences will be shown in this chapter on the published results.

2.6.8.1 Quasi-static loading

Electrical resistance measurement during quasi-static loading and low number of loading cycles is conducted mainly for determining of piezoresistive behavior of the composite material. It is necessary to determine the dependency of measured electrical resistance to applied loads in order to be able to separate this effect from the effect of damage on the measured electrical resistance.

2.6.8.2 Tension-compression

Measured values can be strongly influenced by the quality of preparation of electrical contacts [45], [59]. Poor electrical contact with carbon fibers can cause measurement of negative piezoresistivity measured in fiber direction, when loaded along fiber direction. Negative piezoresistivity means that measured electrical resistance decrease with increasing longitudinal strain (Fig. 27).

Negative piezo resistivity can be measured also on specimen prepared by contact lamination [44].

One of the most extensive research was described in [45] and [46]. Positive piezoresistivity was measured for unidirectional (Fig. 26), cross-ply and quasi-isotropic laminate [45] for configuration depicted on Fig. 28.

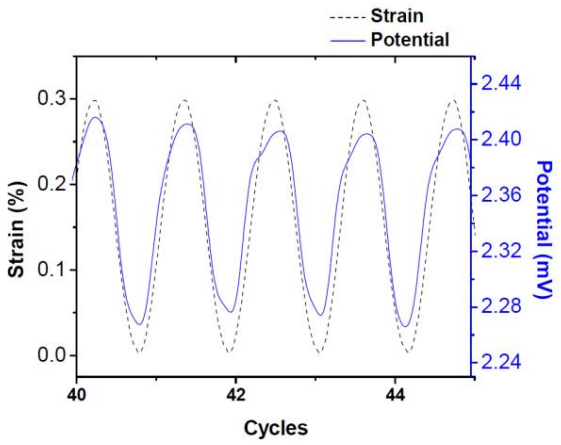

Fig. 26 Positive piezoresistivity measured on unidirectional composite [45]

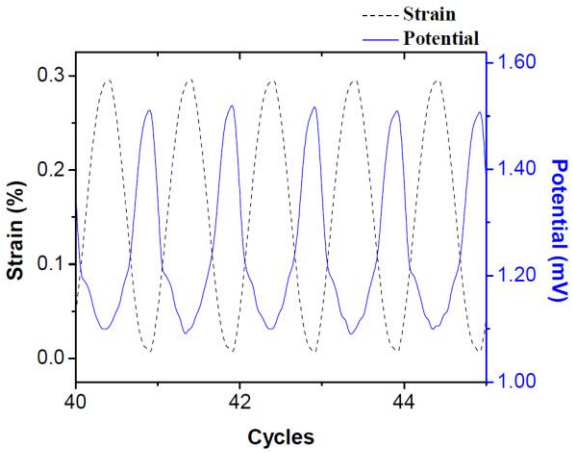

Fig. 27 Negative piezoresistivity caused by bad electrical contacts [45]

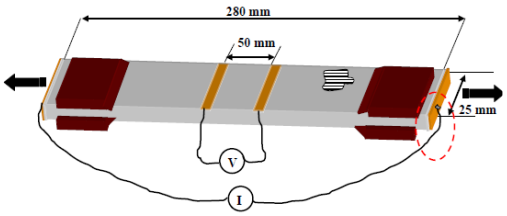

Fig. 28 Configuration of measurement type A [45].

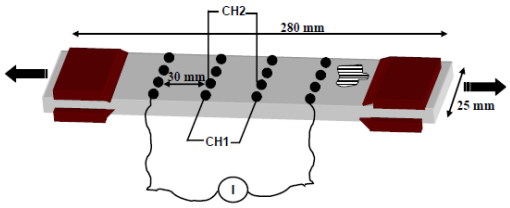

Fig. 29 Configuration of measurement type B [45].

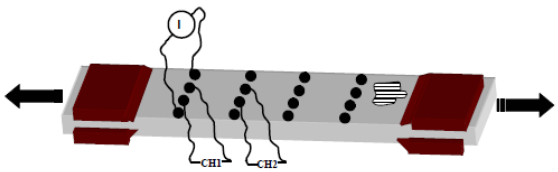

Fig. 30 Configuration of measurement type C [45].

For unidirectional composite for measurement configuration B (Fig. 29) and channel CH1 positive piezo resistivity was also measured, but on channel CH2 negative piezo resistivity was measured. When measured transversal resistivity, see Fig. 30, positive piezo resistivity is observed. For cross-ply laminate, positive piezo resistivity was observed, when measured according to configuration B (channel 1 and channel 2). For cross-ply and quasi-isotropic laminate negative piezo-resistivity was observed under measurement configuration C.

According to described results the piezoresistive behavior is dependent on layup of unidirectional layers and also on the measurement configuration, which was confirmed also in [46].

In paper [46] there are presented results measured on quasi-isotropic laminate specimen during repeated longitudinal tension and compression loading. Resistance measurement was conducted in longitudinal and through-thickness direction (Fig. 31). Unlike results from [45] discussed before, electrical change in through-thickness direction during tension test was also measured. Applied strain was at most equal to 0.03 μm/m. It can be seen, that change in through-thickness resistance is much higher than in longitudinal direction, see Fig. 32 - Fig. 35.

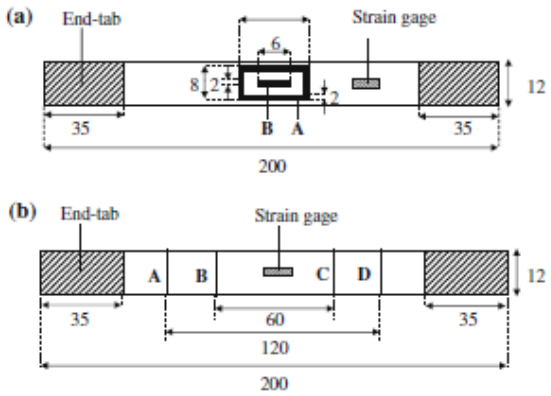

Fig. 31 (a) Configuration for measurement of the through-thickness resistance. (b) Configuration for measurement of the longitudinal resistance. All dimensions are in mm. Measurement configuration in [46].

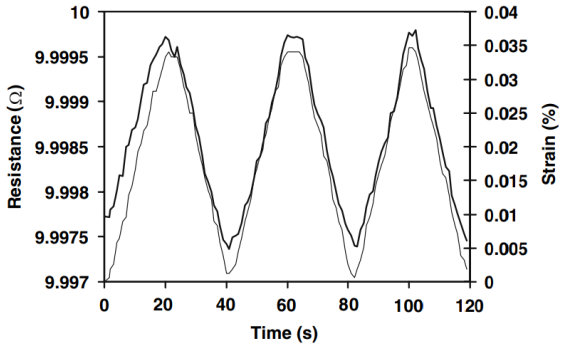

Fig. 32 Variation of the through-thickness resistance (thick curve) with time and of the strain (thin curve) with time during repeated longitudinal tension at a fixed stress amplitude of 17.5 MPa. Results presented in [46].

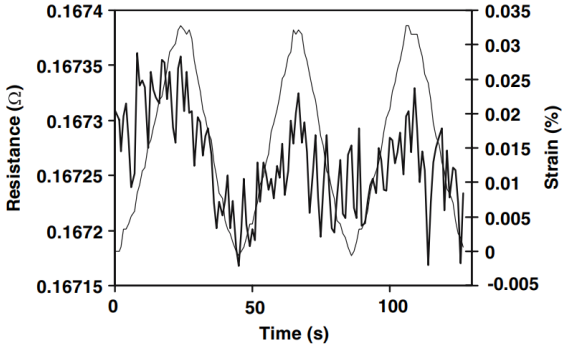

Fig. 33 Variation of the longitudinal resistance (thick curve) with time and of the strain (thin curve) with time during repeated longitudinal tension at a fixed stress amplitude of 17.4 MPa. Results presented in [46]

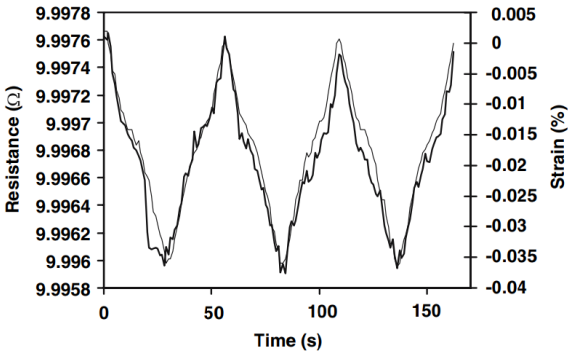

Fig. 34 Variation of the through-thickness resistance (thick curve) with time and of the strain (thin curve) with time during repeated longitudinal compression at a fixed stress amplitude of 17.4 MPa. Results presented in [46].

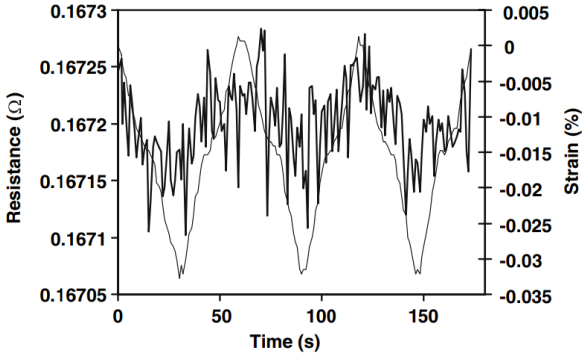

Fig. 35 Variation of the longitudinal resistance (thick curve) with time and of the strain (thin curve) with time during repeated longitudinal compression at a fixed stress amplitude of 17.3 MPa. Results presented in [46].

According to investigations published in [45], we can assume linear increase in longitudinal resistance for tension loading up to 0.5 % strain, or up to 0.6 % strain for unidirectional composite [41], see Fig. 36. These investigations were made on monotonic loading or on low number of cycles (up to 1000 cycles in [60]). Increase or decrease of measured electrical resistance is described as piezoresistivity.

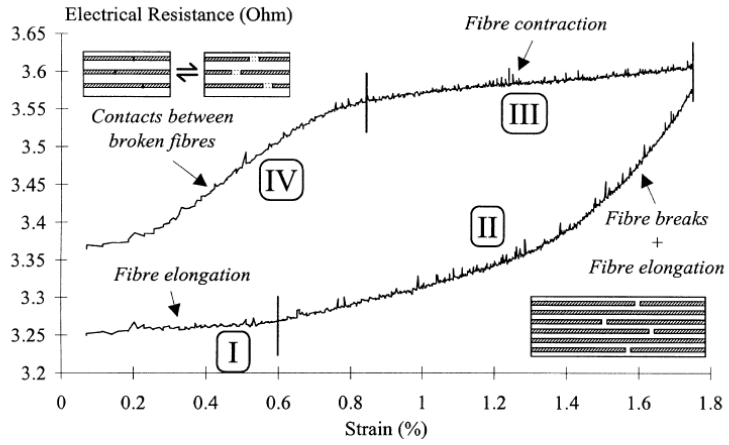

Fig. 36 Schematic of different processes occurring during a monotonic loading/unloading cycle below the strain failure [41].

In [48] is presented a FEM aided approach to determine the gauge factor for unidirectional CFRP composite plate during tension loading.

2.6.8.3 Bending

In [61] and [41] results for ER measurement method during flexural loading are presented, which confirm possibility to deformation and damage detection. Electric resistance measurement on tension or compression side of the specimen can serve for deformation detection, oblique resistance measured during unloading can serve for damage detection [61].

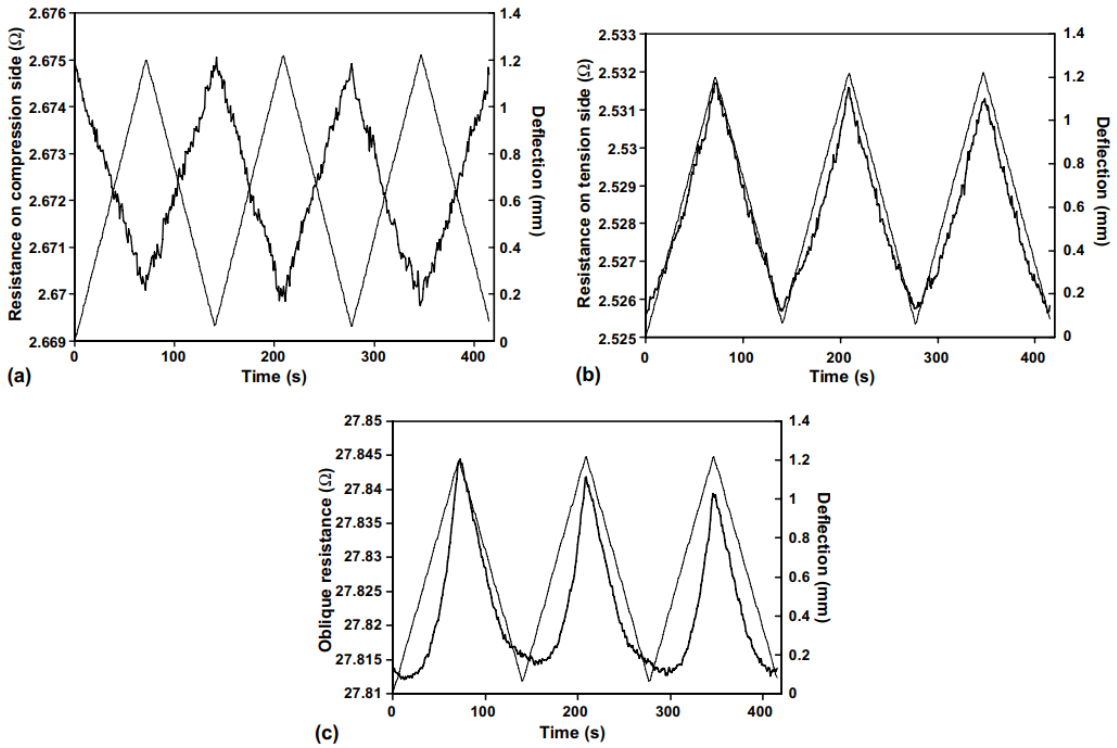

Fig. 37 Resistance (thick curve) during deflection (thin curve) cycling at maximum deflection of 1.999mm (stress amplitude 218.5 MPa). (a) Compression surface resistance, (b) tension surface resistance, (c) oblique resistance [61].

2.6.8.4 Cyclic loading and fatigue damage

The change in measured electrical resistance during repeated longitudinal loading can be observed in Fig. 38 and Fig. 39. The dependency of electrical resistance measured in longitudinal direction is depicted in Fig. 38 Fractional change in longitudinal resistance vs. time and longitudinal strain vs. time during repeated longitudinal loading at maximum stress amplitude of 53 % of the tensile strength . The dependency of electrical resistance measured in through-thickness direction is depicted in Fig. 39. It is evident that the response of measured electrical resistance for different directions show different response.

During measuring electrical resistance on specimens in the longitudinal direction, decrease of measured electrical resistance with increasing number of cycles was observed, see Fig. 38. In [44] the assumption is described, that decrease of measured electrical resistance is caused by better fiber alignment. According to presented theory better fiber-fiber contact is caused by a minor matrix damage. In work [45] positive piezoresistivity was observed for unidirectional, cross-ply and quasi-isotropic laminate manufactured using prepreg sheets, but in [44] negative piezoresistivity was observed for unidirectional laminate also manufactured from prepreg sheets.

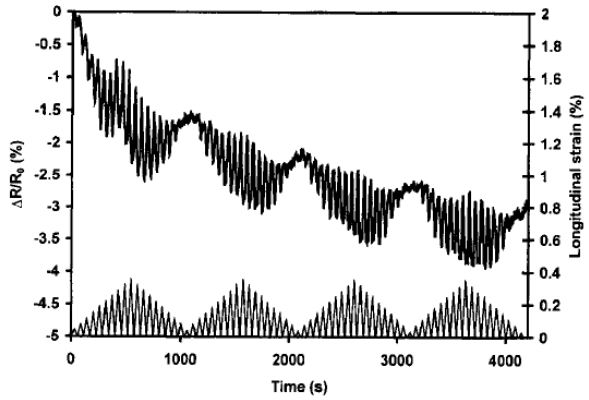

Fig. 38 Fractional change in longitudinal resistance vs. time and longitudinal strain vs. time during repeated longitudinal loading at maximum stress amplitude of 53 % of the tensile strength [44]

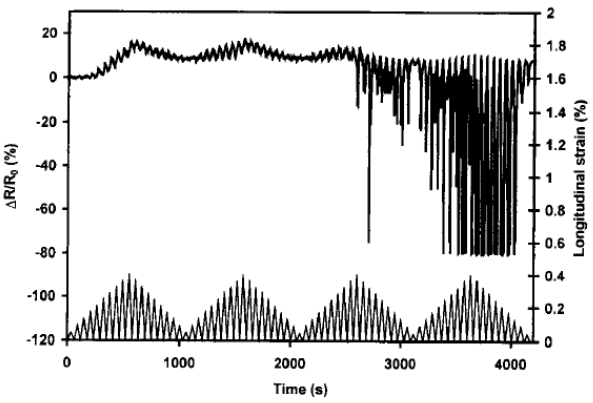

Fig. 39 Fractional change in through-thickness resistance vs. time and longitudinal strain vs. time during repeated longitudinal loading at maximum stress amplitude of 53 % of the tensile strength [44]

Measurement of through-thickness resistance is more sensitive to major matrix damage as reported also in [62]. With increasing number of cycles and the extent of delamination damage, the measured through-thickness resistance increases [62], see Fig. 40. In case of a major damage, noise can be also associated with the electrical resistance measurement, see Fig. 39.

The specific resistivity in the through-thickness direction increases with increasing angle between adjacent plies [63].

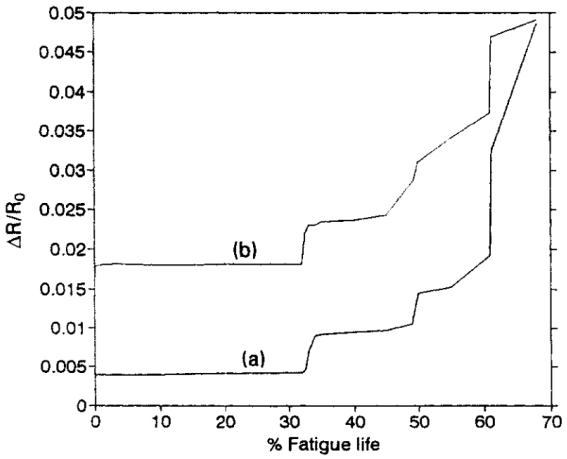

Fig. 40 Fractional change in through-thickness resistance vs. time and longitudinal strain vs. time during repeated longitudinal loading at maximum stress amplitude of 53 % of the tensile strength [62].

Change in measured longitudinal electrical resistance during fatigue loading (maximal strain was 20 % of fracture strain – considering 2 % strain as fractural strain, then 20 % = 0.4 % strain) was observed also in [42]. Change in through-thickness resistance depending on number of loading cycles (maximal strain 0.35 % of breaking stress (respond to approx. 0.6 % strain) was observed also in [62]. Results for fatigue sensing by means of electrical resistance for CFRP composite made from fabric layers are not conclusive [64].

2.6.9 Electrical resistance response to impact damage, delamination, debonding

Although change in electrical resistance can be observed during loading of undamaged specimen, the main goal of the ER measurement method lies on the defect detection of CFRP composites. So far most of the work is done separately either on investigation of response of electrical resistance to loading, or on response to impact damage or delamination.

2.6.9.1 Impact damage

Delamination area is created near the impact location after the impact., This delamination can strongly influence strength of the material during subsequent loading [6]. Thus, impact location, extend of damage and growth is one of the most investigated topics. Nevertheless, during impact also fiber breaks and transversal cracks occurs, which also influences measured electrical resistance change. Because of this impact detection is studied separately from delamination.

Basic information about impact detection can be found in [65], where impact damage detection was investigated on strip type specimens and different electrode configuration was investigated on unidirectional and quasi-isotropic specimens, see Fig. 41.

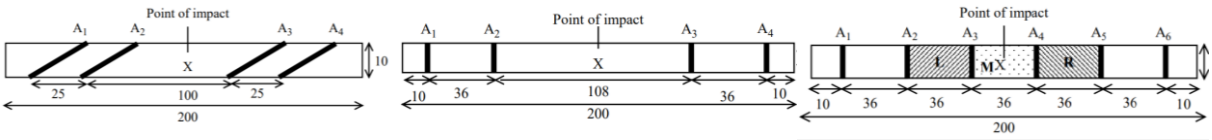

Fig. 41 Measurement configuration used in [65]

It was shown that measurement of oblique resistance with contacts not directly opposite to each other is more effective than measurement with electrodes on one surface for both unidirectional and quasi-isotropic composite. For unidirectional composite measurement on one surface with electrodes directed at angle 45° to the fiber direction is more effective than electrodes, which are positioned perpendicular to the fiber direction.

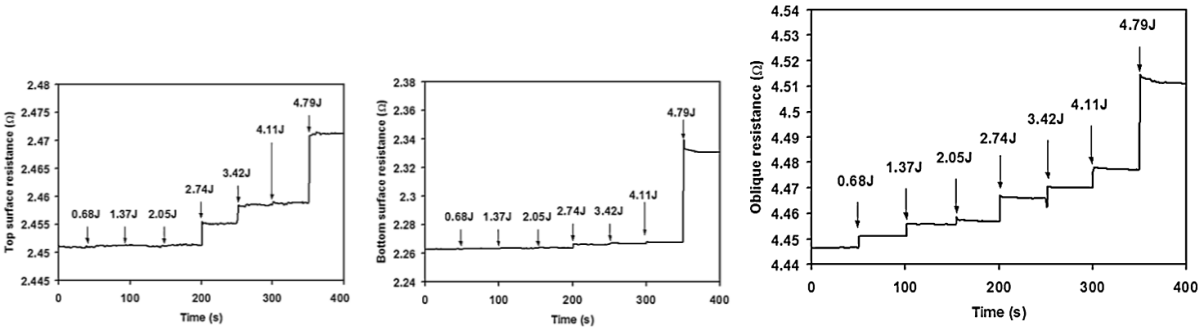

(a) Electrical resistance measured on impacted surface **(b) Electrical resistance measured on the opposite surface to the impacted surface** **(c) Oblique electrical resistance measured on quasi-isotropic specimen made of 8 layers**

Fig. 42 Results for quasi-isotropic specimen made of 8 layers [65]

Results for impact detection on plate specimens are published in [52], [45], [66], [67], [68], [69], [50], [51], [70]. Different electrode configurations were used, some of them are depicted on Fig. 18, Fig. 19 and Fig. 20. Maximum sample dimensions were 200 x 200 mm, but maximum distance between electrodes was 100 mm for electrodes on opposite edges of the specimen in [50]. Both 4-probe and 2-probe measurements were conducted. Electrical contacts are placed mainly on edges of the specimen or on one surface. Approach when flexible printed circuit interleaves are inserted between CFRP composite layers is described in [69].

2.6.9.2 Delamination

Delamination is one of the most significant damage when impact occurred, so some of the researches tried to simulate such effect in order to estimate possibility of impact detection for different specimens and CFRP composite materials [71], [11] , [57]. Results of measurement during experiments with classic delamination DCB specimen were published in [72]. Suggestion of an analytical model was also presented in [72]. Influence of plate thickness and resistivity rations were also discussed.

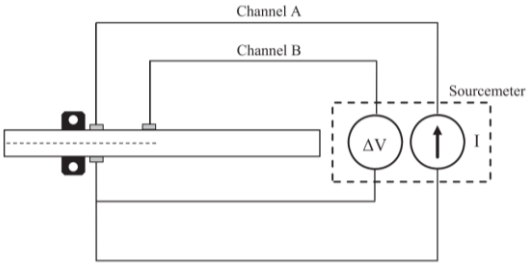

Fig. 43 Schematic of the electrical configuration used in the experimental investigations [72].

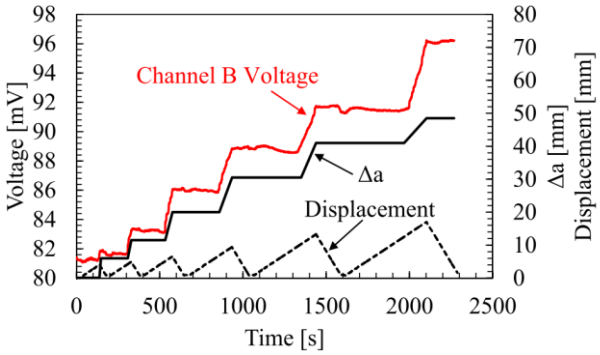

Fig. 44 Plot of the voltage, displacement, and delamination length vs. time of a combined mechanical/electrical DCB test. [72].

Delamination does not occur only after impact damage, there are also lot of other application for which delamination is the main damage scenario, see Fig. 1.

2.6.9.3 Debonding

In [73] [74] results of ER measurement on DCB bonded joint specimen are presented. Bonding was conducted using conductive adhesives with carbon nanotubes (CNTs).

2.7 Conclusions of chapter 2 and potential areas for further creative research

2.7.1 Conclusions on the carbon fiber sensors section

- Number of experimental campaigns have proven possibility of utilization of CF sensors for strain sensing.
- The sensing properties of CF sensors depends on the carbon fiber tows used for the fabrication of the sensor and on the manufacturing process itself. **Therefore, it is necessary to design and verify the own manufacturing process of the CF sensor.**
- Influence of temperature and humidity on sensing using CF sensors made of several carbon fiber tows were published. It is necessary to quantify this influence for new carbon fiber tows used for sensing. **It is necessary to quantify this influence for new carbon fiber tows used for sensing.**
- One campaign showed that microcrack detection using CF sensors is possible on GFRP composite. Idea of impact damage detection using CF sensors was shown, nevertheless no detailed information regarding this approach were given. **The author believes that impact damage detection by the mean of integrated CF tow could be an efficient way for impact damage detection on larger structures rather than ERCM method itself.**
- When speaking about SHM systems and sensors, there is also question, how to distinguish between sensor damage and damage of the structure itself. **A method for checking of the CF sensors would be beneficial.**
- CF sensors were used so far only for component made of GFRP composites or concrete structures. CF sensors were integrated in non-conductive materials. **It would be beneficial to verify the feasibility of integrating CF sensors directly into wound composite parts made of carbon fibers.**

2.7.2 Conclusions regarding electric resistance change measurement (ERCM) method on CF composites

- The number of influences, which can affect results of ERCM method were described (mechanical loading, environmental effects, fatigue loading, material parameters, configuration of electrical contacts, type of damage). **Each of the mentioned effect must be considered during preparation of experimental measurement.**
- Several configurations for determination of electrical resistivity and piezoresitivity of the CFRP material are used. **However, it is needed to develop your own expertise to use such a method in practice.**
- Although the ERCM method is investigated for several decades the contact configurations for determination of the electrical resistivity has not been compared so far. **The influence of measurement configuration on the accuracy of the determined electrical resistivity and further predictions of FE analysis is not given and should be investigated**.
- Best results for impact and delamination detection show experimental campaigns when trough-thickness and oblique resistance was measured. **A more detailed investigation of such configurations would be worth exploring.**
- For practical use of electrical resistance measurement method, **adjusting of the method will be necessary according to loading of examined component.**

- Although a lot of researchers work on algorithms for impact damage detection, the detection is possible only on plate specimens with limited dimension so far. **The author sees a greater potential in practical application of the method for the delamination detection.**
- Only a few papers deal with the delamination or debonding monitoring. **It is desirable to broaden the portfolio of similar own experiments.**
- No mention of the use of the method on CF reinforced thermoplastic and filament wound composites has yet been found. **Therefore, it would be beneficial to expand the base of experimental data and the development of measurement methods here as well.**
- The quantification of the influences on the delamination detection using ERCM is limited so far. **This area should be investigated as well.**
- In the review of current state, several contacting methods for ERCM were described. Most of them are not possible to use for preparation of electrical contacts on the internal surface of the component during manufacturing. **It would therefore be appropriate to find and validate a contacting methodology for these cases.**

3 Aims of the thesis

In the previous part of the work the state of the art of the usage of electric resistance measurement for strain measurement and damage detection on carbon fibers and carbon fiber composites was described. It was shown that there is a variety of possible measurement configurations and evaluation algorithms. However, several unresolved questions and problems emerged because of the method is influenced by many factors such temperature change, material used, loading type, damage type and other aspects highlighted in the previous two subsections. It is not possible to find answers on all of them. The focus of the work is to find versatile approaches, which could be used during further utilization of the investigated methods also on different materials and for different loading scenarios.

The aim of this thesis is to propose a versatile, cheap, and easy to use approach for damage detection of composite structures.

In the first part of the work the possibility of usage of CF sensors for impact damage detection will be investigated. This new approach for impact damage detection has to be verified and possible influences on the sensor's response arising from the operational loads should be analyzed. Other aspects that could influence the successful use of this method are also investigated.

The first objective of attention was established:

A. Development of impact detection method using CF sensors.

The main goals in the frame of this aims were established as follows:

1. Verify possibility of impact damage detection using CF sensors – find appropriate CF tow.
2. Determine the influence of cyclic mechanical loading of the structure to damage detection.
3. Determine the influence of temperature to damage detection.
4. Determine the influence of positioning of the sensor in the stacking sequence of the composite to damage detection.
5. Propose inspection of CF sensors and verify the proposal.
6. Quantify the influence of the length of the sensor to change of electrical resistance after impact.
7. Describe the relationship between electrical resistance change measured on integrated CF sensor after impact and mechanical response of the structure to the impact.

Detection of delamination using the Electrical Resistance Change Measurement (ERCM) method will be examined, and practical aspects of its application will be discussed in the second part of this work. There are a lot of construction where delamination can occur, and which are difficult to monitor by other methods because of their complex shape (for instance corners). The ERCM method should not be limited by the complexity of the shape of investigated part. For this reason, the author focused on the delamination detection using ERCM method.

In literature, there are published several contact configurations for determining electrical resistivity of CFRP composites. Influence of such configurations on the electrical resistivity determination need to be quantified. The following possibility of prediction of delamination detection by the means of FE analysis should be evaluated. The influence of distance of electrical contacts on the detectability of delamination needs to be evaluated and the influence of temperature changes also needs to be evaluated.

The second objective of attention was established:

B. Methodology of delamination detection using electrical resistance measurement on the CFRP composite.

The main goals in the frame of delamination detection were established as follows:

1. Based on experimental investigation and numerical simulation determine the appropriate procedure for electrical resistivity determination in longitudinal and through-thickness direction.
2. Determine the electrical resistivity of CF composite with thermoplastic matrices and compare it to the electrical resistivity of the CFRP composite.
3. Specify the influence of temperature change, electrical resistivities of the material and electrical contact configuration.

It is necessary to gather knowledge and experience for the practical utilization of CF sensors and ERCM method on real components. The objective of the third section is to deal with the requirements on the utilization of the approaches on the carbon fiber filament wound component.

The third area of investigation was defined as:

C. Experimental verification on component level.

Key objectives within this framework have been identified as follows:

1. Propose and verify the method of electrical insulation of CF sensors incorporated into a carbon fiber composite structure.
2. Propose and verify a methodology for electrical contact preparation for ERCM method on the filament wound components.

4 Impact damage detection of GFRP using of CF sensors

Impact damage is one possible source of damage initiation for composite structures. For instance, the aircraft structures can be impacted on the ground through collisions while loading and unloading or during flight by hail, bird, or tire fragment [75]. There are specific structural elements which are highly exposed to impacts, like the door surroundings and the leading edge. Such impact damage can cause a significant decrease of strength of these components and poses a safety risk. The possible use of sensors for impact damage detection is shown schematically in Fig. 45 and Fig. 56.

Fig. 45 Possible impact damage scenarios during flight [76] (left); photo from bird strike test of material for aircraft structure [77] (right).

The potential use of CF sensors for impact damage detection is investigated in this chapter. Several different types of carbon fiber tows were used for sensing purposes. The response of the prepared sensors to mechanical strain, damage and temperature was described. Impact damage was quantified by electrical resistance measurement of the CF sensor before and after loading. The change in electro-mechanical response to cyclic loading with regard to impact damage was also evaluated. A sensitivity test on the influence of the sensor's position in the material for impact damage detection was also conducted. The findings gathered in this section were presented in several publications by the author [A6],[A1].

The influence of the length of the CF sensor was also investigated, as well as the size of the impact on the sensor's response. A correlation between impact damage size, response of the CF sensor and mechanical response of the specimens was found. These findings were published in [A18].

4.1 The structure of the experimental program

Three experimental campaigns were conducted. The campaigns started with initial tests and individual aspects of the usage of CF sensors for impact damage detection were examined.

- In the **first campaign,** it was investigated whether impact damage detection using CF sensors is possible. The influence of the type of carbon fiber tow and the number of filaments were analyzed. The CF sensors were placed on top of the specimen (on impacted site). Several types of CF rovings were chosen and their response to mechanical strain and incision was compared. Sample preparation was done using hand lamination. The influence of short-term cyclic loading during three-point bending (3PB) on different types of sensor material was also investigated. Investigations were published in [A6]. The results of this campaign are summarized in section 4.2.

- In the **second campaign,** the carbon fiber tows which succeeded in the first campaign were used. The influence of the positioning of the CF sensor in the composite layup was investigated. CF sensors were integrated into different position in the composite layup to find the best position for damage monitoring. Sample preparation was done using prepreg sheets and an autoclave. The influence of short-term cyclic loading during 3PB was again analyzed. The influence of temperature change was also examined. Thermography inspection was used for the inspection of CF sensors. Investigations were published in [A1]. The results of this campaign are summarized in section 4.3.

- In the **third campaign,** the carbon fiber tows which succeeded in the second campaign were used. The positioning of the CF sensor in the composite layup that best fit the damage monitoring in the second campaign was used. The same procedure for sample preparation as in the second campaign was used. The sensor length was double that in the second campaign. The influence of long-term cyclic loading was investigated before and after impact damage initiation during a four-point bending (4PB) test. The correlation between size of impact and response of the structure a response of the sensor was investigated. The results of this campaign are summarized in section 4.4. and were published in [A18].

4.2 First experimental campaign - Impact damage detection using CF sensors

The aim of the first study was to investigate:

- the possibility of using embedded carbon fiber tows to detect impact damage,
- the influence of cyclic flexural loading on the possibility of damage detection,
- the influence of damages to embedded carbon fiber tows on measured signals.

For our experimental campaign flat specimens made of glass fiber reinforced polymer. Sensors made of carbon fiber tows were embedded to the specimens as the final layer. In order to offer a thorough understanding of the influence of damage to CF sensors on measured signals, some of the specimens were embedded in undamaged condition, and others were embedded with incised CF senosrs. Following the initial set of loading cycles, the specimens with undamaged CF sensors were subjected to impact and subsequently subjected to another set of cyclic loading. Measurements of electric resistance were conducted during the loading. In order to evaluate their suitability as sensors for structural health monitoring applications, a comparative analysis was conducted on four different carbon-fiber tows, namely two ex-PAN types, ex-Pitch, and nickel coated.

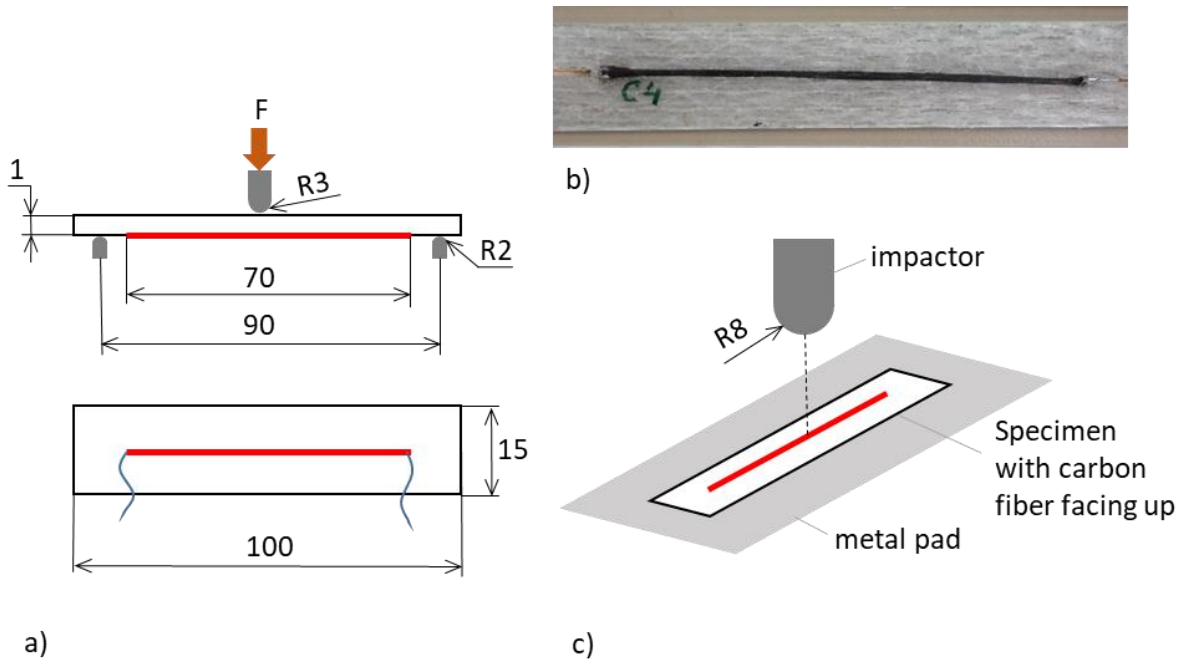

Fig. 46 Specimen and loading description (a); Impacted specimen with embedded carbon fiber (b); Configuration during impact loading (c). [A6]

4.2.1 Experiments and evaluation methods

4.2.1.1 Specimen preparation

Flat specimens as depicted in Fig. 46 were prepared for the experimental procedure. The specimens consisted of two layers $[0]_2$ of unidirectional glass non-crimp fabric with a weight of 600 g/m². These fabric layers were provided by R&D Faserverbundwerkstoffe GmbH, L20 epoxy resin and EPH 161 hardener were used. The specimens were cured for 15 hours at a temperature of 60°C. CF sensors were placed on one side of the fabric before curing. All specimens were cut from a single plate after curing.

4.2.1.2 Carbon fiber sensors (CF sensors)

From each of the tested carbon-fiber tows, CF sensors measuring 70 mm in length were prepared. The methodology for the manufacturing of CF sensor was described in [12], and the identical approach was implemented in this investigation. A nickel electrolyte coating was applied to the ends of each roving. Subsequently, thin copper wire was used to establish electrical connections, as depicted in Fig. 47 and Fig. 48.

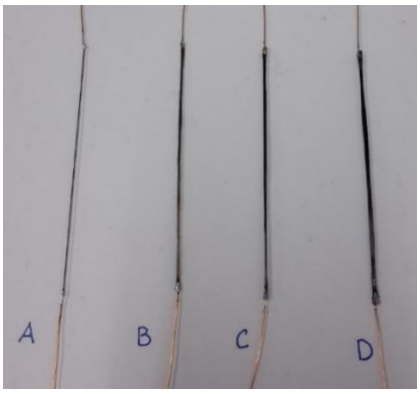

Fig. 47 CF sensors prepared for installation into the specimens

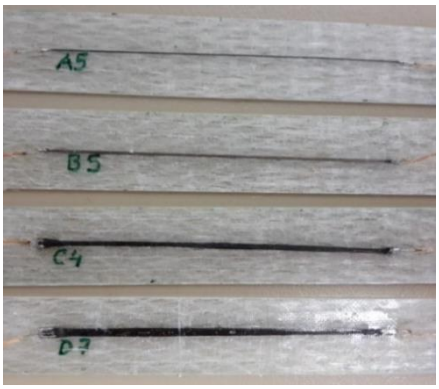

Fig. 48 Specimens with integrated CF sensors

In Table 4 are given properties of the carbon fibers used for preparation of CF sensors in this study. The first type is Toray T300 (label A), which has already been used successfully for strain and damage monitoring [7], [33]. The second type is also a PAN fiber, but with nickel metallization (label B), produced by Toho Tenax. This material was used to investigate the influence of the nickel layer. The original nickel-coated PAN fiber consisted of 12,000 filaments. For the investigation we wanted to use a thinner tow, so the carbon fiber tow was divided. The part of the tow that was used consisted of 7,720 filaments. To ensure a relevant comparison, with no influence of the production process of the nickel coating, the same PAN fiber manufactured by Toho Tenax, without a nickel layer (label C), was included in the test matrix. The tow was also divided into two parts, and the part for preparing CF sensor contained 6,000 filaments. The fourth fiber examined in this study was PITCH-fiber, which was produced by Nippon Graphite Fiber Corporation (label D).

4.2.1.3 Loading and damage preparation

Two types of damage to CF sensors were investigated. Two groups of specimens were prepared from each type of CF sensor. The specimens in the first group were prepared with undamaged CF sensors. The second group were equipped with CF sensors that were incised using a scalpel. The incisions resulted in breakage of about 30 to 50 % of the filaments in the roving. The cutting of the carbon fibers was observed using a Tescan LYRA 3 electron scanning microscope. Images of the cuts of the carbon fibers A and D are depicted in Fig. 49 and Fig. 50. The brittle behavior of the ex-pitch fiber is indicated by the morphology of the filament breakage. The morphology of the filament breakage for all ex-PAN fibers (A, B and C) look the same. All specimens were exposed to cyclic flexural loading. A three-point bending test was chosen in order to prevent possible damages in the area where the electrical contacts had been soldered. The test was configured in such a way that the tension stress in the area of the electrical contacts of the CF sensor was negligible. The loading was performed using a Zwick Roell Retroline 1145 universal testing machine, under the following configuration: support distance 90 mm, maximal loading force 12 N, preload 1.1 N, loading velocity 50 mm/min.

Table 4 An overview of the examined carbon fiber tows.

Label of the fiber		**A**	**B**	**C**	**D**
	[-]	T300 1000-50A	HTS40 A23 12K 1420TEX MC	HTS 40 MC	CN-80-30S
Type	[-]	PAN	PAN	PAN	PITCH
Producer		Toray	Toho Tenax	Toho Tenax	Nippon Graphite Fiber Corporation
Number of Filaments	[-]	1,000	12,000	12,000	3,000
Number of Filaments Used	[-]	1,000	7,720	6,000	3,000
TEX-number	[-]	66	1,437	1,430	-
Metalization	[-]	-	Nickel	-	-
E	[GPa]	230	215	230	780
R_m	[MPa]	3,530	2,760	2,900	3,430
Elongation	[%]	1.5	1.28	1.3	0.5
Thermal conductivity	[W/mK]	10.46	-	10	320
Volume resistivity	[μΩm]	17	-	16	5

Strain gauges were applied to determine the cyclic load in such a way that the strain level was 3,000 μm/m for the outer layer of the bending specimens. In order to investigate the changes in electrical resistivity, 300 load cycles were applied to each specimen (with undamaged CF sensors, and with incised CF sensors). The specimens with undamaged CF sensors were exposed to impact loading after the first loading series. Impact loading was performed using an impactor 16 mm in diameter. During impacting, the specimen was placed on a metal pad with the CF sensor facing upwards, see Fig. 46. The impact energy was 2 J and 3 J, according to Table 5. After impacting, the specimens were exposed to the second loading series of 300 cycles. The influence of the damage in combination with cyclic loading was characterized and was compared with the behavior of the specimens with undamaged carbon fiber sensors.

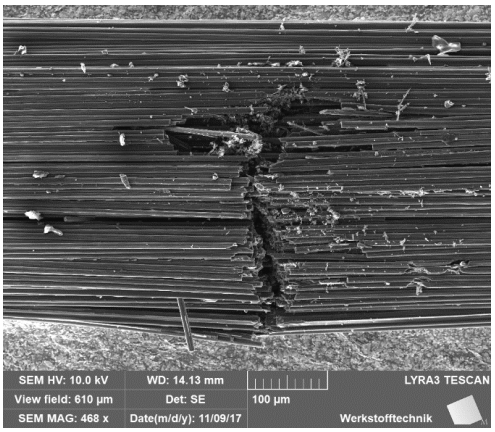

Fig. 49 Detail of the cut of the Toray T300 carbon fiber (A)

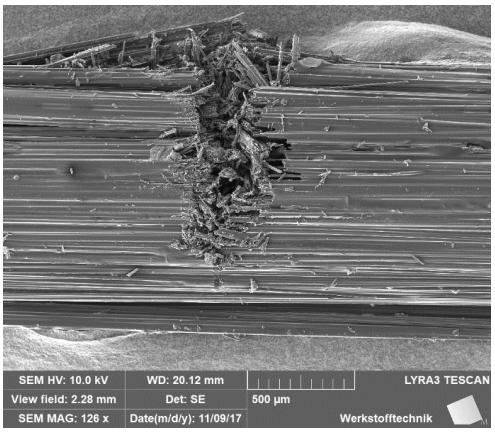

Fig. 50 Detail of the cut of the Nipon CN-80-30S carbon fiber (D)

4.2.1.4 Electrical resistance measurements

Measurements of the changes in electrical resistance change were performed using a Quantumx MX 1615 strain gauge amplifier, manufactured by Hottinger Baldwin Messtechnik GmbH. The output of the Wheatstone bridge was used to determine the changes in the electrical resistance of the measured carbon fiber sensor embedded in the specimens. A half bridge connection was used in order to eliminate changes in the electrical resistance change due to changes in temperature during the measurements. In each branch, one specimen with the same type of carbon fiber sensor was connected to an additional resistance (R_{ad}), because the minimum electrical resistance in each branch has to be 80 Ω. The changes in electrical resistance were calculated using the following equations, where U_O is output voltage and U_I is input voltage.

$$\frac{U_O}{U_I} = \frac{1}{4} \cdot \frac{\Delta R}{R} \quad \left[\frac{mV}{V}\right] \rightarrow \left[\frac{m\Omega}{\Omega}\right], \tag{11}$$

$$\Delta R = 4 \cdot \frac{U_O}{U_I} \cdot R_0 \, [m\Omega], \tag{12}$$

$$R_0 = R_{CFS} + R_{ad}, \tag{13}$$

$$Relative\ change\ in\ electrical\ resistance\ = \frac{\Delta R}{R} = \frac{\Delta R}{R_{CFS}}. \tag{14}$$

The relative change in the electrical resistance of each specimen was determined according to equation (14) The value was used in the subsequent evaluation, and is marked $\Delta R/R$. An overview of the measured electrical resistivity for all specimens is given in Table 5.

4.2.2 Results and Discussion

For the purposes of SHM, the following two factors are of great interest:

- the change in the electrical resistivity of the CF sensor due to the damage in composite,
- the change in the electrical resistivity of the damaged CF sensor due to cyclic loading.

Smooth, almost linear dependence of the measured relative resistance of the fiber on the loading was measured for all types of carbon fibers in the pristine state, see Fig. 51, Fig. 53 and Fig. 54.

The incision of the fibers was the first type of damage investigated. Incision simulates the interruption of filaments that can occur during tension or compression loading, and after an impact. It was assumed that incising the fibers before embedding can have a significant influence on the measured signal during the subsequent three-point bending test. A significant change in the signal was also observed for some specimens with CF sensor made of type B and C fibers, see Fig. 53 and Fig. 54. Small changes in the shape and size of the signal were also observed for specimens A4 and A8 (Fig. 52). No change in measured signal compared to undamaged specimens was observes for specimens equipped with CF sensor type D pitch fibers.

Table 5 An overview of the specimens with measured electrical resistance.

A	Toray T300					
Undamaged	[Ω]	Impacted	Impact energy [J]	[Ω]	Incised	[Ω]
A1	29.2	A1	3	45.5	A3	32.2
A2	31.3	A2	3	31.3	A4	33.5
A5	29.7	A5	2	29.9	A7	32.4
A6	29.5	A6	3	30.9	A8	30.8
					A9	31.3
					A10	-
B	Tenax Ni-coated					
Undamaged	[Ω]	Impacted	Impact energy [J]	[Ω]	Incised	[Ω]
B1	0.40	B1	3 (2x)	0.46	B3	0.45
B2	0.41	B2	3 (2x)	0.48	B4	0.43
B5	0.60	B5	3	0.60	B7	0.56
B6	0.60	B6	2	0.60	B8	0.63
					B9	0.58
					B10	0.60
C	Tenax HTS 40 MC					
Undamaged	[Ω]	Impacted	Impact energy [J]	[Ω]	Incised	[Ω]
C1	4.83	C1	3 (2x)	4.97	C5	4.96
C2	4.82	C2	3	4.86	C6	5.38
C3	4.79	C3	3	4.82	C7	5.45
C4	4.74	C4	2	4.76	C8	5.14
D	Nippon CN-80-30S					
Undamaged	[Ω]	Impacted	Impact energy [J]	[Ω]	Incised	[Ω]
D1	1.63	D1	3	2.02	D5	2.40
D2	1.75	D2	3	2.36	D6	2.16
D3	1.82	D3	3	2.13	D7	2.77
D4	2.04	D4	2	2.28	D8	2.51

Differences in change of measured signal may have been caused by the way in which the incised specimens were prepared and in the way in which the incised CF sensor was embedded in the specimens. For further experiments, it is suggested that the CF sensor should be interrupted after the specimens have been prepared. Nevertheless, the experiments as they were conducted provided information about the behavior of partly interrupted CF sensor.

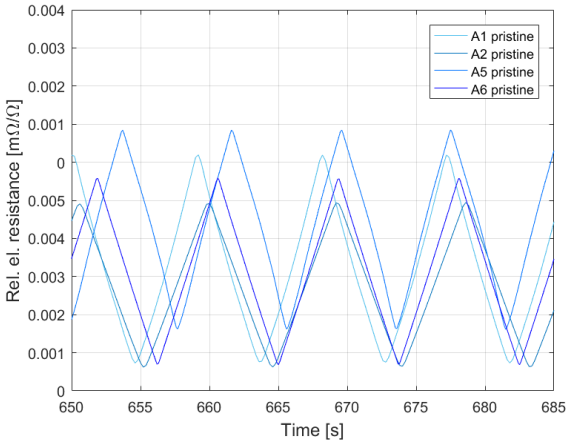

Fig. 51 Electrical resistivity of type A embedded CF sensor - pristine during cyclic loading

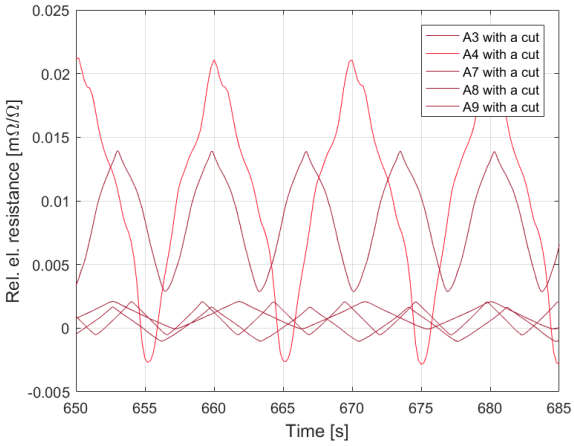

Fig. 52 Electrical resistivity of type A embedded CF sensor - incised during cyclic loading

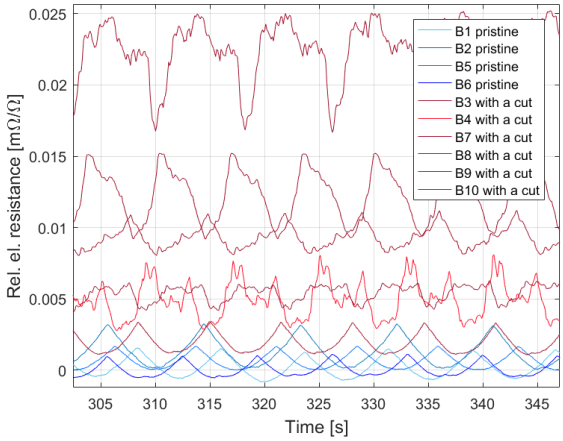

Fig. 53 Electrical resistivity of type B embedded CF sensor - pristine and incised during cyclic loading

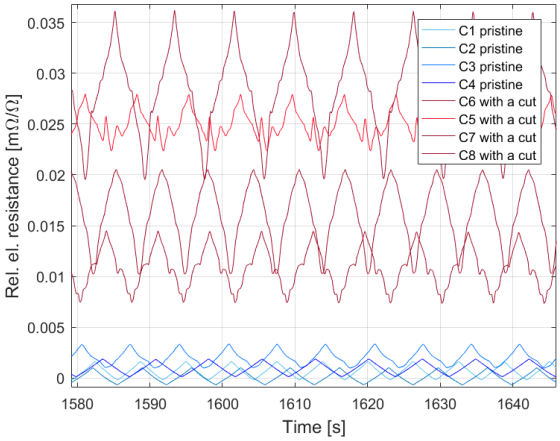

Fig. 54 . Electrical resistivity of type C embedded CF sensor - pristine and incised during cyclic loading

Impact was the second investigated damage mechanism. Specimens with embedded CF sensor according to

Table 5 were loaded before and after impact. The electrical resistivity of the embedded carbon fibers was measured before flexural loading and during 300 subsequent cycles. After the impact on the specimens, the resistivity of the embedded CF sensor was measured again, and it was also measured during the subsequent 300 cycles of flexural loading. The graphs in Fig. 55 summarize the results of these measurements. For each specimen, the measured resistance for three states of an undamaged (pristine) specimen is given for each specimen. The following states are compared: before loading, during the first cycle of flexural loading at a deflection of the specimen of 2 mm (corresponds to a strain of 900 µm/m), and during cycle number 300 at a deflection of 2 mm. The same data are given for all

specimens for the state after impact. Fig. 55 (A) presents data for type A CF sensors. There are great differences among the tested specimens, and no clear conclusions can be drawn. The situation is similar for nickel-coated carbon fiber (Fig. 55 (B)). The data obtained for type C CF sensor (Fig. 55(C)) shows that the change in electrical resistivity after impact is only from 0.5 % to almost 3 % in the unloaded state.

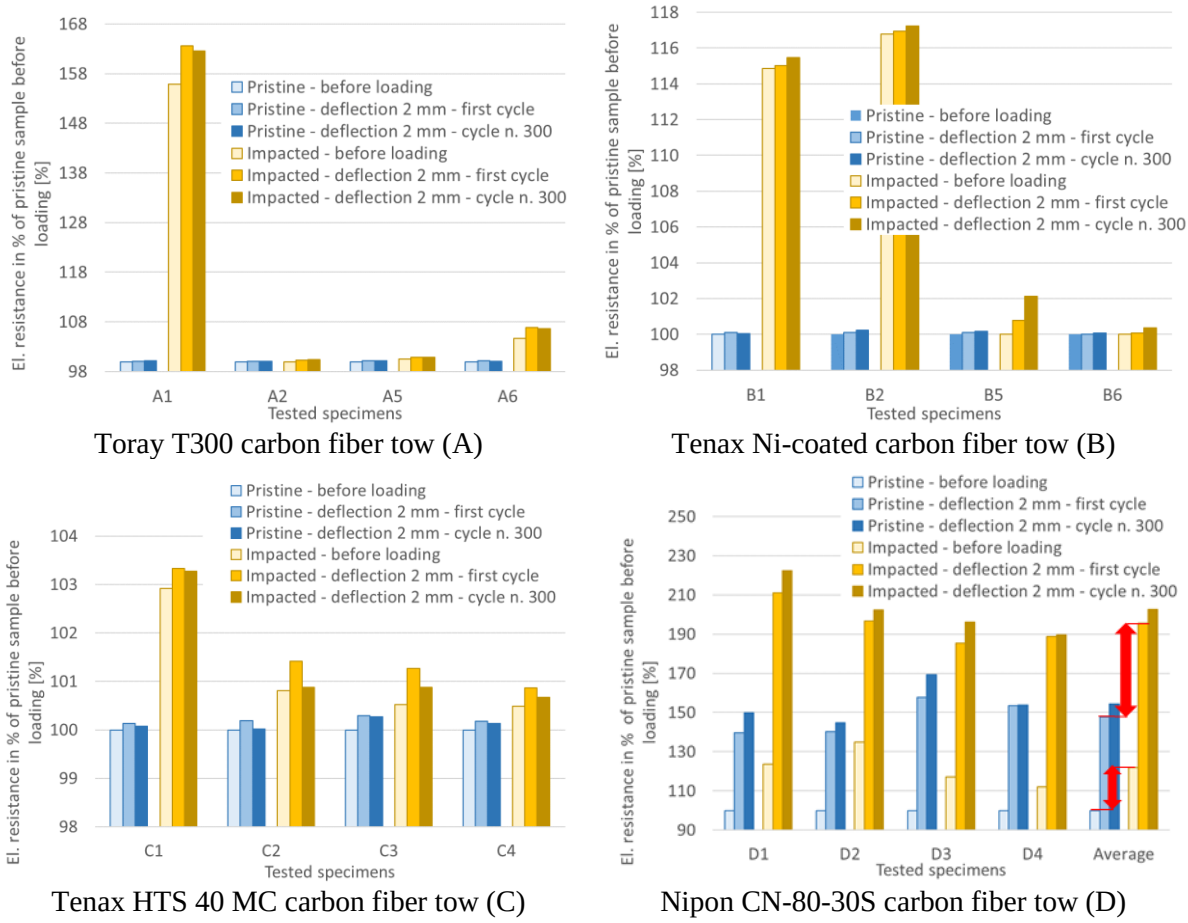

Toray T300 carbon fiber tow (A)

Tenax Ni-coated carbon fiber tow (B)

Tenax HTS 40 MC carbon fiber tow (C)

Nipon CN-80-30S carbon fiber tow (D)

Fig. 55 Measured data for the pristine state and for the impacted state of the specimens with embedded CF sensors

The change is slightly higher for the loaded state, but it decreases as the number of cycles increases. A significant change in measured electrical resistivity was observed for the pitch carbon fiber (Fig. 55 (D)). The change in the measured electrical resistivity values for all specimens was similar and was one order of magnitude higher than for the other tested types of carbon fibers. The average change in electrical resistance after impact for an unloaded specimen is greater than 20%, and for loaded specimens the change is even much greater. The electrical resistivity of pitch carbon fibers increases due to cyclic loading.

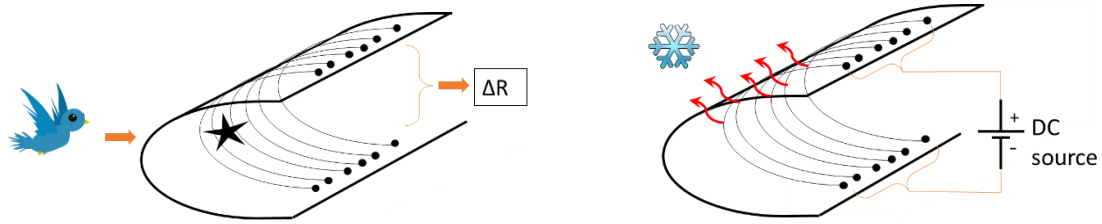

Fig. 56 Possible applications of CF sensor-network during impact detection, and as a heating element in a leading edge

4.2.3 Conclusions drawn from the first experimental campaign

The following conclusions can be drawn from the investigation:

- The changes in measured electrical resistivity due to impact on the specimens are most significant for the tested ex-PITCH fiber. These changes are higher by an order of magnitude than for the tested ex-PAN fibers.
- Cyclic loading has a more significant influence on changes in the electrical resistivity of damaged ex-PITCH fibers than on changes in the electrical resistivity of ex-PAN fibers.
- The changes in electrical resistance are more pronounced in the loaded state for tested type C and type D fibers, while no decisive conclusions can be drawn in this area for other types of fibers.
- Changes in the measured dependency between electrical resistivity and flexural loading of incised CF sensors are most likely to occur in specimens with type B and type C embedded fibers.
- The different characteristics for ex-PITCH fibers compared to ex-PAN fibers can be attributed to the brittle behavior of the carbon structure of pitch fibers. Further investigations will follow.

The characteristics investigated here are of strong interest because they can help in the development of a complex CF sensor network for use in various aspects of Structural Health Management (SHM).

4.3 Second experimental campaign - Impact damage detection using CF sensors

Based on the findings from the first experimental campaign, a second campaign focusing on impact damage detection was prepared. The ex-PAN carbon fiber Toray T300 was chosen as a reference fiber tow, because it has shown stable and repeatable behavior in other sensing applications, such as those reported in [27] and [33] although it has shown different results regarding impact damage detection. Since the highest sensitivity to impact was observed for the ex-PITCH fiber tow, it was hypothesized that this could be related to its low limit of maximal elongation. For the second experimental campaign, two types of pitch carbon fiber tows with low maximal elongation were chosen.

4.3.1 Materials and methods

4.3.1.1 Sample preparation

The specimens were made of glass woven fabric prepreg sheets, commonly used in the aerospace industry. The autoclave curing technique was selected for this purpose. A laminate lay-up of $[+45/0/-45/90]_{sym}$ was used for preparing the specimens. The chosen prepreg material, made of woven fabric with epoxy resin HexPly 1454 GM/50%/1035, underwent the following curing process: 125 °C for 90 minutes under pressure of 6 bar. The specimens were then cut into strips measuring 140 mm × 23 mm, with a thickness of 1.3 mm.

Table 6 Overview of specimens for mechanical tests.

Material of CF sensor	Specimen numbers	Placement of CF sensor between layers
T300 1000-50A (PAN)	**30**[4], 31, 32, 33	1 and 2
	34, 35, 36, **37**	4 and 5
	16, 17, **18**	7 and 8
YS-95A-30S (PITCH)	1, **2**, 4	1 and 2
	5, 7, **8**	4 and 5
	9, 11, **12**	7 and 8
YSH-70A-30S (PITCH)	1, 2, **3**	1 and 2
	4, 5, **6**	4 and 5
	7, **8**, 9	7 and 8

Three different integration arrangements were applied for the carbon fiber sensors. They were placed between the first and second layer, in the middle of the specimen 's thickness (between the fourth and fifth layer), and between the seventh and eighth layer. Table 6 presents an overview of the specimens used for the mechanical tests and the different CF sensor materials that were employed.

[4] The specimens with numbers written in bold underwent computer tomography after the mechanical loading and impact test.

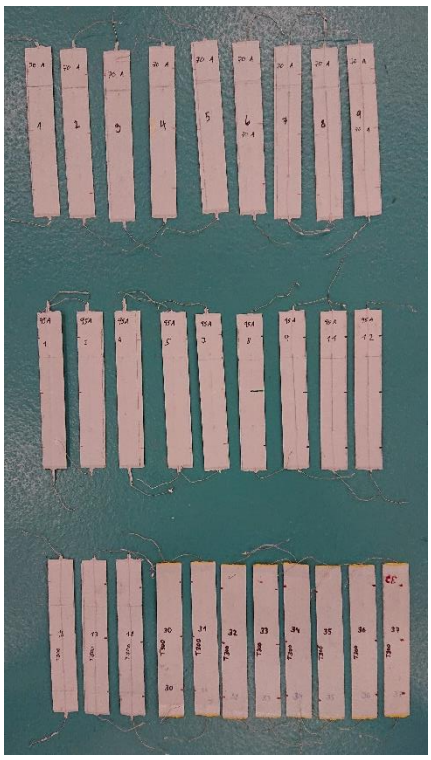

(a)

(b)

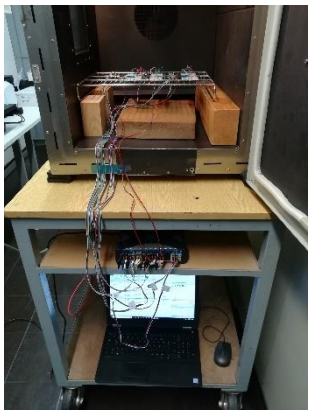

(c)

Fig. 57 (a) Specimens after mechanical loading; (b) CF sensors type 70A during implementation in the composite lay-up; (c) Specimens during temperature loading. [A1]

4.3.1.2 Carbon fiber sensors (CF sensors)

The carbon fiber sensors were fabricated from three different fiber tows. The material properties of each type are detailed in Table 7. The selection of materials for the preparation of the CF sensors was made to assess the influence of ultimate elongation on the detection of impact damage.

The objective was to find whether an impact can damage the sensor fiber, and how such damage influences the signal. The T300 1000-50A PAN tow was chosen for this purpose, because it was already employed in a previous comparative study [A6] and various sensing applications, see references [27] to [33].

Table 7 An overview of the carbon fiber tows examined here.

Label of the fiber tow		**T300** **T300 1000-50A**	**95A** **YS-95A-30S**	**70A** **YSH-70A-30A**
Type		PAN	PITCH	PITCH
Producer		Toray	Nippon Graphite Fiber Corporation	
Number of filaments	[-]	1,000	3,000	3,000
Tensile modulus E	[GPa]	230	893	714
Tensile strength R_m	[MPa]	3,530	3,600	3,600
Ultimate elongation	[%]	1.5	0.3	0.5
Thermal conductivity	[W/mK]	10.46	600	250
Volume resistivity	[μΩm]	17	2.2	5

4.3.1.3 Mechanical testing and impact loading

All specimens underwent a three-point bending (3PB) test. This type of cyclic flexural test was chosen to prevent damage in the area of the electrical contacts. The loading configuration, as shown in Fig. 58 results in tension/compression loading of the sensor fiber due to its nonsymmetrical integration (see also Fig. 62). The cyclic loading was performed using the hydraulic testing system MTS Mini Bionix (MTS, Minnesota, USA).

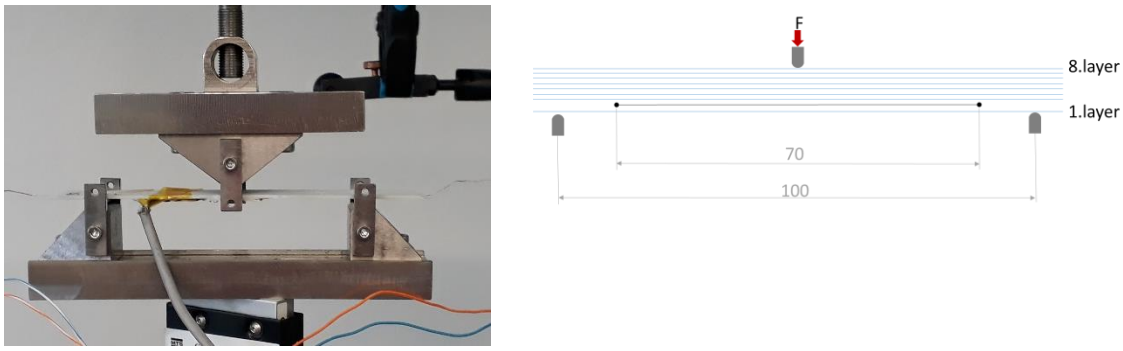

(**a**) (**b**)

Fig. 58 Configuration of the 3-point-bending test: (a) specimen during cyclic flexural loading; (b) configuration of the composite lay-up during cyclic flexural loading.

The specimens were loaded with a force ranging from 1.5 to 15 N (load ratio = 0.1) at a frequency of 0.1 Hz. The maximum loading force was established during a preliminary test, where a strain gauge was installed in the middle part of the outer surface of the specimen. The maximum loading force of 15 N corresponded to a measured longitudinal strain of 3,200 μm/m during the preliminary test. This strain level corresponds to a maximal loading level in many applications to avoid intralaminar matrix cracks. The specimens were subjected to 200 load cycles before impact loading and another 200 load cycles afterward. Measurements of changes in electrical resistance were performed using a Keysight 344401A multimeter, employing the 4-wire resistance measurement method to eliminate test lead resistances.

The potential for detecting impact damage using CF sensors was investigated through a drop weight impact test. The test configuration, different from the first experimental campaign, is illustrated in Fig. 59. Due to changes in the manufacturing process, the sensors protruded slightly from the surface. The supports were adjusted to prevent any cantilevers from damaging the sensor during impact. An impactor 16 mm in diameter and weighting 410 g was dropped from the height of 0.5 m generating an impact energy of 2 J.

No visible damage was observed on the impacted side of the specimen (the mold side) after the 2J impact. However, damages to the opposite side of the specimens were visible and could be detected by visual inspection in some cases.

Specimens T300-32, T300-33, T300-36, T300-37 were subjected to a second impact as the first impact was outside the area of the CF sensor. Specimens T300-34 and T300-35 did not undergo impact loading.

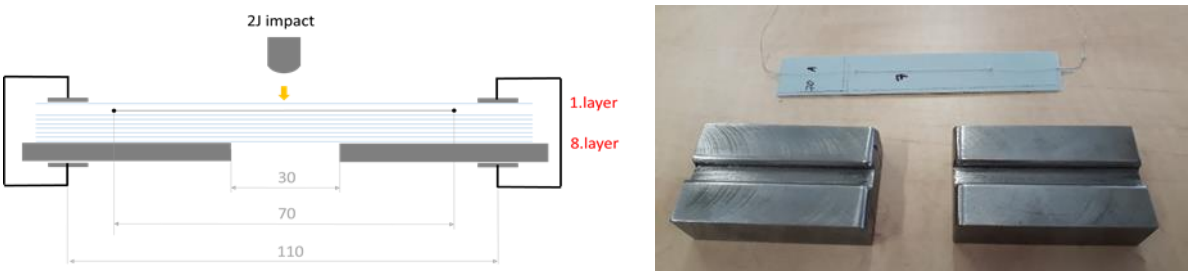

(a) (b)

Fig. 59 Configuration of the drop weight impact test: (a) schema of the impact test; (b) supports for the impact test.

4.3.2 Results and discussion regarding mechanical testing and impact loading

Most composite structures, where impact damage detection is a critical aspect, are also exposed to cyclic loading. Therefore, understanding the influence of cyclic mechanical loading on the measured signal of impact sensors is of great interest. The purpose of the mechanical testing was to describe the response of the measured signal of the investigated sensors with regard to:

- the number of cycles;
- the positioning of the CF sensor in the composite lay-up;
- the influence of different materials on the CF sensor signal.

Specimens with integrated sensors were subjected to cyclic flexural loading both before and after impact loading. During mechanical loading, room temperature was monitored to exclude its influence. The influence of temperature change on the measured signal of CF sensors is discussed in section 4.3.4.

In practical applications, it is not always feasible to conduct simultaneous temperature measurements at the location where impact detection is needed. One approach is to use temperature compensation of the half-bridge circuit as is done for instance for strain gauges [78]. Another option is to evaluate the peak-to-peak values of cyclic loading [79] (see Fig. 60). The schematic representation illustrates the evaluation procedure applied for different experimental steps. Using this procedure, temperature measurements become unnecessary.

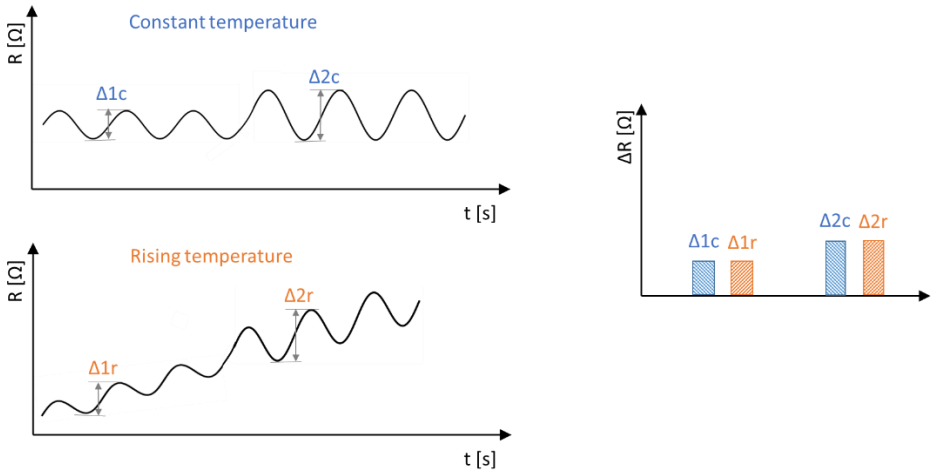

Fig. 60 Evaluating the peak-to peak data [A1].

Fig. 61 presents the peak-to-peak relative values of the measured electrical resistance for all specimens that underwent both mechanical and impact loading.

The relative values were determined to allow an easier comparison of sensors made from different carbon fiber tows. The peak-to-peak relative values were determined for the first and last cycle before impact loading (cycles 1 and 200) and for the first and last cycle after impact loading (cycles 201 and 400). The peak-to-peak values were related to the measured value of the electrical resistance of the sensor after implementation. For the Xth cycle of the loading the equation for the relative electrical resistive range ΔR_{REL} is as follows:

$$\Delta R_{REL(CYCLE\ X)} = \frac{R_{\max loading(CYCLE\ X)} - R_{\min loading(CYCLE\ X)}}{R_{after\ implementation}}. \quad (15)$$

According to the measured data, it is evident, that all types of carbon fiber tows investigated here show piezoresistive behavior. A positive change in measured electrical resistance was observed for specimens, in which the sensor was integrated on the tension side of the specimen (between layers 1 and 2), as shown in Fig. 61 and Fig. 62.

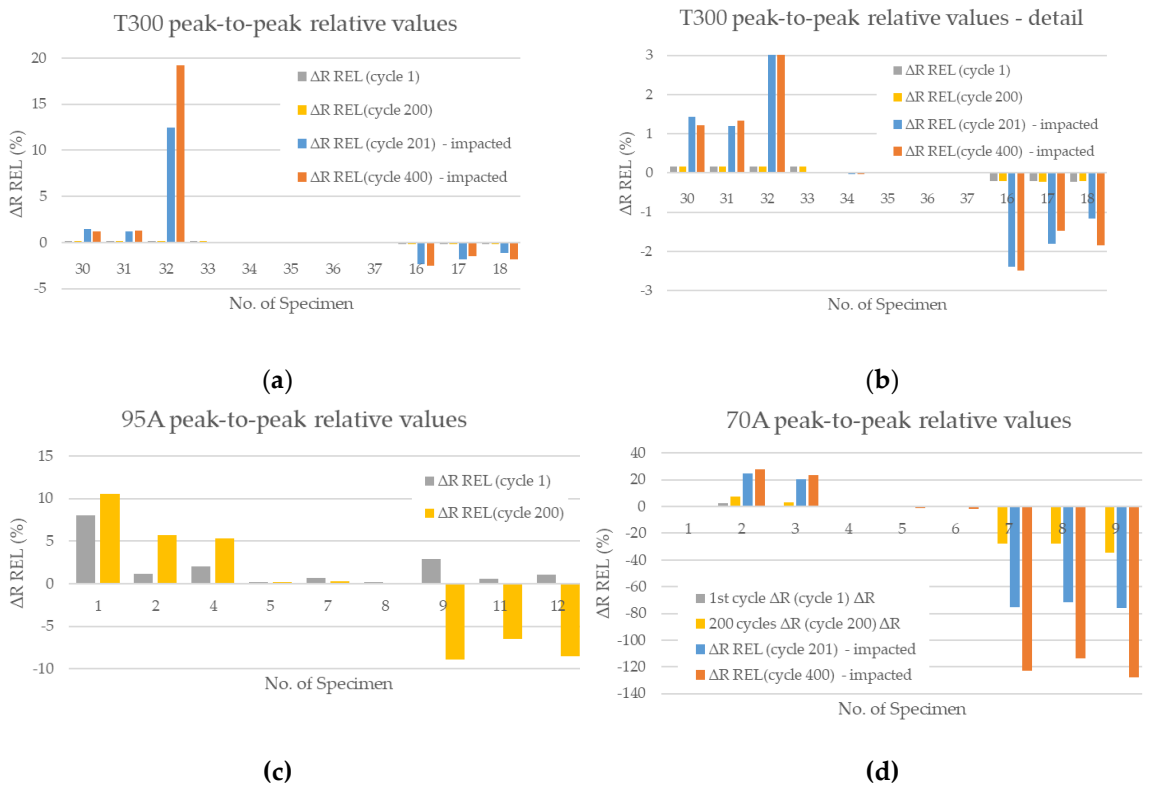

Fig. 61 Peak-to-peak relative values of the measured signal from CF sensors integrated into the specimens before and after impact loading: (a) results for specimens T300; (b) results for specimens T300 – detail; (c) results for specimens 95A; (d) results for specimens 70A.

Specimen with CF sensor between the 1st and 2nd layer during 3PB	Specimen with CF sensor between the 4th and 5th layer during 3PB	Specimen with CF sensor between the 7th and 8th layer during 3PB
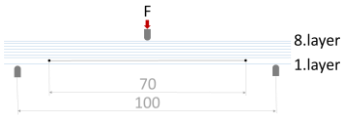	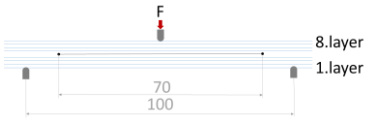	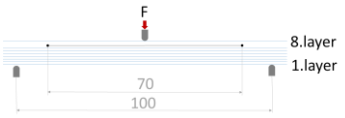
Specimen T300-30	Specimen T300-37	Specimen T300-16
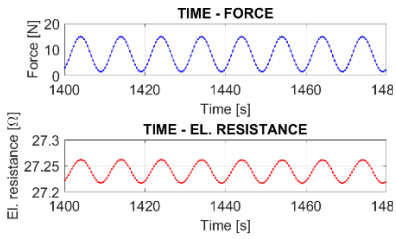	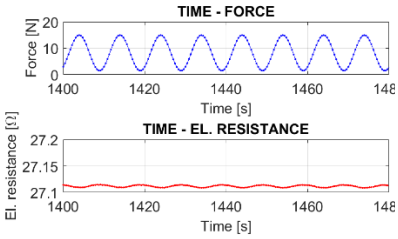	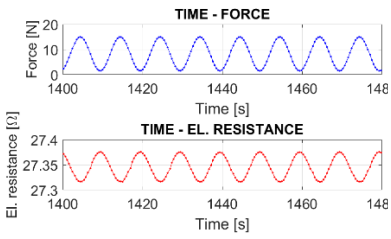

Fig. 62 Configuration of the 3PB test and the measured signal from the integrated CF sensor.

The relationship between the number of cycles and the measured resistance for the T300 material sensors can be considered negligible before impact. Sensors made of T300 material also exhibit a limited dependency between the number of cycles and measured resistance after impact. All specimens displayed a change of less than 0.7 % in the peak-to-peak relative values between the first and the 200th cycle. The influence of the number of cycles on the measured signal is much more pronounced in specimens with integrated sensors made of pitch carbon fiber tows 95A and 70A. Compressive loading has a more significant impact on the change in the measured signal for both materials.

For the 70A material, we also have data on cyclic loading after impact. Fig. 64 illustrates that the greater the change in measured electrical resistance after impact, the larger the influence of the number of post-impact cycles on the change in measured electrical resistance. Peak-to-peak values for sensors made of the most brittle material 95A are not provided. The reason is that specimens with this type of sensor were not subjected to a second campaign of cyclic loading due to detected damage in the contact area after implementation, as discussed in section 4.3.3.

After 200 cycles of flexural 3PB loading, the specimens were subjected to impact loading according to the configuration shown in Fig. 59. Supporting our hypothesis and in line with previous experimental investigations published in [A6], sensors made of material with lower ultimate elongation are more sensitive to impact loading. Therefore, the relative change in the measured electrical resistance of the integrated sensor after impact is expected to be greater for sensors made of more brittle carbon fiber tow.

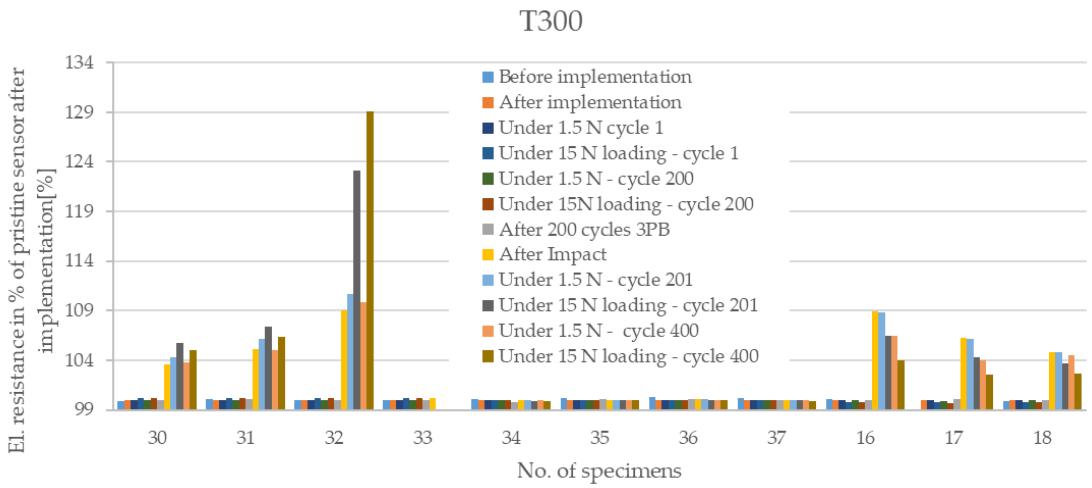

Fig. 63 Electrical resistance of integrated sensors as a percentage of the value of a pristine sensor after implementation - results for specimens with CF sensors made of material T300

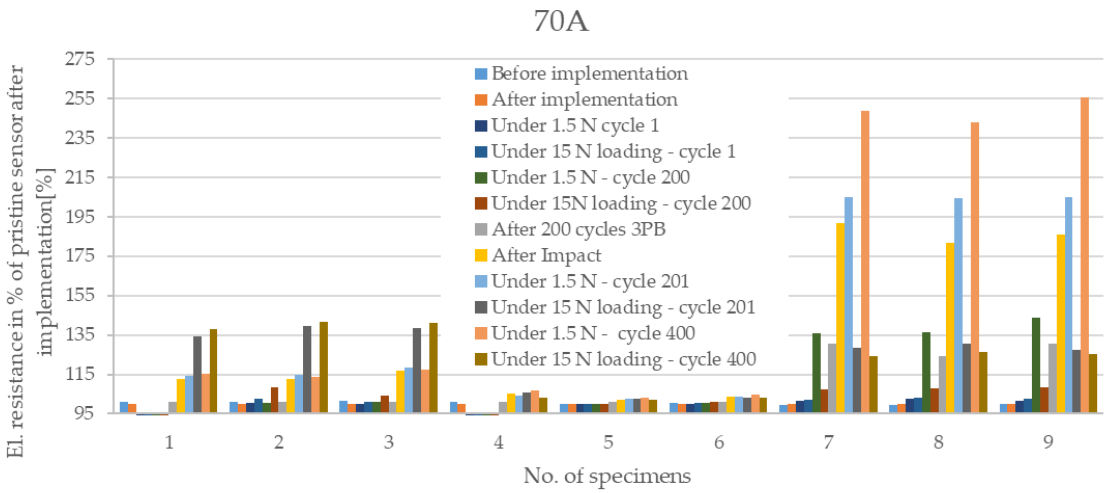

Fig. 64 Electrical resistance of integrated sensors as a percentage of the value of a pristine sensor after implementation - results for specimens with CF sensors made of material 70A.

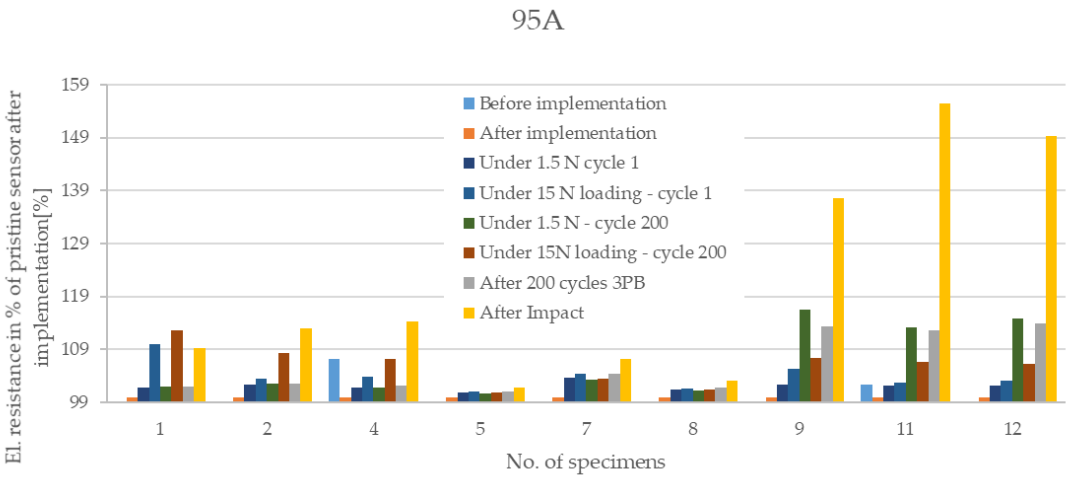

Fig. 65 Electrical resistance of integrated sensors as a percentage of the value of a pristine sensor after implementation - results for specimens with CF sensors made of material 95A.

This hypothesis was not confirmed for all specimen types. The largest change in electrical resistance was noted for material 70A. This difference might be attributed to the fact that sensors made of 95A had damaged electrical contacts already after implementation.

Based on the measured data, positioning the CF sensor on the side opposite to the impact seems more appropriate. This was observed in specimens T300-16, T300-17, T300-18; 70A-7, 70A-8, 70A-9; 95A-9, 95A-11, 95A-12, where the change in measured electrical resistance was the most significant (refer to Fig. 63, Fig. 64 and Fig. 65).

Peak-to-peak values after impact for sensors made of the most brittle material, 95A, are not provided, because these specimens were not subjected to the second campaign of cyclic loading. Non-destructive thermographic testing (detailed in section 4.3.3) revealed that the electrical connections of the 95A material sensors were damaged.

The detection of impact damage using sensors made from different types of carbon fiber tows was demonstrated on rectangular coupons made of a prepreg glass fabric composite. The study explored various sensor positioning within the lay-up. Detailed conclusions from this investigation can be found in section 4.3.5.

Section 4.3.4 details the response of CF sensors to temperature variations.

4.3.3 Active thermography and CF sensors for impact damage detection

The active thermographic inspection of CF sensors was proposed for two main purposes:

- To inspect CF sensors after sample production, as they might be damaged during integration, curing, or sample handling.
- To visualize sensor damage after impact, which can be practically used in practical applications to locate damage along the length of the CF fiber.

During the second experimental campaign, a FLIR A325sc infrared camera was used to perform an active thermographic inspection of all specimens for impact detection using the CF sensor. The CF sensor is supplied with electric current, and the thermographic camera displays a temperature field that indicates where local heating is occurring. As previously mentioned, damage to the CF sensor results in increased electrical resistance of the CF sensor, leading to localized heating.

All specimens were inspected after manufacturing and again following drop-weight impact testing. Several specimens also underwent additional inspection after 200 cycles of flexural loading, before the impact test.

The inspections focused on the mold side of the specimen, which is both the impacted side and the outer surface during the cyclic flexural test. In practical applications, the mold side is typically accessible. During the thermographic inspection, an electric current was applied to the integrated CF sensors for 10 minutes using a direct current source (Agilent E3631A). The type T300 CF sensors were subjected to an electric current of 0.09 A, while 0.3 A was used for CF sensor type 95A, and 0.24 A for type 70A CF sensors.

4.3.3.1 Active thermographic inspection - results and discussion

An active thermographic inspection of the specimens before loading revealed damage to the electrical contacts of the sensors made of pitch carbon fiber tow 95A. The temperature profile along the sensor with damaged contact areas is shown Fig. 66. In Fig. 67 the temperature profile of a sensor without any pre-damage is depicted. Six out of nine specimens with implemented sensors made of material 95A were damaged during manufacturing or during implementation. Two specimens were indeterminate regarding sensor damage, and no data were provided for one specimen. This demonstrates the sensitivity of the structural integration of carbon fiber sensor made of brittle ex-pitch filaments.

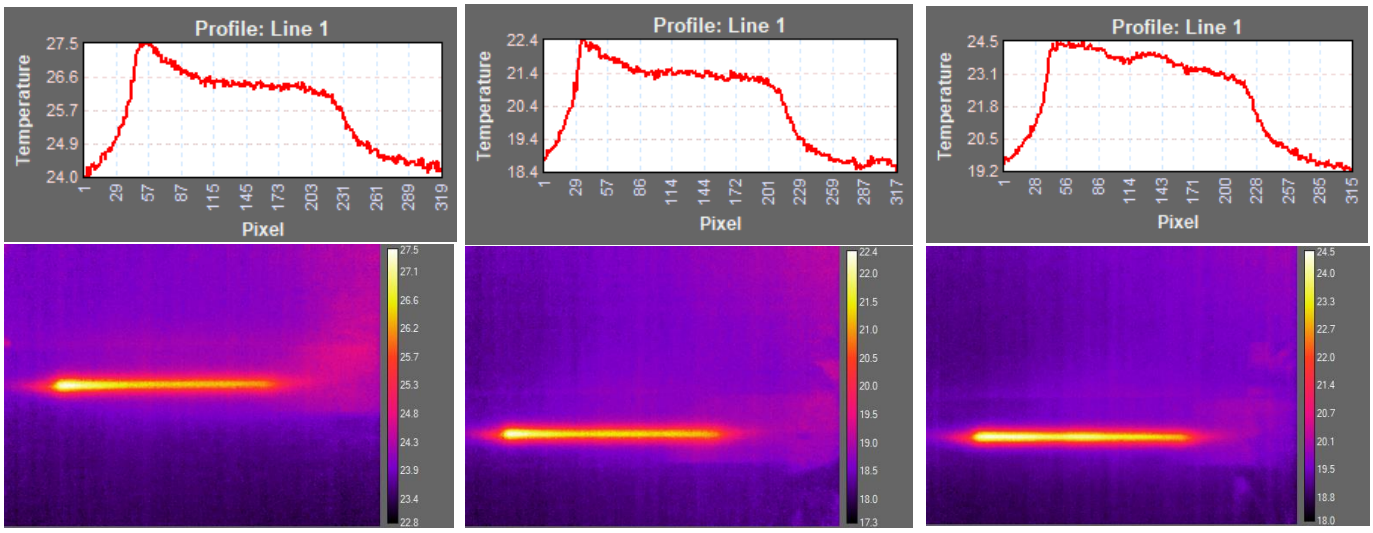

(a) **(b)** **(c)**

Fig. 66 Active thermographic inspection: (a) 95A-11 before loading, (b) 95A-11 after 200 cycles of cyclic flexural loading, (c) 95A-11 after impact.

Sensors made of pitch 70A carbon fiber tow and sensors made of PAN T300 carbon fiber tow showed no signs of pre-damage before loading.

Specimens T300-16, T300-17, 95A-11, 95A-12, 70A-8 and 70A-7 were investigated after 200 cycles of flexural loading and before impact loading. No signs of damage caused by flexural cyclic loading were observed for specimens with a T300 sensor. However, damage to the electrical contacts was detected for specimens 95A-11, 95A-12. The temperature profile along the sensor changed slightly after cyclic loading in the case of sensors 70A-7 and 70A-8.

The specimens were subjected to thermographic inspection once again after impact loading. The results of this observation are given in Table 8. According to our measurements, T300 has the greatest potential for use as a heating element for active thermography. It was possible to detect impact damage both when the sensor was located on the impacted side and when it was on the opposite side of the specimen.

Table 8 Results of a thermographic inspection after impact loading.

CF sensor between layers	T300		95A		70A	
1 - 2	30	IV	1	IV	1	DEC
	31	IV	2	IV	2	CH
	32	IV	4	ND	3	DEC, CH
	33	INV				
4 - 5	34	ND	5	INV	4	IV
	35	ND	7	INV	5	INV
	36	INV	8	INV	6	INV
	37	INV				
7 - 8	16	IV	9	INV	7	ND
	17	IV	11	IV	8	IV, DEC
	18	IV	12	INV	9	DEC

[1] data description: IV – impact visible, INV – impact not visible, ND – no data, DEC – damage of electrical contacts after impact, CH – change of temperature profile along CF sensor.

Observations with CF sensors made of material 95A revealed that impact damage can be detected even by a sensor with damaged electrical contacts. For specimens with an integrated CF sensor made of material 70A, some showed signs of damage to the electrical contacts after both cyclic loading and impact loading. However, based on the active thermography data, it is not possible to conclusively determine whether the damage was caused by the impact loading or the cyclic loading.

Several conclusions have been drawn regarding active thermographic inspection in combination with CF as heating element, see section 4.3.5.

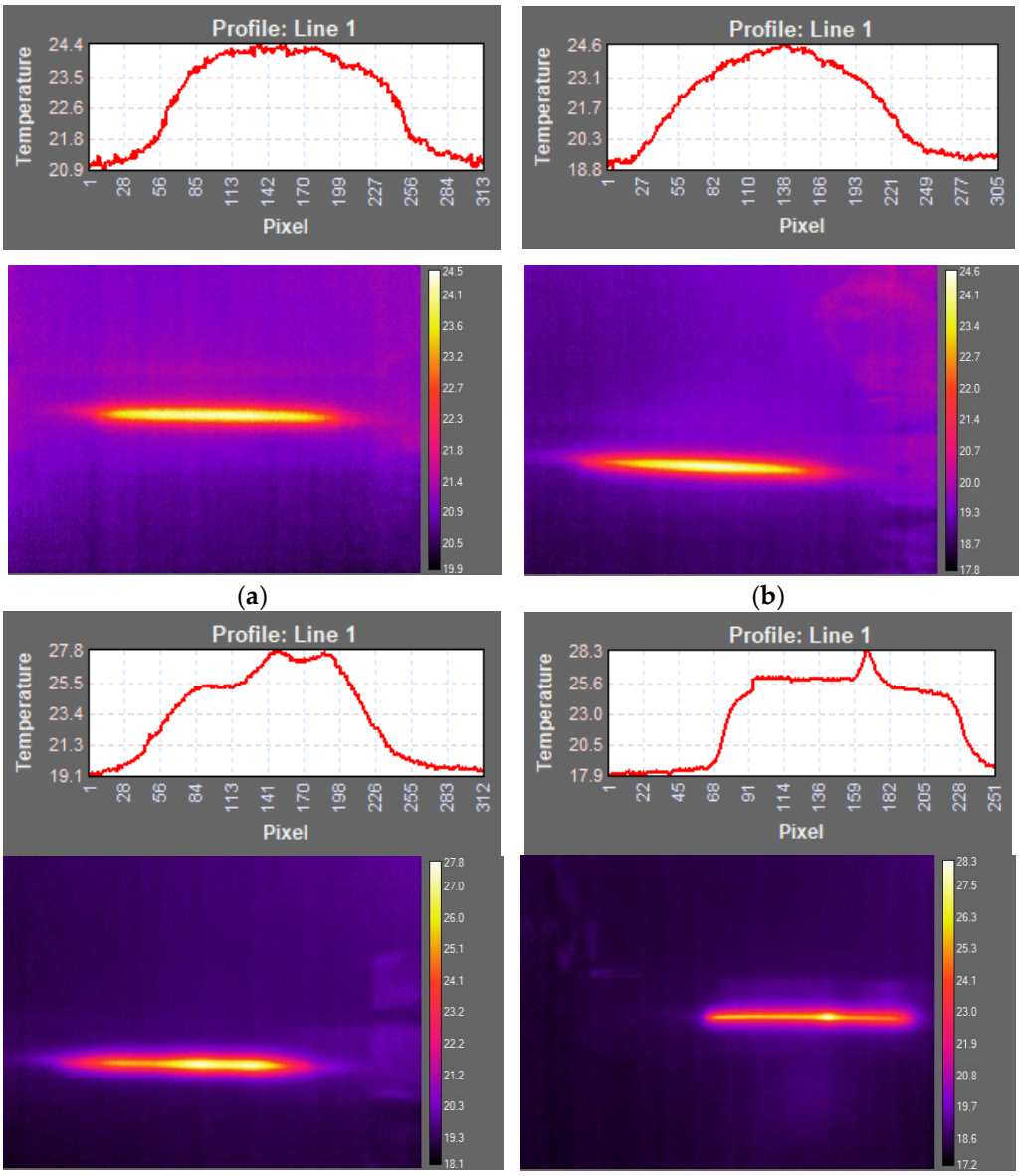

Fig. 67 Thermographic inspection: (a) 70A-8 before loading, (b) 70A-8 after 200 cycles of 3PB, (c) 70A-8 after impact, (d) T300-30 after impact.

4.3.4 Influence of temperature on measured signal from CF sensors

For practical applications of CF sensors, it is necessary to consider the temperature dependency of the measured electrical resistance. This temperature dependency can be either compensated during measurement by connecting the sensors in a half-bridge configuration within a Wheatstone bridge, or through numerical compensation. The temperature coefficients of the investigated CF sensors made of various materials were determined. These coefficients can be further used for numerical compensation of the influence of temperature changes during measurements using such CF sensors.

4.3.4.1 Temperature Loading - experiment description

Several specimens with integrated CF sensors were manufactured for the experimental study on the influence of temperature on the electrical resistance of CF sensors made of different materials (see Fig. 14). The CF sensors were embedded between the same layers for all specimens (between the first and the second layer). The HBM QuantumX MX 1615 measuring amplifier was used at a 50 Hz sampling rate. The CF sensor probes were connected by a 2-wire resistance measuring circuit. In addition, two PT100 temperature sensors (Heraeus Nexensos M222, tolerance: F 0.1) were connected by a 4-wire resistance measurement (see Fig. 68). One PT-100 temperature sensor was placed in such a way that the flowing air could pass freely. The other sensor was attached to the surface of the specimen to measure the temperature near the inertia of the specimen. The temperature of the oven (Zwick temperature chamber EC75A) was incremented with 20 °C temperature steps with a hold time of 30 min to a maximum temperature of 120 °C. After the maximum temperature was reached, the door of the oven was opened for a cool down period of 60 min.

4.3.4.2 Temperature Loading – results and discussion

Fig. 68 presents the raw measured values. In Fig. 68 (a) the measured temperatures show the behavior of the temperature control of the oven. After a new temperature value has been set, the oven needs up to 15 minutes to reach a constant temperature level. The differences between the PT100 sensors just after a new temperature has been set due to the air flow inside the oven and the different location of the temperature sensor. At lower temperatures the two PT100 sensors show a difference in the measured values of about 0.02 °C, which increases to about 1.97 °C or 1.64 % at 120 °C. For further evaluation, the data of the sensor attached to the surface of the specimen was used.

Fig. 68 (b) presents the measured values of the T300 ex-PAN samples. The curve looks like an upside-down version of the curves in Fig. 68 (a) since the CF sensors reduce their resistance with increasing temperatures. An offset of the resistance values of about 0.02 Ω can be seen. The curves in Fig. 68 (d) of the 70A ex-pitch CF sensor show quite similar behavior to the curves in Fig. 68 (a). The measured values are smaller since the ex-pitch CF sensors have a much lower resistance of about 3.1 Ω in comparison with the 27.3 Ω resistance of the T300 CF sensor.

An increase in resistance with an increase in temperature can be observed for the 95A CF sensor in Figure 4 (c). This effect is more pronounced with higher resistance values before the temperature measurement and can probably be attributed to pre-damage at the electrical contact point during manufacturing (see section 3.3). No further examination was made of 95A-CF sensor.

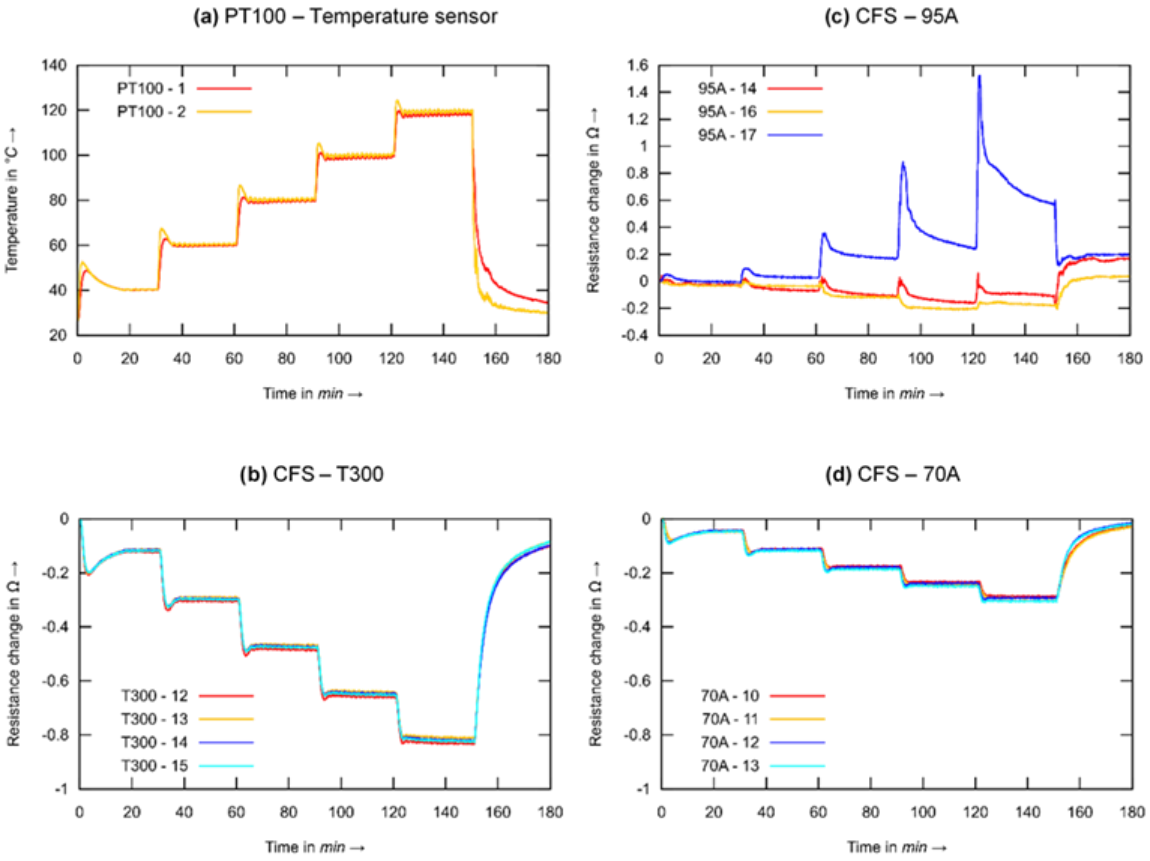

Fig. 68 Temperature dependence of the measured electrical resistance of the investigated types of CF sensors

The T300 samples show a resistance drop of 3 % (0.8 Ω) while the 70A samples show a drop of 8.5 % (0.3 Ω) at a temperature level of 120 °C. This means that the effect of the temperature on the fiber resistance is greater for 70A than for T300-CF sensor.

For practical applications, it is necessary to calculate the linear fit model from the measured data. For this purpose, the measured values were taken between 15 minutes after setting a new temperature and the next increase in temperature. For each temperature level, the mean values of the measured temperature were calculated, and were used for the linear fit model (see Fig. 69).

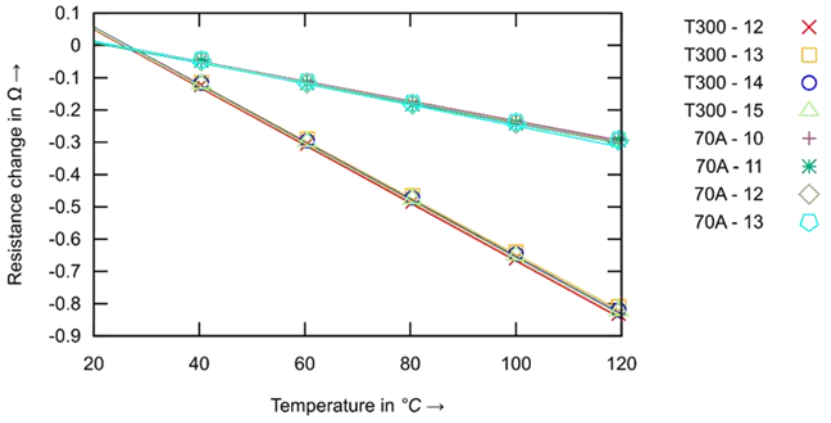

Fig. 69 A linear fit function for the measured mean values of the CF sensor

A linear fit model was chosen, seen Equation 1, with the slope of the linear fit m, the resistance at 0 °C of the CF sensor $R_{0°C}$, and the measured resistance of the CF sensor R_T.

$$T_{CF\ sensor} = (R_T - R_{0°C})/m. \quad (16)$$

Table 9 The calculated values of the linear fit, and also the R2 and RMSE values.

Specimen nos.	m [Ω/°C]	$R_{0°C}$ [Ω]	R^2	RMSE [°C]
T300-12	$-9.10 \cdot 10^{-3}$	27.79	$1 - 3{,}368 \cdot 10^{-5}$	0.206
T300-13	$-8.93 \cdot 10^{-3}$	27.76	$1 - 5{,}498 \cdot 10^{-6}$	0.083
T300-14	$-9.02 \cdot 10^{-3}$	27.91	$1 - 1{,}286 \cdot 10^{-6}$	0.128
T300-15	$-9.04 \cdot 10^{-3}$	27.90	$1 - 1{,}123 \cdot 10^{-6}$	0.119
T300 mean	$-9.02 \cdot 10^{-3}$	27.84		
70A-10	$-3.12 \cdot 10^{-3}$	3.49	0.9985	1.365
70A-11	$-3.17 \cdot 10^{-3}$	3.54	0.9978	1.682
70A-12	$-3.19 \cdot 10^{-3}$	3.53	0.9986	1.309
70A-13	$-3.32 \cdot 10^{-3}$	3.48	0.9983	1.462
70A mean	$-3.20 \cdot 10^{-3}$	3.51		

The calculated coefficients of the linear model, and also the R^2 and root mean squared error (RMSE) values, are summarized in Table 9 The high R2 values show, that the CF sensor signals show good linear behavior. The RMSE values show the magnitude of the error between the liner fit function and the measured mean values of the CF sensor samples.

4.3.5 Conclusions drawn from the second experimental campaign

4.3.5.1 Mechanical loading and impact loading –partial conclusions

- According to our investigation, it is better to position CF sensors on the side opposite the impact, rather than on the impacted side. Placing a CF sensor on the opposite side increases the probability of detecting an impact. This is probably caused by the nature of impact damage in composite layups, where greater damage tends to occur closer to the surface opposite the impacted side.
- The PAN type of fiber tow used for integrated CF sensor showed stable behavior under cyclic loading.
- Sensors made of pitch carbon fiber tows were more sensitive to cyclic loading.
- Manufacturing CF sensors using extremely brittle pitch carbon fiber tows (Pitch 95A) is not recommended. Ensuring contact quality is challenging, and difficulties arise in sensor manufacturing and handling, especially during integration into structures.
- The influence of mechanical loading on the change in electrical resistance of integrated PAN T300 and Pitch 70A CF sensors is minimal compared to the effects of barely visible impact damage. It has been shown that the change in electrical resistance due to mechanical loading for all types of CF sensors.
- CF sensors made of PAN T300 and 70A carbon fiber tow have proven to be highly effective and suitable for detecting impact damage.

4.3.5.2 Active thermographic inspection – partial conclusions

- Active thermography proves to be a successful method for inspection of CF sensors after manufacturing. It can reveal damage in the area of electrical contacts.
- It was demonstrated that active thermography, in combination with a CF sensor, can effectively visualize barely visible impact damage (BVID) in components.
- In practical applications, changes in measured electrical resistance can serve as an indicator of impact damage to the structure. Subsequently, active thermographic inspection combined with the CF sensor as a heating element, could be employed to localize the impact damage across a larger area.

4.3.5.3 Temperature Loading –partial conclusions

- The temperature coefficients for CF sensors made of T300 and 70A materials were determined through experiments on sensors integrated into GFRP composites.

4.4 Third experimental campaign - Response of CF sensors to cyclic loading, influence of the length of the CF sensor to the impact damage detection, correlation between sensor data and mechanical response of the specimen to the impact damage

The third experimental campaign was designed to investigate the following:

I. The potential influence of sensor length on the ability of a CF sensor to detect impact damage.
II. The impact of a higher number of cycles on the response of the CF sensor.
III. The possibility of establishing a correlation between measured signal from CF sensor after impact and mechanical response of the structure to the damage.

4.4.1 Experiments and evaluation methods

4.4.1.1 Specimen description

Specimens were manufactured using autoclave technology with the same lay-up and process. Let us recall here that the sample consisted of a total of 8 layers. The only variation was the size of the specimens: they were cut into strips measuring 180 mm × 23 mm and had a thickness of 1.3 mm. A total of 10 specimens were manufactured. The CF sensors were integrated between the seventh and eighth layers of the composite lay-up during manufacturing. The same method for preparation of CF sensors was used as in previous experimental campaigns. The material used for the CF sensors was Toray T300 1000-50A, with a sensor length of 140 mm, which is double that used the length as in the second experimental campaign.

4.4.1.2 Experiment description

All specimens were exposed to a four-point bending (4PB) test, with a loading span of 50 mm and a support span of 100 mm, using the same testing machine as in the second campaign.

The specimens were subjected to harmonic loading with a force ranging from 3 to 30 N (load ratio = 0.1) at a frequency of 0.1 Hz. The maximum loading force, established during the preliminary test, corresponded to a measured longitudinal strain of 3,000 μm/m. During this test, a strain gauge was installed on the middle part of the specimen's outer surface.

Three specimens underwent 1,000 cycles of loading, followed by a 2 J impact. These specimens were then exposed to another 1,000 cycles of loading after the impact loading.

Fig. 70 Specimens with strain gages and optical fibers for distributed sensing installed on the top surface (mold side of the specimen).

Fig. 71 The specimen with CF sensor integrated between 7th and 8th composite layer.

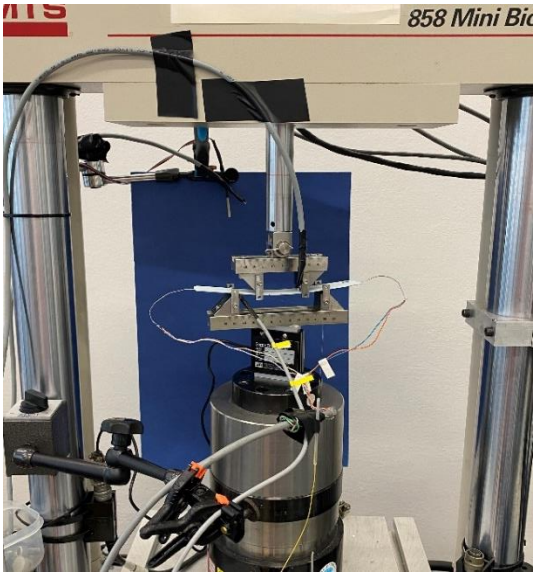

Fig. 72 Configuration of 4PB cyclic mechanical test

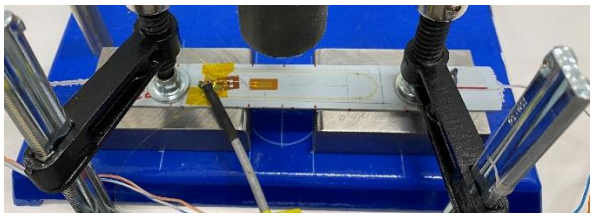

Fig. 73 Configuration of impact damage test

4.4.2 Part I - Influence of the length of the sensor to impact damage detection

Comparison of the electrical resistance values of the CF sensor after implementation and after impact was conducted. The results for two sensor groups with lengths of 70 mm and 140 mm, are presented in Fig. 74 and Fig. 75. The absolute values of electrical resistance change were found to be the same, indicating that the relative resistive change is smaller for the longer sensors.

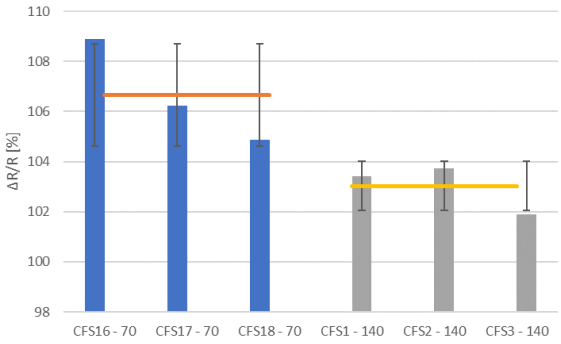

Fig. 74 Relative electrical resistance change after BVID impact of 2J of sensors with length of 70 mm and 140 mm

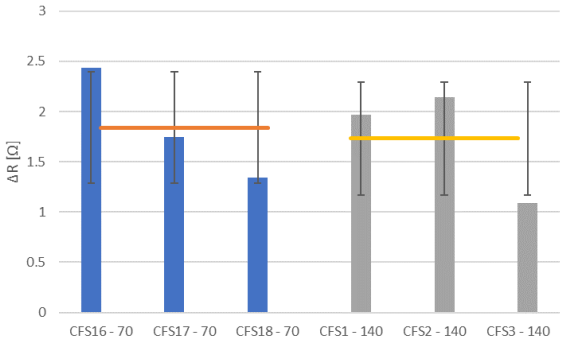

Fig. 75 Absolute values of electrical resistance change of integrated CF sensor after BVID impact of 2J

The relative change in electrical resistance caused by the 2J impact, using the same configuration, was 107% for CF sensors with a length of 70 mm, and 103% for those with a length of 140 mm. The measured electrical resistance of the sensors increased after the impact loading in average by 1.84 Ω for the sensors with the length of 70 mm and by the 1,73 Ω for the sensors with the length of 140 mm.

It is possible to record the signal from the CF sensor during impact loading using a strain gauge amplifier. Fig. 76 shows recorded electrical resistance of the integrated CF sensor during impact loading, alongside the measured signal from a strain gauge (SG) installed on the specimen's surface. The electrical resistance change of the integrated sensors is also documented in Table 10. It can be observed that the measured electrical resistance change of the integrated CF sensor differs from the values shown in graph in Fig. 76. This is caused by the additional loading of the sensors caused by clamping.

Table 10 Overview of measured values after impact

	R	After impact including load caused by the mass of the impactor			After impact without any additional load	
	[Ω]	$\Delta R/R$ [%]	ΔR [Ω]	$\Delta\varepsilon$ [µm/m]	$\Delta R/R$ [%]	ΔR [Ω]
CFS1-140 mm	57.3	4.2	2.4	-166	3.4	2.0
CFS2-140 mm	57.2	5.5	3.1	89	3.7	2.1
CFS3-140 mm	57.4	2.5	1.4	176	1.9	1.1
Average	57.3		2.3			1.7
Std. Dev.	0.1		0.9			0.6

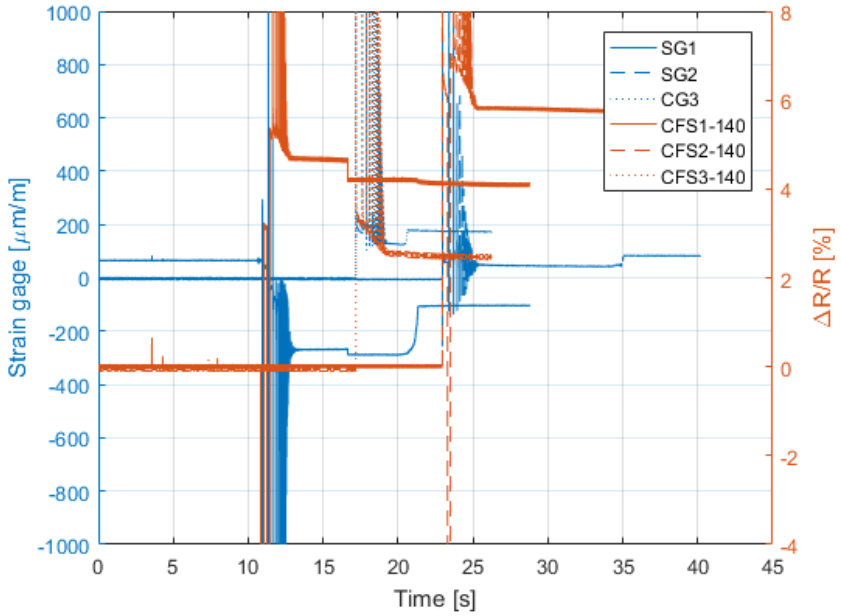

Fig. 76 Measured signal from strain gages installed on the impacted surface and from integrated CF sensors during impact loading (including removal of impactor)

Additionally, the effect of cyclic loading on damaged CF sensors after Barely Visible Impact Damage (BVID) was also investigated. The results of this investigation are summarized in the following section.

4.4.3 Part II - Influence of the number of cycles to the response of CF sensor

The influence of cyclic loading to the sensor's behavior was evaluated in the same manner as in the second experimental campaign, but the amount of loading cycles was extended from 200 to 1,000 cycles. In the second campaign, sensors underwent 200 cycles of a three-point bending (3PB) test, subjected to a loading force of 1.5 – 15 N (load ratio = 0.1) at a frequency of 0.1 Hz. The sensors were integrated at various positions in the lay-up.

In this third campaign, sensors were exclusively integrated between the 7th and 8th layers of the composite lay-up. This position demonstrated the largest change in measured electrical resistance after impact loading (refer to section 4.3.2) among the investigated scenarios. Additionally, it is subjected to compressive stress during the four-point bending (4PB) cyclic test. Further details regarding the configuration of the test can be found in section 4.4.1.2.

Switching the loading configuration from 3PB to 4PB resulted in a larger area of constant deformation under maximal loading. The loading was set such that the maximal deformation matched that of the previous 3PB test, which was 3,000 μm/m.

The stability of the sensor output during 4PB test is compared using the relative electrical resistive range ΔR_{REL} according to equation (15).

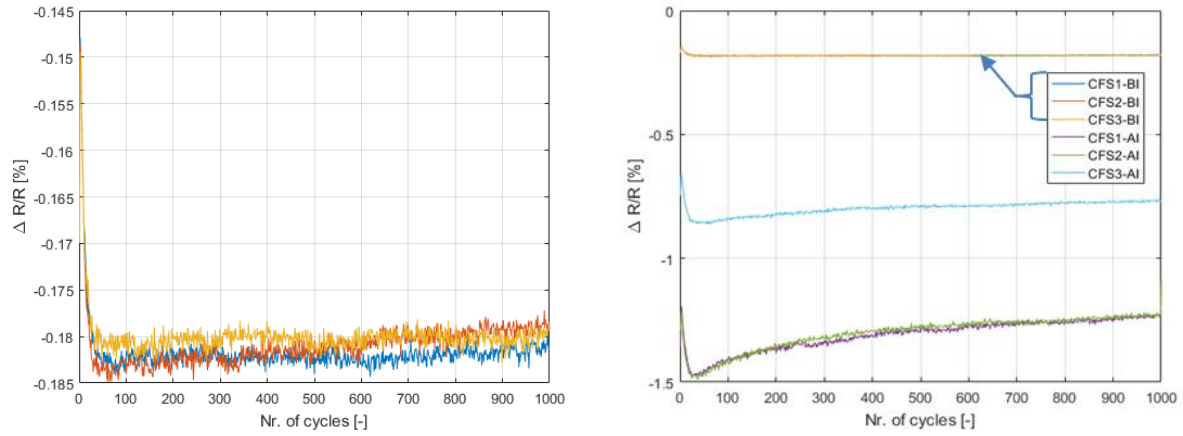

(a) (b)

Fig. 77 (a) Relative electrical resistance of the CF sensors during cyclic test before impact for specimens CFS1, CFS2 and CFS3; (b) Relative electrical resistance of the CF sensors during cyclic test before impact (BI) loading and after impact loading (AI).

4.4.4 Part III - Correlation between sensor response and structure response to the impact

Given that CF sensors can be used to detect impact damage to structures, it was investigated whether it is possible, based on the measured change in electrical resistance of the integrated CF sensor, to predict the amount of damage after impact and the resulting structure's response to mechanical loading.

Let us consider a beam of a manipulator with a working head drive. Different working heads with different masses are moving within the beam. We must consider the variable loading of the beam. During the operation of the manipulator, a collision may occur. We can assume decrease of the maximum loading capacity of the beam due to damage. Detecting such collisions and predicting the residual strength of the structure would be useful. We have established our specimen to be such a beam. We wanted to show a correlation between damage size and the measured response of the CF sensor. Moreover, we aimed to measure the changes in the response of the sensor to the loading at different levels of impact.

4.4.4.1 Details about experimental campaign

Several specimens were exposed to different sizes of impact and afterwards loaded to the maximal bending moment. It was investigated whether there is a correlation between mechanical response and electrical resistance change measured through the integrated sensors. Based on preliminary tests, three sizes of impact were chosen. The same configuration of impact loading as in previous experiments was used, as depicted in Fig. 59 and Fig. 73.

The intention was not to create damage that could be easily revealed by the naked eye. The same specimens previously used for cyclic tests, which underwent impact of 2 J, were used, see Fig. 78. There was no visible sign of impact damage on the impacted side. It was revealed that an impact of 4 J causes a crack of the specimen (Fig. 80), so another three specimens were impacted by an energy of 3 J, as shown Fig. 79.

Subsequently, the specimens were subjected to 4PB loading. Initially, the plan was to load the specimens until final rupture, but the specimens were too flexible.

Despite the loading span was set to 20 mm and the support span length to 70 mm to achieve maximum bending moment, only the specimen impacted by 4 J underwent final rupture. Table 11 provides an overview of the impacted specimens.

Table 11 Overview of specimens

0 J	2 J	3 J	4 J
T300-140-7	T300-140-1	T300-140-5	T300-140-4
T300-140-8	T300-140-2	T300-140-6	
T300-140-9	T300-140-3	T300-140-10	

The configuration of the 4PB test was chosen in such a way that the loading force in both types of 4PB tests (loading span/support span for static test 20 mm/70 mm and for cyclic test 50 mm/100 mm) corresponded to the same bending moments and so to the same strain. We set the loading limits for cyclic tests so that the maximum strain equals to 3,000 μm/m. This value also corresponds to a loading force of 30 N and a displacement of 2.65 mm, as seen in Fig. 82. As mentioned in the previous chapter, this strain level corresponds to a maximal loading level in many applications to prevent intralaminar matrix cracks.

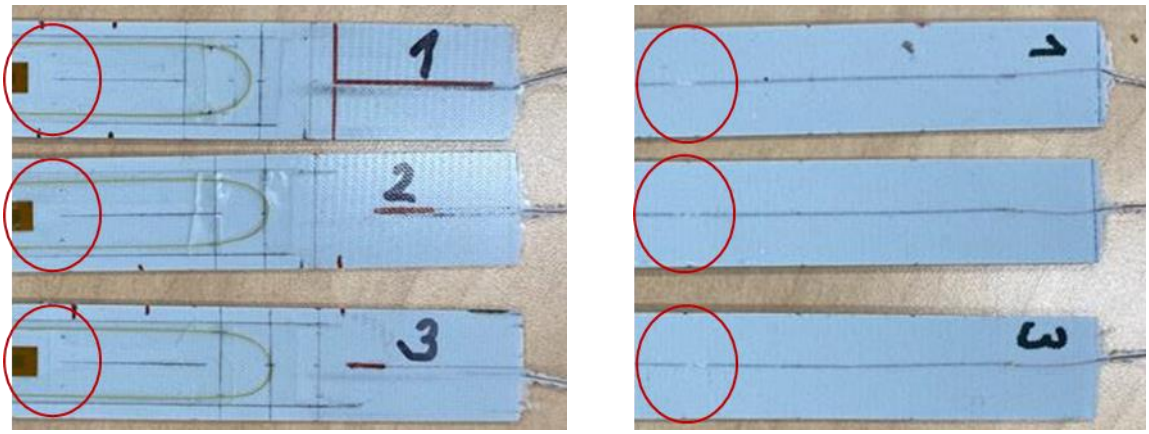

Fig. 78 Specimen CF sensor -140-1, CF sensor-140-2, CF sensor-140-3 after 2J impact, impacted side (mold side of the specimen) on the left, bottom side of the specimen on the right side. The red circle indicates the impacted area.

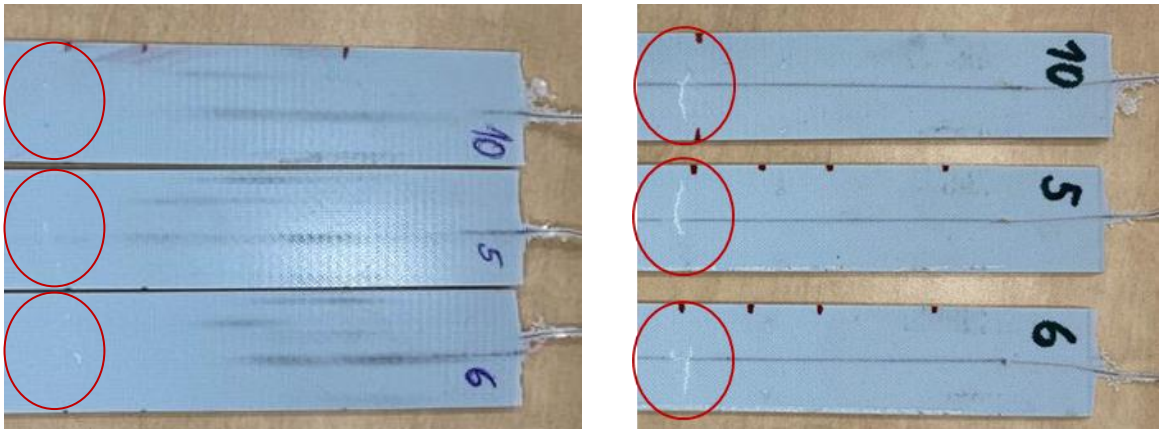

Fig. 79 Specimen CF sensor -140-5, CF sensor-140-6, CF sensor -140-10 after 3J impact, impacted side (mold side of the specimen) on the left, bottom side of the specimen on the right side. The red circle indicates the impacted area.

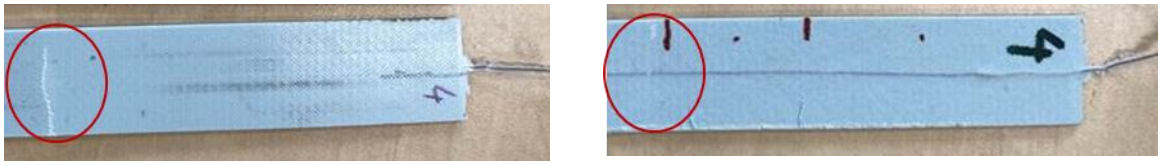

Fig. 80 Specimen CF sensor -140-4 after 4J impact, impacted side (mold side of the specimen) on the left, bottom side of the specimen on the right side. The red circle indicates the impacted area.

4.4.4.2 Results and discussion

A record of the force and displacement measurement data is shown in the figures Fig. 81 and Fig. 82. The plot in Fig. 82 reveals, that the specimen with CF sensor 140-4, which was impacted by 4 J show significantly lower stiffness compared to the rest of the specimens. The decrease in stiffness is easily observed in Fig. 82, where the maximum loading force on the graph corresponds to the maximum loading force during cyclic loading (30 N). This decrease in stiffness was caused probably by significant damage of the specimen. We can also observe that the rest of the impacted specimens displayed lower stiffness than the pristine specimens. The greater is the applied load, the larger are the differences in induced displacement.

Fig. 83 shows data of the change in measured electrical resistance for each specimen, which was calculated according to the following formula.

$$\Delta R_{(x\ mm)} = R_{at\ the\ beginning\ of\ loading\ (deflection = 0\ mm)} - R_{(deflection = x\ mm)}. \quad (17)$$

According to the 3D graph of dependency of ΔR, deflection, and force in Fig. 83, the greater is the deflection, the more pronounced is the effect of stiffness loss caused by impact damage. The influence of increasing impact energy, when compared between test specimens impacted by 2 J and 3 J, is relatively small. However, the effect of increasing impact energy between 3 J and 4 J is significant. This is probably caused by the fact, that different damage mechanisms are present in the specimen impacted by 4 J, see Fig. 77.

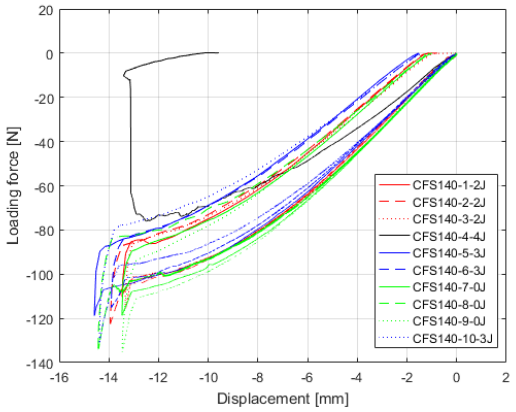

Fig. 81 Force displacement dependency during 4PB of pristine and impacted specimens

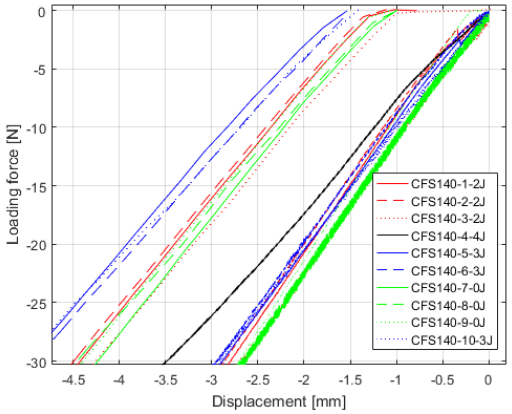

Fig. 82 Detail of force displacement dependency during 4PB of pristine and impacted specimens

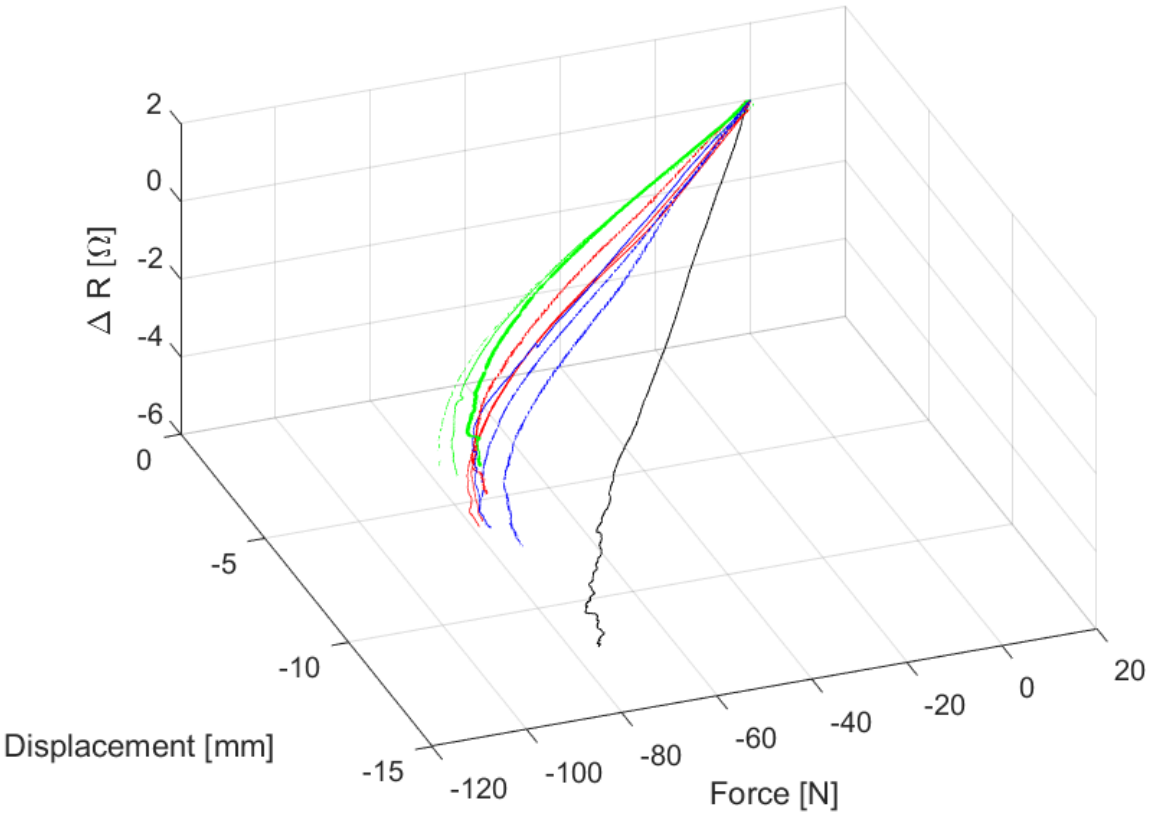

Fig. 83 3D Force-displacement-ΔR from integrated CF sensor during 4PB test

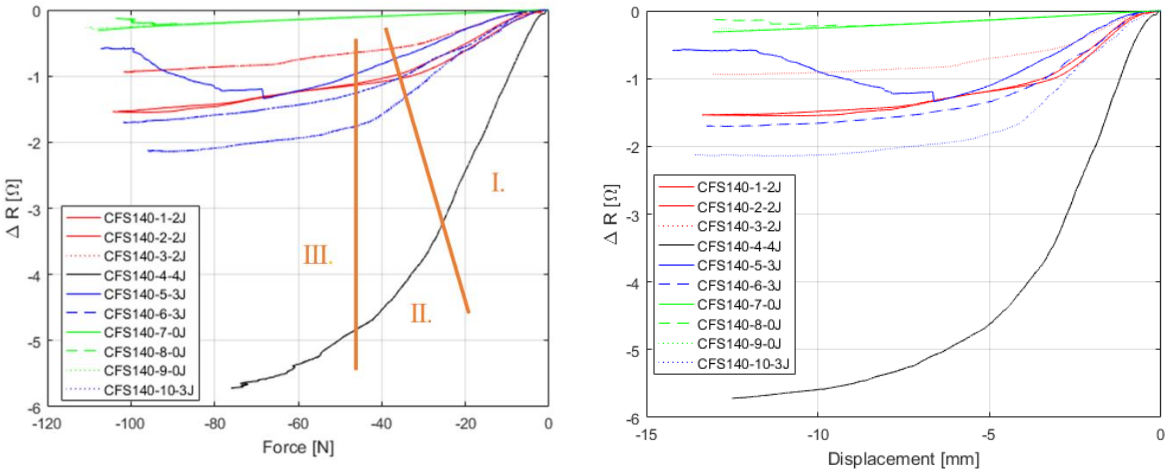

Fig. 84 Change of electrical resistance of the integrated CF sensor depending on applied force during 4PB (on the left), change of electrical resistance of the integrated CF sensor depending on applied displacement during 4PB (on the right).

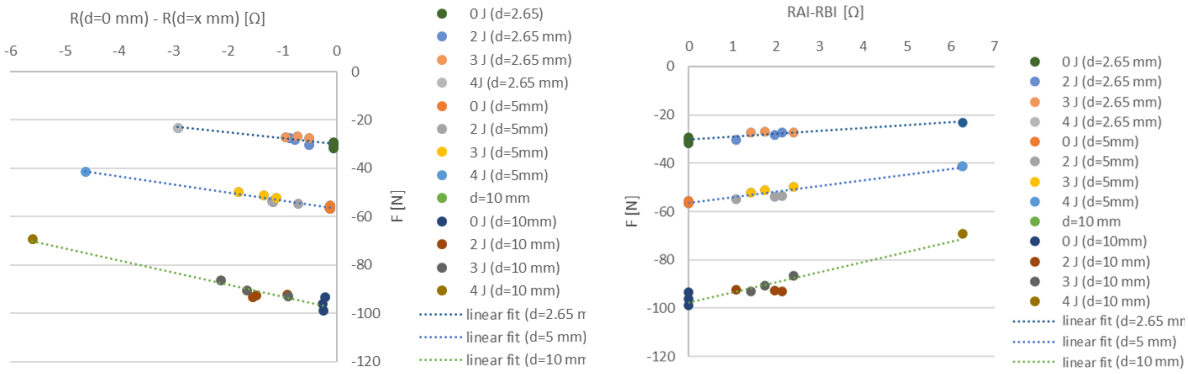

Fig. 85 Graph of force – change of measured electrical resistance during loading (for different impact energies and displacements) (on the left side), graph of force – change of measured electrical resistance AI (after impact) and BI (before impact) (for different impact energies and displacements) (on the right side).

It can be seen in Fig. 83 and Fig. 84, that for the investigated specimens it is not completely possible to distinguish between 2J and 3J impacts. However, when we compare measured data of all specimens (no impact, 2J, 3J and 4J impact) a correlation can be seen between lower stiffness (less energy required for the same size of deflection) and a larger change in the measured electrical resistance of the CF sensor caused by the impact. The higher the impact energy, the lower the force needed for the same displacement of the sensor, and the greater the change in measured electrical resistance during loading.

In Fig. 83 and Fig. 84 it is evident that the relationship between the depicted quantities is not consistent across the entire load range. We can distinguish areal s of two different slopes in the loading curve, sections I and III. The section II. can be called a transition area.

The graphs in Fig. 85 demonstrate that it is possible to predict the decrease in force needed for a defined displacement of the specimen (structure) from the electrical resistance change measured during loading, as well as from the electrical resistance change measured before and after impact on the unloaded structure.

The measured data can serve as a background for predicting the behavior of a structure after impact. Although the specimens were not loaded to final fracture, it can be deduced, that the force needed for final fracture of the construction correlates with the size of the impact and the magnitude of the measured

change in electrical resistance of the integrated CF sensors. The CF sensors could be utilized to indicate the necessity of reducing the maximum operational loading for impacted structures.

A specific loading state could be proposed for inspection purposes. For example, loading to a defined deflection can be established. It has been shown that the sensor response does not change considerably depending on cyclic loading. Therefore, limits can be set for the electrical resistance change of the sensor, indicating whether the structure was not impacted, was impacted within a defined range, or was impacted beyond a defined range.

4.4.5 Conclusions drawn from the third experimental campaign

4.4.5.1 Influence of the length of the sensor - partial conclusions

- The change in measured electrical resistance after impact loading is comparable for CF sensors of the same size but double the length. Using longer sensors for detecting small impact damage is feasible. This could be advantageous, allowing the mapping of impact occurrences over a larger area of the component.

4.4.5.2 Influence of the number of cycles - partial conclusions

- The response of the CF sensor to cyclic mechanical loading is stable. The measured ΔR_{REL} was similar for all three investigated sensors.
- The sensor's response to impact loading is evident during subsequent loading. The measured ΔR_{REL} is four to seven times larger than the sensor's response prior to impact loading.
- Based on the presented measurements, it is possible to reveal impact damage on the structure loaded by defined cycles by measuring during shutdowns. A special loading scenario can be established (in this study we used loading by 4PB from 3 to 30 N) and the response of the integrated sensor can be measured during these shutdowns. It is not necessary to consider the influence of temperature.

4.4.5.3 Correlation between sensor and structure response - partial conclusions:

- A correlation was found between the measured change in electrical resistance of the integrated CF sensors and the decrease in stiffness of the specimens caused by impact loading.
- The decrease in stiffness of the specimen due to impact can be predicted from the measured change in electrical resistance of the integrated sensors during loading.
- The decrease in stiffness of the specimen due to impact can be predicted from the measured change in electrical resistance of the integrated sensors before and after the impact.

5 Damage detection – delamination

In this chapter, we will discuss the possibility of delamination detection and the influences that could affect the measurement and determination of delamination length. For crack length determination based on electrical resistance measurement and FE simulation, it is essential to define the resistivity of the investigated composite. Two sets of specimens were examined. The first set was prepared from CFRP composite material, and the second one was prepared from carbon fiber reinforced thermoplastic matrix composite (CFRTP). The electrical resistivities of CFRTP composites were not found in existing literature. Initially, the nominal resistivities of each material were determined.

The procedure and findings regarding different measurement configurations are described in sections 5.1 and 5.2, with findings published in [A12]. Section 5.3 details the experimental data from delamination detection, and FE analysis of this detection is described in section 5.3.4. Results from the sensitivity analysis are given is section 5.4., presented results were published in [A7], [A10] and [A11].

5.1 Determination of electrical resistivity of CFRP composite

In section 2.6.3 are described published approaches for electrical resistivity determination. The author has not found any comparison of electrical contact configurations published in the literature. In this section will be presented results of such comparison.

Accurate determination of the electrical resistivities of investigated composite materials is crucial for the numerical simulation of damage detection configurations. Numerical simulations of damage detection scenarios can be used for decision whether the electrical contact configuration is well-designed for detecting specific sizes of damage. They can also be useful in determining how precise a measurement device should be for damage detection. The comparison of numerical investigations and experimental measurements during delamination growth (section 5.4.1) will illustrate the influence of electrical contact configuration on the accuracy of numerical analysis.

Three contact configurations were tested for the determination of in-plane resistivity. The resistance in the through-thickness direction was determined using two contact configurations. The obtained values were then compared and subsequently used for the numerical simulation of delamination specimen tests.

5.1.1 Experimental procedure

For specimen preparation, Hexply AGP 193PW/8552S RC40 composite material was used. The $[45/0]_{4S}$ lay-up was used. After curing, electrical contacts (made of conductive epoxy and thin copper strips) were prepared. The specimens' surfaces were slightly sanded with P120 and P600 sandpaper before being degreased. Electrical contacts were made with a conductive epoxy called CHO-BOND® 584-29 and thin copper strips.

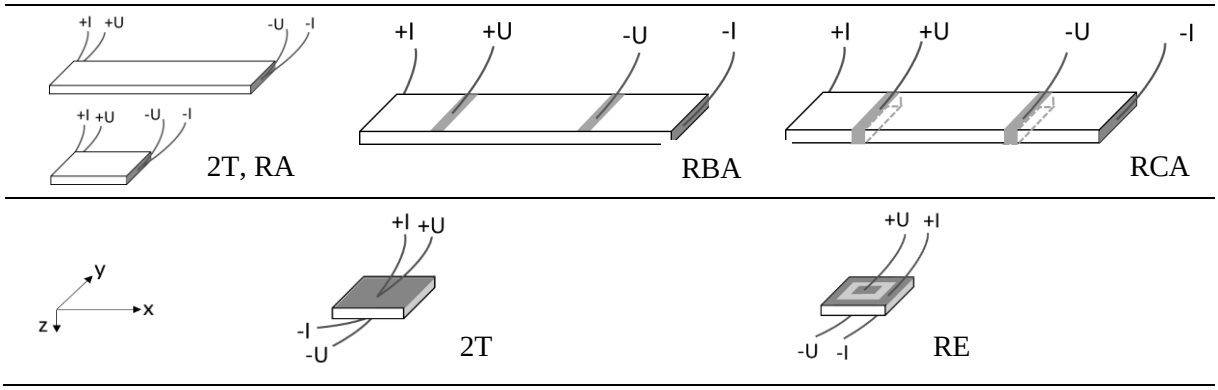

Fig. 86 Configurations of electrical contacts for determination of in-plane and through-thickness resistivity

5.1.2 Measurement procedure

The configurations of the electrical contacts used for electrical resistance measurement are shown in the Fig. 86. Detail description of different electrical contact configurations was already given in section 2.6.3. The measurement was performed using the HP E3631A current source and two Agilent 34461A multimeters. The series comparison measurement method was performed.

5.1.2.1 In-plane resistivity

There were several contact configurations used in literature. Here are compared methods based on two wire measurements. A configuration here called RA is based on 2T measurement. For neglecting the size of a contact resistance (see Fig. 86), measurement must be performed on several specimens with different length. Compared to RA method, the two-wire (2T) contact configuration assumes that the contact resistance can be neglected.

The most accurate method should be 4-wire (4-terminal, 4T) measurement configuration, when separate terminals for current and voltage measurement are used. Two measurement configurations, which are also used in literature were used. These were configuration RBA – voltage terminals only on top surface of the specimen and RCA – voltage terminals around the specimen surface, see Fig. 86.

5.1.2.2 Through-thickness resistivity

For determination of through thickness resistivity, we used 2T and 4T measurement configurations as depicted in Fig. 86. For each of the two measurement configurations (2T and RE) four specimens with dimensions (15 mm × 15 mm × 1.6 mm) were prepared. The RE electrical configuration was prepared according to Fig. 86. The inner voltage electrodes dimensions were 5 mm × 5 mm. There was distance of 2 mm between the inner voltage and outer current electrodes.

5.1.3 Experimental Results

5.1.3.1 In-plane resistivity.

Six specimens L1 - L6 were prepared for determination of the in-plane resistivity (ρ_x). Because of the lay-up of the material, we assume that the resistivity in the x and y direction (see Fig. 86) is the same. First 2T and RA method was adopted. Results of 2T measurements are given in Table 12. It was found that measured resistivity of specimen L2 and L4 is outlying from other measured values. For this reason, five more specimens L10 – L14 were prepared and results for specimens L2 and L5 were not considered.

If we assume that it is possible to neglect the contact resistivity, we can determine the electrical resistivity using 2T configuration. Following formulas was used for determination of 2T in-plane resistivity.

$$R_x = \rho_x \cdot \frac{l}{A} = \rho_x \cdot \frac{l}{w \cdot t} \ . \tag{18}$$

$$\rho_x = R_x \cdot \frac{A}{l} \ . \tag{19}$$

Results of 2T measurements are given in Table 12.

Table 12 Overview of specimens used for determination of in-plane resistivity and measured electrical resistivity using 2T method.

	Length [mm]	Width [mm]	Thickness [mm]	1/Thickness [1/m]	2T - R [Ω]	2T- ρ_x [Ωm]	Temp. t [°C]
L1	88.4	25.2	3.1	0.328	0.293	0.000254	21.4
~~L2~~	~~88.4~~	~~25.2~~	~~3.2~~	~~0.317~~	~~0.792~~	~~0.000711~~	~~21.5~~
L3	87.6	25.2	3.1	0.319	0.316	0.000284	21.8
L4	93.6	25.2	1.6	0.61	0.476	0.000209	21.8
~~L5~~	~~93.1~~	~~25.2~~	~~1.6~~	~~0.63~~	~~1.074~~	~~0.000465~~	~~21.8~~
L6	91.9	25.1	1.6	0.61	0.498	0.000222	21.8
L10	92.5	25.1	1.6	0.63	0.502	0.000218	23.5
L11	92.5	25.1	1.6	0.63	0.412	0.000179	23.7
L12	92.5	25.2	1.6	0.63	0.388	0.000169	23.8
L13	46.3	25.1	1.6	0.63	0.344	0.000298	23.8
L14	46.3	25.1	1.6	0.63	0.270	0.000234	23.7
					Av.	0.000201	
					St.dev.	0.000041	

When we consider that the contact resistance (R_C) is not negligible, but constant, we can determine the resistivity of the specimen and the value of the contact resistance. Here the method is marked as RA. For this approach it is necessary to evaluate 2T measurement on specimens with different dimensions. It is possible to use linear regression for measured data for specimens, which differ in their thickness according to following formula:

$$R_x = R_{C1} + \rho_x \cdot \frac{l}{w} \cdot \frac{1}{t}. \tag{20}$$

For the linear regression equation of measured data

$$R_x = 0.6286 \cdot \frac{1}{t} + 0.1012. \tag{21}$$

We can calculate the resistivity for the material as follows:

$$\rho_x \cdot \frac{l}{w} = 0.6286 \rightarrow \rho_x = 0.6286 \cdot \frac{w}{l} = 0.162 \ \Omega mm = 0.000017 \ \Omega m. \tag{22}$$

First, we evaluated only data for specimens L1, L3, L4, L6 and obtained value of in-plane resistivity ρ_x = 0.000174 Ωm, see Fig. 87. After preparing specimens L10 - L14 we also performed linear regression for measured data of group of specimens L1, L3, L4, L6, L10 - L12, see Fig. 89 . According to formula (23), we also proceed linear regression for specimens which differ only in its length (group of results for specimens L10 - L14, see Fig. 88, and group of results for specimens L4, L6, L10 - L14, see Fig. 90.

$$R = R_C + \rho \cdot \frac{1}{w \cdot t} \cdot l \tag{23}$$

Measured electrical resistivity, equation of linear regression and determined values of in-plane resistivity are given in Fig. 87 - Fig. 90. The lowest value of in-plane resistivity according to RA configuration was 0.00011 Ωm.

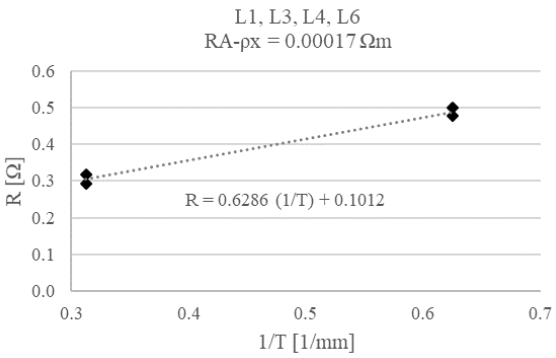

Fig. 87 Evaluation of RA measurement on specimens L1, L3, L4, L6

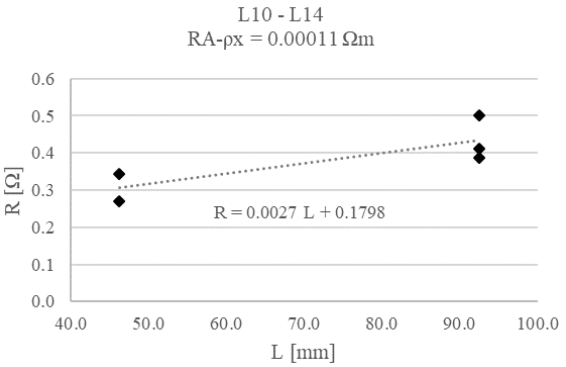

Fig. 88 Evaluation of RA measurement on specimens L10 – L14

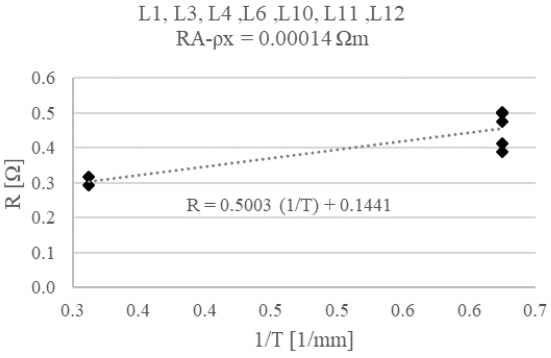

Fig. 89 Evaluation of RA measurement on specimens L1, L3, L4, L6, L10, L11, L12

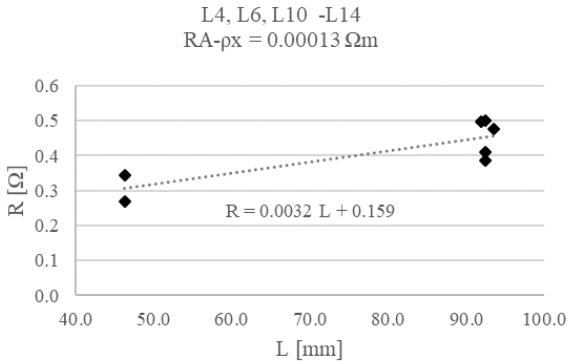

Fig. 90 Evaluation of RA measurement on specimens L4, L6, L10 – L14

The RBA and RCA electrical contact configurations were prepared on specimens L1-L6. The distance between the inner voltage electrodes according to (Fig. 86) was 30 mm for both configurations. For the resistivity determination the same formula as for the 2T configuration (eq.(19)) was used, but the distance between inner electrodes was considered in the formula. Measured data are given in Fig. 91. Although the measurement for the 2T configuration on specimens L2 and L4 were outlying, measurements with RBA and RCA on these two specimens were not outlying.

Table 13 Overview of results of measured electrical resistivity using RBA and RBC method.

Specimens	RBA [Ωm]	RBC [Ωm]
L1	0.000075	0.000075
L2	0.000082	0.000085
L3	0.000086	0.000084
L4	0.000068	0.000080
L5	0.000081	0.000078
L6	0.000067	0.000074
Av.	0.000076	0.000079
St.dev.	0.000007	0.000004

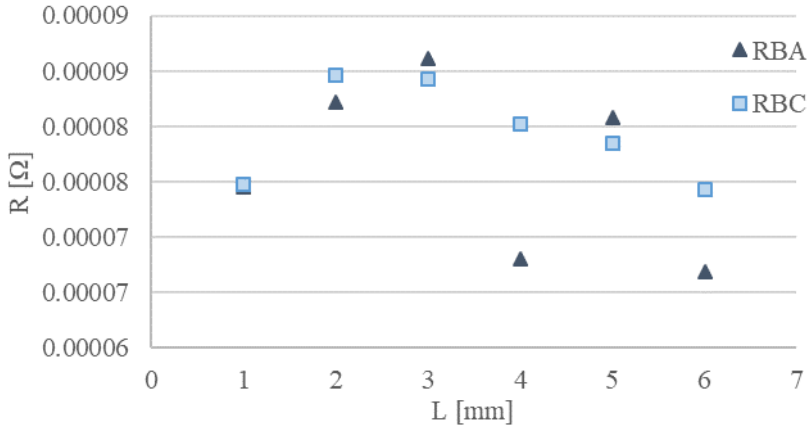

Fig. 91 Results of measured electrical resistance using RBA and RBC method.

The RA method was not studied for the through-thickness direction. For the 2T electrical contact configuration electrical resistivity ρ_z was determined to be 0.12 ± 0.034 Ωm.

5.1.3.2 Through-thickness resistivity

The through-thickness electrical resistivity ρ_z according to RE contact configuration was determined to be 0.06 ± 0.005 Ωm.

5.1.3.3 Partial conclusions

- Contrary to the results presented in [41], we used conductive epoxy instead of electroplating to prepare electrical contacts for configuration RA. We discovered that the contact configuration RA exhibits higher electrical resistivity compared to contact configurations RBA and RCA.
- Based on the obtained values of through-thickness resistivity, it is not possible to neglect the contact resistance and employing the 2T configuration for measurements in the through-thickness direction, despite the fact that through-thickness resistivity is an order of magnitude larger than in-plane resistivity.
- A negligible difference in the measured data was observed between configurations RBA and RCA.
- According to our investigation it is more advantageous to use separate current and voltage electrodes when using conductive epoxy for electrical contact preparation.

5.2 Determination of electrical resistivity of CF composite with thermoplastic matrix

For the determination of electrical resistivities of CF composite with thermoplastic material (CF-PPS) the configuration of electrical contacts was used based on the findings of previous sections.

5.2.1 Experimental procedure

Nominal resistivities of the material was determined using four-wire measurement method. Electrical contact configurations for the determination of the nominal resistivities are shown in Fig. 92.

Six specimens with dimensions 5 mm × 15 mm × 60, 80, 128, 147, 180, 250 mm were used for determination of the longitudinal resistivity (ρ_x), distance between the inner voltage and outer current electrodes was 20 mm, the width of the voltage electrodes was 3 mm. Seven other specimens with dimensions 5 mm× 15 mm × 27 mm were used for determination of through-thickness resistivity (ρ_z). The distance between inner voltage and outer current electrode was 2 mm, dimension of the inner voltage electrode was 14 mm × 4 mm.

The obtained nominal resistivities were used also for numerical simulations of the delamination growth and are given in Table 14.

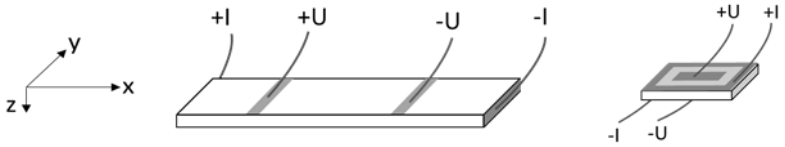

Fig. 92 Configurations of electrical contacts for determination of in-plane (left) and through-thickness resistivity (right).

Table 14 Nominal electrical resistivities.

	ρ_x [Ωm]	ρ_z [Ωm]	ρ_z / ρ_x [-]
CF-epoxy	0.000079 ± 0.000004	0.06 ± 0.005	0.8 x 10^3
CF-PPS	0.000116 ± 0.000032	0.11 ± 0.008	1.0 x 10^3

5.2.1.1 Partial conclusions

- The electrical resistivity of CF-PPS composite material was determined and will be further used in FE simulation of delamination growth in CF-PPS specimen.

5.3 Delamination detection using electrical resistance change method

Delamination detection using the Electrical Resistance Change Method (ERCM) was investigated on two types of materials: CFRP composite and CF composite with a thermoplastic matrix. The mechanism of delamination growth was different for each type of material, because the experimental setup for each material group was different, but the delamination growth was observed in both test groups. Detailed descriptions of the materials and methods are provided for each material type.

5.3.1 Material and specimen preparation

5.3.1.1 CFRP composite (CF-epoxy)

The Mixed-Mode Bending (MMB) specimens were extracted from CFRP composite made of 16 layers of the material Hexply AGP 193PW/8552S RC40 (CF-epoxy). The lay-up $[45/0]_{4S}$ was used. Dimensions of the specimens were 3.3 mm × 25 mm × 185 mm. A 25 mm long non-adhesive plastic foil sheet was inserted to the plate edge during manufacturing to the neutral axis to initiate the delamination growth between the 8th and 9th layer. Total number of five MMB specimens was tested. Nominal values of resistivity were obtained using the four-probe configuration, see Fig. 92.

The specimens made of CF-epoxy were loaded simultaneously by mode I and mode II loading (Mixed-Mode Bending - MMB specimens). Experimental results were already published in [A7].

5.3.1.2 CF composite with thermoplastic matrix (CF-PPS)

The specimens made of CF-PPS (carbon fiber, polypropylene sulphide matrix, fabric with 5H satin weave) composite, material sheet AIMS05-09-002. Six specimens with the dimensions 5 mm × 15 mm × 54 mm were cut from one plate, which was manufactured by thermoforming process. Surface of the specimens was slightly sanded at first with sandpaper P120 and P600 and then degreased. Electrical contacts were prepared using a CHO-BOND® 584-29 conductive epoxy and copper strips. The configuration of the electrical contacts on the specimens are given in Fig. 94 and Fig. 95.

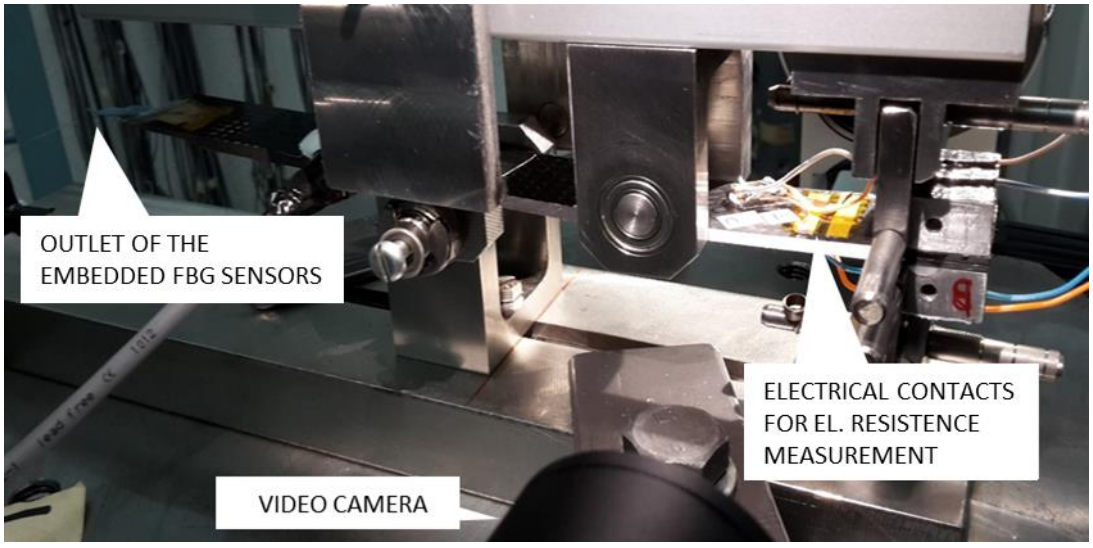

Fig. 93 MMB Specimen during testing

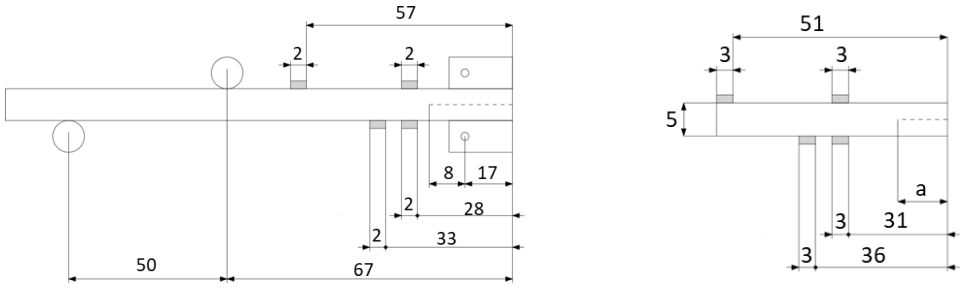

Fig. 94 Configurations of electrical contacts for determination of in-plane (left) and through-thickness resistivity (right).

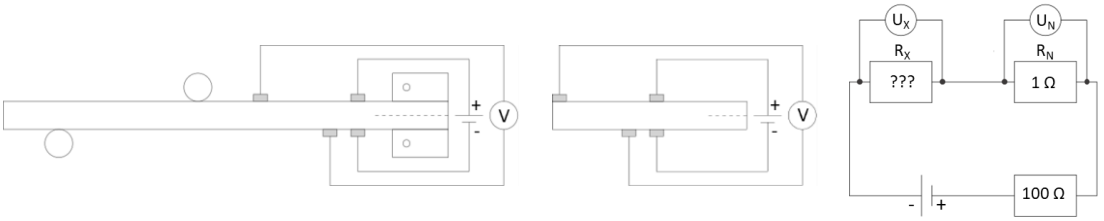

Fig. 95 Measurement configuration of the electrical resistance measurement - configuration of duty current injection and voltage change measurement on the CF-epoxy specimen (a), CF-PPS specimen (b), schematic of the series comparison measurement method (c).

5.3.2 Experimental procedure

5.3.2.1 CF-epoxy

The specimens were loaded by mixed-mode bending according to ASTM D6671M-06 standard. The configuration of the loading is shown in Fig. 93. MMB specimens were clamped using bonded aluminum blocks into INOVA ZUZ 50 loading machine, with a LTC 116-0.1 load cell, which has a capacity of 1 kN. The crack propagation during the loading was monitored using the cameras at 12.5 frames per second. Sinusoidal loading with displacement control set to δ_{max} = 7 mm and δ_{min} = 0.7 mm, and a frequency of 5 Hz was applied. The cycling was stopped for each measurement.

5.3.2.2 CF-PPS

The specimens were not loaded, the specimens were clamped into a jig during the test. To initialize the delamination, specimens were partly cut in the half of the thickness. Afterwards the delamination growth was forced mechanically. Delamination growth was recorded using a Nikon camera. The propagation of the delamination crack during the measurement is shown in the Fig. 96.

5.3.3 Measurement procedure

The determination of electrical resistivity of CF-epoxy and CF-PPS specimens was performed using the HP E3631A current source and two Agilent 34461A multimeters. The change in electrical resistance was determined using the series comparison measurement method.

Series comparison measurement method is used to achieve high measurement accuracy when measured resistance of low values. The measurement was performed here using the HP E3631A current source and two Agilent 34461A multimeters. The change in electrical resistance was determined using the series comparison measurement method according to the following equation:

$$R_X = \frac{U_X}{U_N} \cdot R_N. \tag{24}$$

We had a resistor of nominal value R_N. In case, when the same current go across both measured and known resistor and we measure the voltage across the known resistor (U_N) and across the measured resistor (U_X). It is possible to calculate the value of unknown resistor (R_X) according to formula (24).

The resolution of the measurement when using mentioned multimeters can be calculated according to equations given in [80]. The resolution was determined ± 0.01 mΩ and the accuracy of the measurement was ± 0.03 mΩ.

The electrical measurement of CF-epoxy specimens was performed also in two static load cases (loaded/unloaded).

The electrical resistance of each CF-PPS specimen was measured before an initialization of the delamination and after each delamination growth (increment).

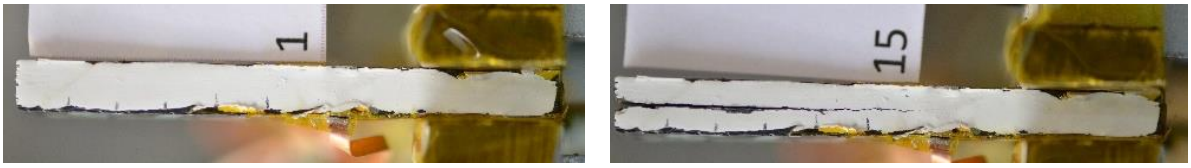

Fig. 96 Delamination propagation on the CF-PPS specimen.

5.3.4 Numerical simulation of delamination specimen test

The numerical analyses were carried out using the commercial code Ansys 19.2. The MMB specimen made of CF-epoxy was prepared as a 2D model, over 31,000 plane elements were used with element size from 0.008 mm to 0.5 mm, see Fig. 97 FE model of MMB specimen. Mechanical loading was not considered during the simulation.

The delamination growth of specimen made of CF-PPS was simulated also in Ansys 19.2 as a 2D model, over 39,900 plane elements with element size from 0.008 mm were used.

Material parameters were entered according to conducted measurements and are given in Table 14.

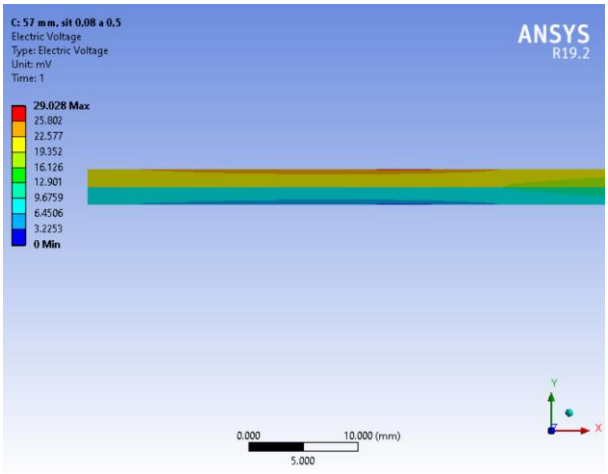

Fig. 97 FE model of MMB specimen.

5.3.5 Results and discussion

Results of the experimental and numerical investigations are given in Fig. 98. Results are given as a relative change of measured electrical resistance. It is calculated according following equation:

$$\frac{\Delta R}{R_0} = \frac{R - R_0}{R_0} \cdot 100 \quad [\%] \tag{25}$$

The R_0 in the equation corresponds to the initial electrical resistance. For the MMB CF-epoxy specimen the initial resistance was measured before delamination growth, when the delamination was only 25 mm. For the DCB CF-PPS specimen the initial resistivity was determined on the specimen without delamination.

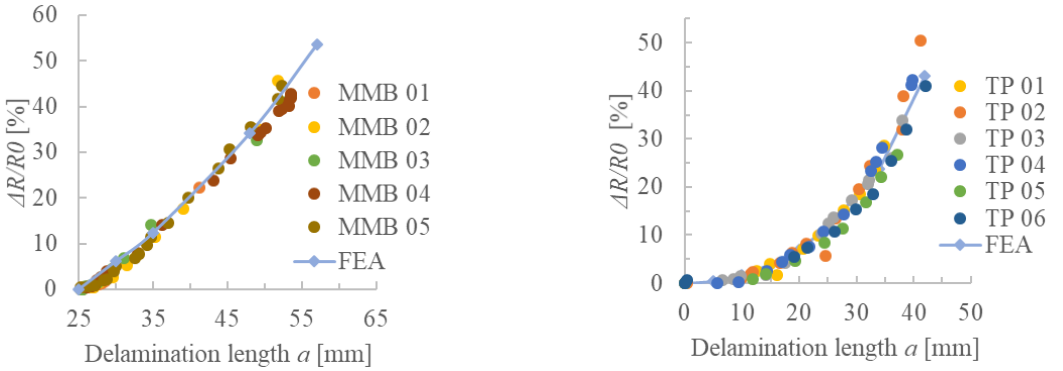

Fig. 98 Comparison of experimental results and numerical simulation results of delamination growth on the CF-epoxy specimen (left) and CF-PPS specimens (right).

5.3.5.1 Partial conclusions

- Delamination detection using ERCM method is feasible.
- Simulation using FEA show good agreement with experimental, when electrical resistivities are determined using four terminal measurements (see Fig. 92).

5.4 Influences on delamination detection

There are many influences, which could affect the delamination detection and prediction of delamination growth. In this part we focus on the influence of the procedure of nominal electrical resistivity determination. The influence of the temperature change and contact configuration is discussed.

5.4.1 Procedure of determination of electrical resistivity of the material – influence on delamination detection prediction

The values of electrical resistivity of the CF-epoxy material obtained in section 5.1.3 were used in the finite element analysis of the delamination growth. An overview of used electrical resistivities is given in Table 15. Simulated data were compared to those obtained during experimental investigations. The FE model used for the analysis was the same as in section 5.3.4.

Results of the conducted finite element analysis are given in Fig. 99 and Fig. 100. It can be seen, that results obtained with electrical resistivities using 2T method do not correspond to the measured data at all. When using data obtained by RA and RE configuration, the longer the delamination, the bigger the difference between measured and simulated data can be seen.

Table 15 Overview of the electrical resistivities used in finite element analysis.

	2T – 2T	RBA – 2T	RBA - RE	RA - RE
ρ_x [Ωm]	0.0002	0.00007	0.00007	0.0001
ρ_z [Ωm]	0.12	0.12	0.06	0.06

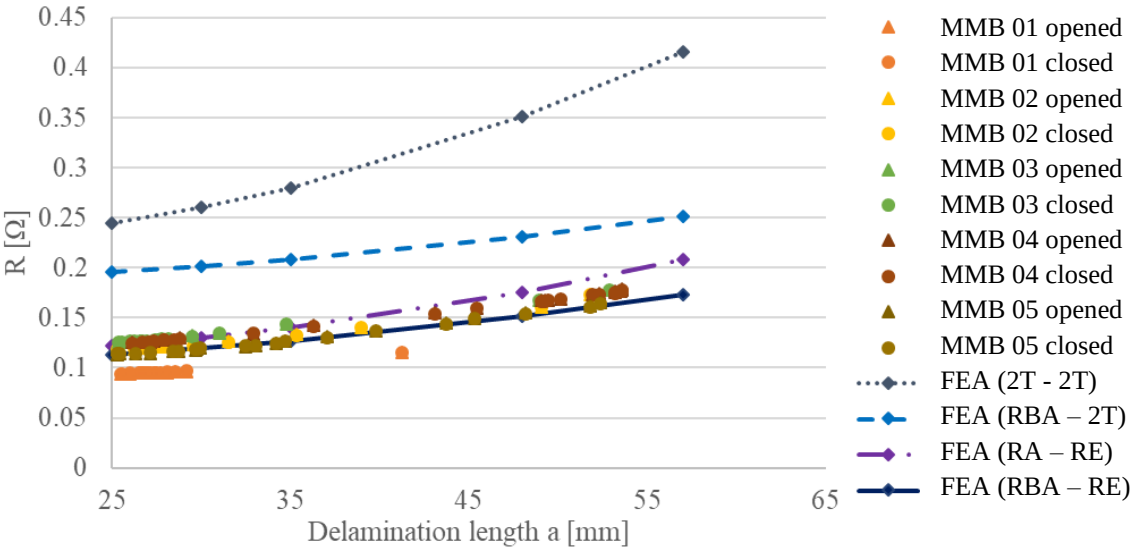

Fig. 99 Results of finite element analysis and measured experimental data.

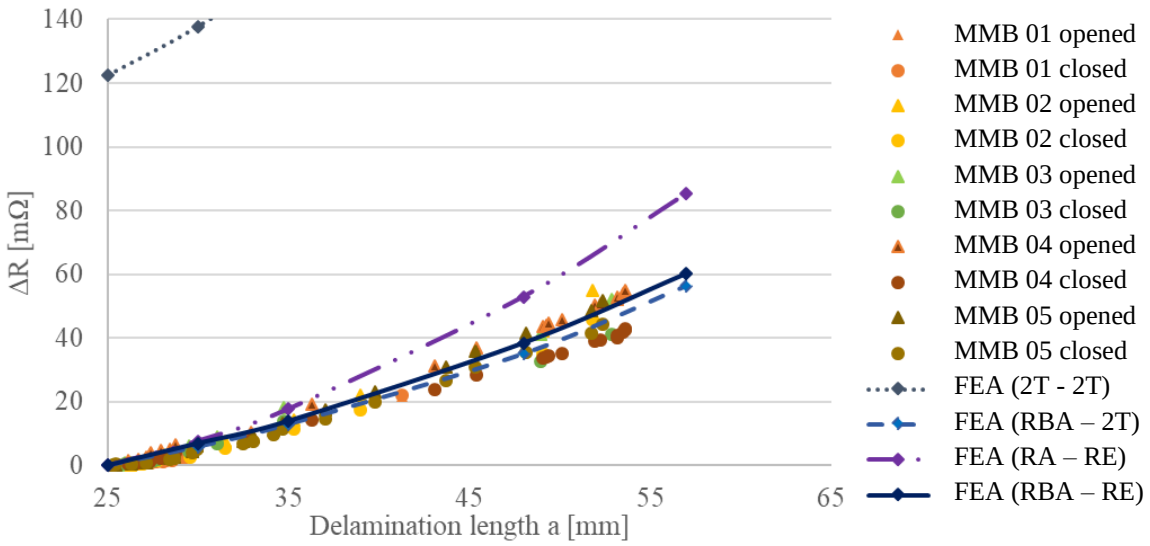

Fig. 100 Results of finite element analysis and measured experimental data.

5.4.1.1 Partial conclusions

- The procedure of electrical resistivity measurement affects the accuracy of delamination growth prediction using the FE model.
- It is not recommended to use two terminal measurement method for electrical resistivity determination.

5.4.2 Influence of the temperature change on delamination detection

For practical applications, in which operating temperature can significantly vary, it is necessary to know its consequences.

Temperature coefficients were taken from literature and used for the calculation of electrical resistance change for different sizes of delamination.

Values of the electrical resistivity vary depending on the temperature [42], [81], [82], see Table 16. Different values of the temperature coefficient of resistivity were used for the numerical simulation of delamination growth at the temperature 20 °C, 40 °C and 60 °C. First temperature coefficient was considered only in the longitudinal direction (α_x = - 0.0006 1/Ωm). Then the temperature coefficient in the longitudinal and through-thickness direction was considered (α_x = -0.0006 1/Ωm, α_z = -0.00094 1/Ωm). The resistivity at different temperatures was calculated according to the following equation:

$$\rho(T) = \rho_{20}[1 + \alpha\ (T - T_{20})], \tag{26}$$

where ρ_{20} is the electrical resistivity at room temperature (20 °C) and α is the temperature coefficient of resistivity. Results of the FE simulations are given in Fig. 101.

Numerical investigation of the influence of the temperature shows that the increment of measured electrical resistance ΔR decrease only by maximal 2.5 % percent for the delamination length 30 mm when the temperature increases from 20 °C to 60 °C.

Table 16 Temperature coefficients of resistivity.

Reference	Material	Lay-up	Direction		
			Fiber (x) [10^{-4} K^{-1}]	Transverse (y) [10^{-4} K^{-1}]	Thickness (z) [10^{-4} K^{-1}]
Takahashi, 2011	UD prepreg	$[0_8]_T$	-5.28	-13.8	-9.41
Todoroki,2014	UD prepreg	$[0/45/-45/90]_s$	-6	-	-
Ogi, 2006	UD	[0]	-5.7	-	-
Ogi, 2006	UD	[45]	-8.2	-	-
Ogi, 2006	UD	[90]	-5.9	-	-

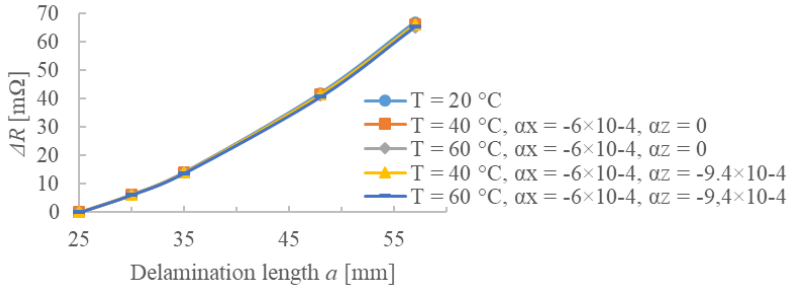

Fig. 101 Influence of the temperature coefficients of the resistivity on the electrical resistance change (FEM simulation).

5.4.2.1 Partial conclusions

- Based on performed simulations, it can be stated that the influence of temperature change on measured change of electrical resistance is relatively small compared to the influence of the delamination growth.

5.4.3 Influence of the values of the nominal resistivities on the delamination detection

Nominal resistivities of composite material can differ a lot. Values of the nominal resistivities are influenced by the orientation of the fibers, stacking sequence and the volume fraction (V_f) of the carbon fibers in the composite material. We used our case example of monitoring of delamination growth on the MMB specimen. The intention was to show possible differences when materials of different material properties would be monitored. Although influence of different electrical resistivity ratios ρ_z/ρ_x were already published (see [72]) the absolute values of such investigations were not given. We prepared the numerical parametric study with electrical resistivities published in [41] (similar values of electrical resistivities were published in [82]), and also electrical resistivities of our investigated CF-epoxy composite material, see Table 17.

Table 17 Nominal electrical resistivities used for numerical simulation.

V_f	Longitudinal resistivity ρ_x [Ωm]	Through-thickness resistivity ρ_z [Ωm]	ρ_z/ρ_x [-]
CF-epoxy	7.9×10^{-5}	6.0×10^{-2}	0.8×10^{3}
0.58 [16]	2.93×10^{-5}	4.82×10^{-2}	1.6×10^{3}
0.49 [16]	3.71×10^{-5}	2.83	76.3×10^{3}
0.43 [16]	4.72×10^{-5}	16	339.0×10^{3}

The nominal resistivities significantly influence the resistance measurement. Although the difference of change of electrical resistance with the increasing delamination was of the same order for the investigated electrical resistivities, the total measured electrical resistance increased by two orders (120 mΩ for $\rho_z/\rho_x = 0.8 \times 10^3$ and 12,000 mΩ for $\rho_z/\rho_x = 339 \times 10^3$), see Fig. 102.

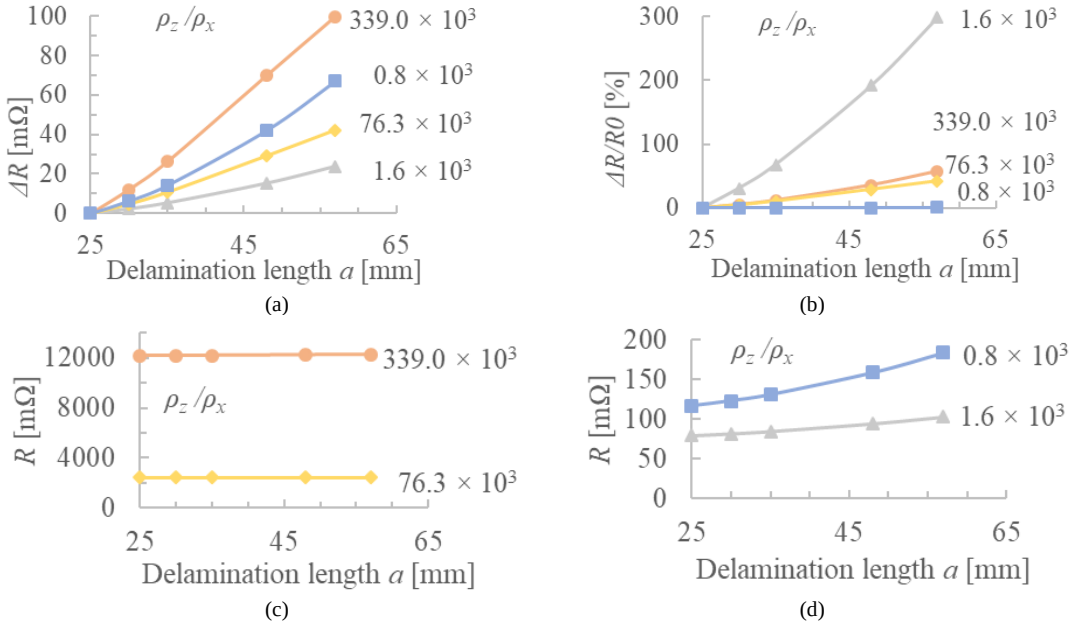

Fig. 102 Influence of the nominal resistivity on the electrical resistance change.

5.4.3.1 Partial conclusions

- The conducted numerical experiment showed that the magnitude of electrical resistance change caused by the delamination growth depends not only on resistivity ratios (ρ_z/ρ_x), but also on the magnitude of resistivity in longitudinal and through thickness direction.

- In scientific papers, the results of simulations are often given only as percentages of the relative resistance change ($\Delta R/R_0$). The results presented in Fig. 102 demonstrate the need to present results also in absolute values for a better understanding of the problem.

5.4.4 Influence of the distance of the electrical contacts on the delamination detection

In this section, is presented a study focused on the influence of the distance between positive and negative voltage electrode *D* (see Fig. 103).

The numerical simulation was carried out for four different distances between the positive and negative voltage electrode. Results of the simulation for the distances between the positive and negative voltage electrode 10, 20, 30, 40 mm are shown in Fig. 103. Electrical resistivities previously determined for CF-epoxy were used, see Table 14.

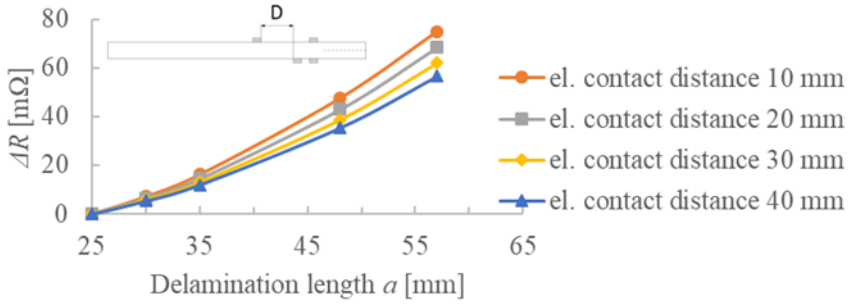

Fig. 103 Comparison of numerical simulation of delamination growth on the CF-epoxy specimen with different distance between positive and negative voltage electrodes.

5.4.4.1 Partial conclusions

- The numerical investigation of the influence of the electrical contact distance shows that the increase of measured electrical resistance may increase by 21 % for the delamination length of 30 mm when we decrease the distance between the positive and negative voltage electrodes from 40 mm to 20 mm.
- This is because the change in measured electrical resistance caused by the delamination growth is relatively small. The resolution of the resistance measurement device could be a limitation for the method. Based on the numerical simulation, it is possible to define the distance between the voltage electrodes in such a way that the appropriate resolution of the delamination growth can be detect.

5.5 Delamination detection - conclusions

- It was shown that the accuracy of the prediction of delamination detection using FE analysis and the ERCM method is influenced by the precision in determining electrical resistivity. It was also shown that it is necessary to present results of FE analysis in comparison with experimental data using absolute values, as relative resistance values can be misleading. In section 5.4.1, the influence of the procedure for determining electrical resistivity on delamination detection prediction using FE is shown.
- Experimental investigation and numerical simulation of delamination growth were conducted on specimens made of CF-PPS and CF-epoxy.

- Electrical contact configurations for determining electrical resistivity from literature were compared. It is recommended to use the 4T (four-terminal) contact configuration for both longitudinal and through thickness direction. The comparison between numerical and experimental results has shown good agreement.
- The influence of temperature on the electrical resistance change during delamination growth is relatively small even for temperature changes as high as 40 °C. This means that temperature changes in the structure do not significant affect the accuracy of delamination indication in the composite during experimental measurement.
- The influence of contact distance was analyzed. The smaller the distance between the positive and negative voltage electrodes, the higher the measured electrical resistance change due to delamination growth. It is recommended to choose the electrode distance based on the resolution of the measurement device and according to the size of the delamination increment that needs to be detected.

6 Experimental verification on component level

In the previous sections, investigations at coupon level were presented. To facilitate practical utilization and spread the investigated methods, it is necessary to address challenges associated with integrating sensors into the production process of composite parts. In previous sections, investigations on CF sensors integrated into the composite layup made of prepregs and cured in autoclave were discussed. This section demonstrates the practical application of CF sensors and the ERCM method on carbon fiber filament wound profiles. These profiles among other applications, are particularly useful in two areas where structural health monitoring for damage would be beneficial.

The first application is in aircraft steering rod. For these applications, profiles over two meters in length with diameters about 30 mm are used. The steering rod could be damaged during operation, for instance after a failed landing, a ground accident, or flight through extreme turbulence. The ability to easy detect cracks or ruptures of the rod through ground inspection would be advantageous.

The second potential utilization of damage detection in filament wound profiles is in the area of construction of robotic arms. Robotic arms in the production industry are often made from filament wound profiles due to their high stiffness and low mass. Possible collisions and resulting overloading can damage the composite profiles. Such damage could be overlooked due to cabling, coating, and casing covering the surface of the robotic arms. Therefore, a method to easily detect serious damage after an impact collision on CFRP wound profiles was investigated.

Fig. 104 Filament wound composite profile for the robotic arm [83]

Several types of damage detection scenarios were investigated as part of a research project regarding investigation of Integrated Loop Technology Joints. There were three areas investigated:

- Crack detection using a CF sensor (Results were published in [A13].)
- Strain monitoring using the CF sensor integrated within the filament wound layup (Results were published in [A15] and [A16].)
- Electrical resistance measurement on the filament wound profiles (Results were published in [A14].)

6.1 Damage detection of filament wound profiles by means of CF sensors

6.1.1 CF sensor attached to the surface – damage detection

The feasibility of damage monitoring by the simple installation of the CF sensor on the surface of the filament wound profile was investigated.

6.1.1.1 Specimen preparation

The specimens were produced using an automated filament winding process. Carbon fibers T700 (supplied by Toray Composite Materials America, Inc., USA) were used in combination with epoxy resin LG900/HG100 (supplied by GRM Systems s.r.o., Czech Republic). Each specimen was manufactured from 5 layers.

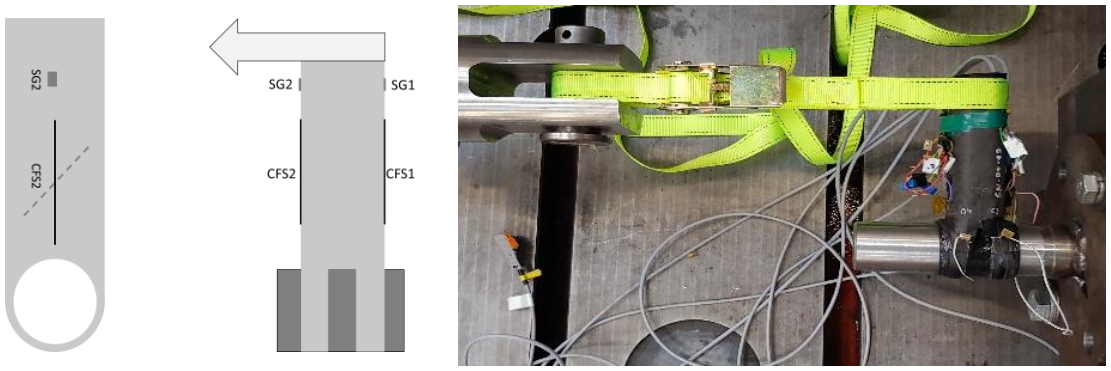

(a) (b)

Fig. 105 Sensor configuration on the specimen (a), Configuration of the flexural test (b)

6.1.1.2 Carbon Fiber Sensors (CF sensors)

The CF sensors were produced using carbon fiber roving from PAN T300 (Toray Composite Materials America, Inc.), based on the technique outlined in [2], and were cut to a length of 80 mm. The distance between the eyelet and the sensor was 10 mm. The CF sensors were bonded with epoxy adhesive CC-33a (Kyowa Electronic Instruments Co., Ltd.) to the surface of seven samples along their longitudinal axis as outlined in Fig. 105. The CF sensors on specimens 8 and 9 were positioned at a 45° angle to the longitudinal axes, as indicated in Table 18. The epoxy adhesive was also utilized to provide electrical insulation between the sensor and the specimen.

Table 18 Specimen overview, configuration of the CF sensors and position of the crack

Specimen number	CFS1 tension side	CFS2 compression side	Crack on the compression side
8	45°	45°	through the sensor
9	45°	45°	through the sensor
13	0°	0°	next to the sensor
14	0°	not installed	-
15	0°	0°	next to the sensor
34	0°	0°	through the sensor
35	0°	0°	next to the sensor

6.1.1.1 *Experimental setup*

The flexural test of the composite profile with the ILT joint was performed in the configuration depicted in Fig. 105. All specimens were tested using an IST Instron PL63N servo hydraulic actuator, with a loading speed of 8 mm/min. The change in electrical resistance of the CF sensors was measured using a strain gauge transducer (HBM QuantumX1645B).

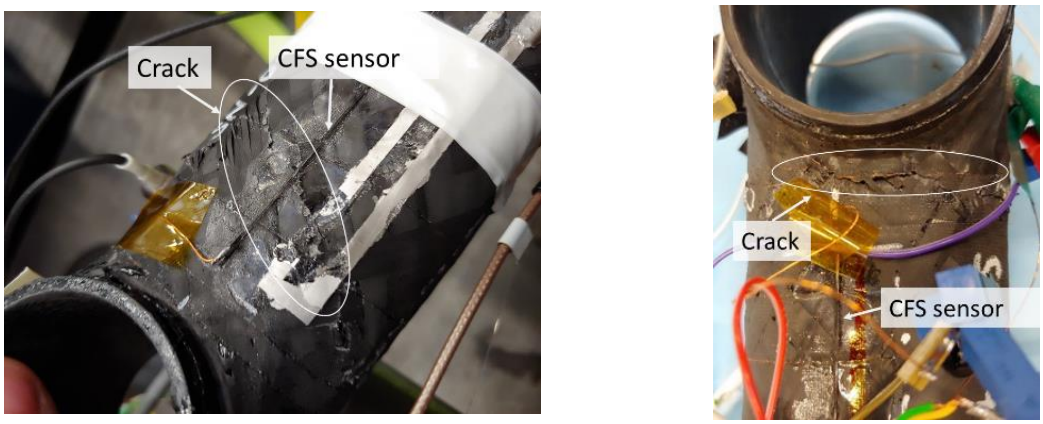

(a) **(b)**

Fig. 106 Specimen 34 with the crack in the area of CF sensor (a), Specimen 13 with the crack next to the CF sensor (b)

6.1.1.2 *Results and discussion*

The specimen fracture occurred on the compression side of the specimens. Two types of fracture were observed. The first type occurred approximately 30 mm from the eyelet (specimens 8, 9, 34) in the area where the CF sensor had been installed, likely due to the buckling of the specimens (refer to Fig. 105 (a). The second type of fracture was detected closer to the eyelet, at approximately 10 mm (specimens 13, 14, 15, 35), as depicted in Fig. 106 (b). The second type of damage occurred next to the installed CF sensor. The electrical resistance of the installed CF sensors was measured during loading.

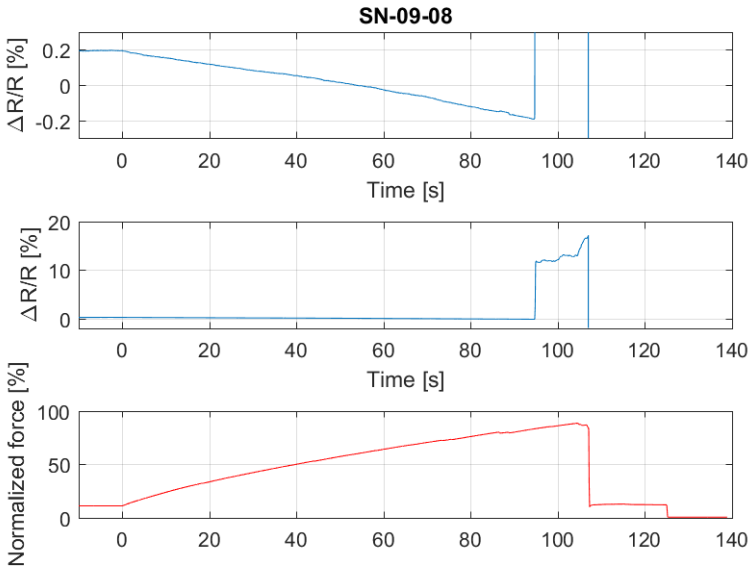

Fig. 107 Measured electrical resistance changes during bending loading of the specimen SN-09-08

Two scenarios for damage detection exist, namely damage detection during continuous measurement and damage detection during production line shutdowns. Table 19 shows the measured step change values of the electrical resistance of the CF sensors installed on the compression side during loading and after final breakage. The measured step change of approximately 0.05 % could be attributed to a temperature change of 1.5 °C, as described in detail in [A1], therefore, it is important to consider the change in operating temperature for practical applications.

Table 19 Measured step change in electrical resistance for CF sensor installed on the compression side.

Specimen number	ΔR [%] during loading	ΔR [%] after final fracture	Position of the fracture
8	11	overload	
9	0.05	overload	In the area of the sensor
34	1.7	20 %	
13	0.12	1	
15	0.1	overload	Next to the sensor
35	0.05	0.3	

6.1.1.3 Conclusions

The epoxy adhesives used for the bonding of the CF sensors to the surface of the CFRP composite tubes successfully serves as electrical insulation.

The possibility of damage detection using a CF sensor attached to the surface was experimentally investigated. The CF sensors attached to the surface were sensitive to damage in the form of cracks.

According to the conducted experiments – it seems possible to detect damage of profiles with ILT joints using a CF sensor attached to the surface during continuous measurement and during production line shutdowns.

6.1.2 Integration of the CF sensor into the filament wound profiles

The possibility of integrating CF sensors into the carbon fiber filament wound profiles for strain sensing and damage monitoring was investigated. A successful approach of electrical isolation, in the form of using a braided sleeve, which cover the CF sensor during integration, was used, as shown in Fig. 108.

Another successful method involved the placement of the CF sensor between two glass fiber filament wound layers. A comparison of such an integrated sensor with a DFOS sensor was published in [A15] and [A16], as indicated in Fig. 109.

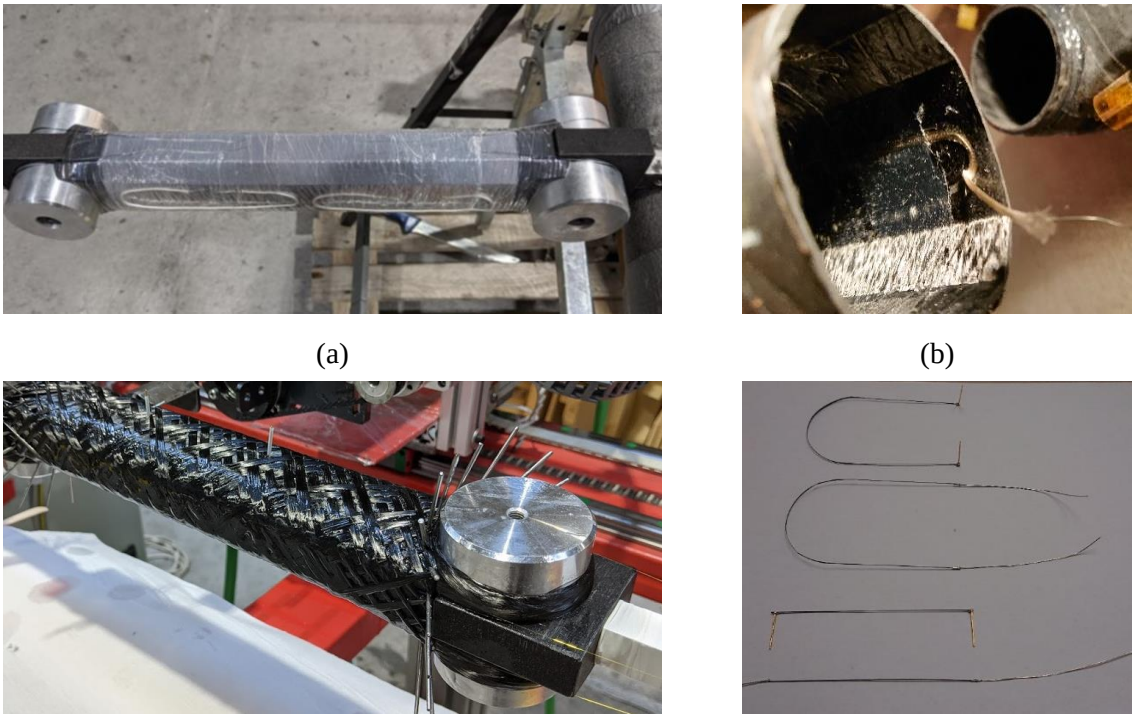

(a) (b)

(c) (d)

Fig. 108 CF sensors with braided sleeve during integrating (a), detail of connecting wire of CF sensors with braided sleeve after manufacturing (b), electrically isolated connecting pins of integrated CF sensor during manufacturing (c), CF sensors of different shapes before integration (d).

6.1.2.1 Conclusions

The technology for manufacturing CF sensors in a specific shape was developed. Two methods for the effective electrical insulation of CF sensors from the rest of the CF filament wound profile were developed. The values of strain determined by the integrated CF sensor during loading are comparable with the results obtained from an optical fiber using the DFOS method and a strain gauge.

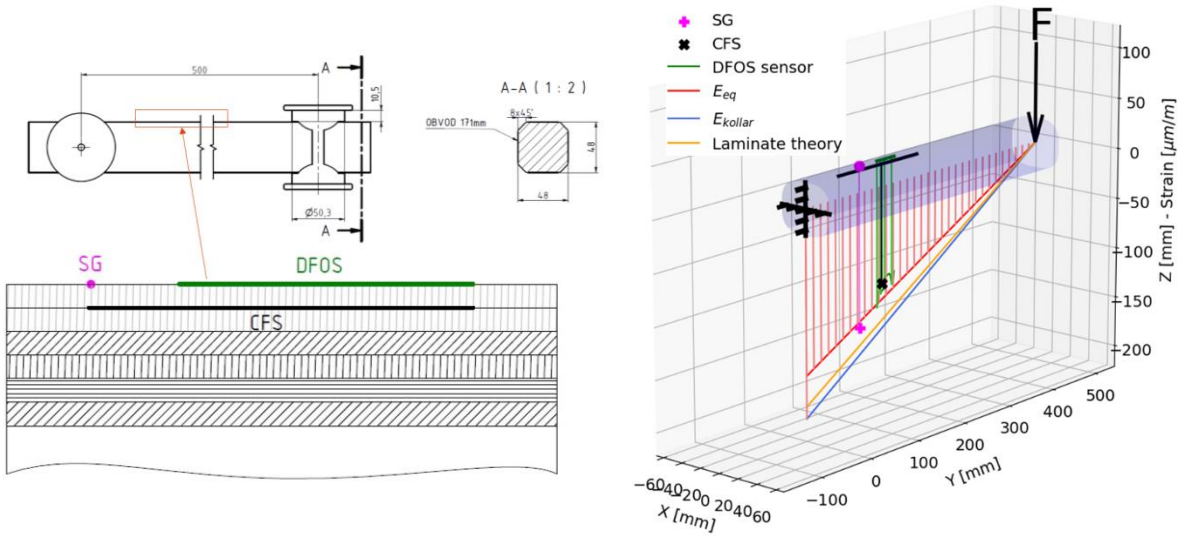

(a) (b)

Fig. 109 Configuration of the specimen with integrated CF sensor (a), Graph of measured mechanical strain compared to calculated values of strain [A16] (b)

6.2 Damage detecting of filament wound profiles by means of ERCM method and electrical contacts prepared of carbon fiber tow

In literature, it has been shown that damage detection using the ERCM method is possible also on composite tubes [84], [85].

Contacts are typically prepared on the outer surface of specimens, as demonstrated in [84], [85]. Usually, conductive epoxy is employed to prepare the electrical contacts. However, this approach has the drawback of requiring specimen polishing before the electrical contacts can be prepared. An alternative is the deposition of a conductive layer, although this method has been only used for outer surfaces, see [51].

A possibility to prepare electrical contacts using carbon fiber tows on the internal surface of carbon fiber filament wound tubes while leaving the external surface intact was investigated. The achieved results were published in [A14].

This approach was necessary because the outer surface of the investigated component can sometimes be used for wiring, and from an aesthetic point of view, should remain intact. To achieve this, we coated the ends of carbon fiber tows with nickel. The carbon fiber tows were then added to the structure during production and used as electrical connections to the structure. One could suggest an inserting of metal wire during manufacturing of the specimen. However, the issue with this approach is that a matrix layer develops between the composite filaments and the metal wire, see Fig. 110.

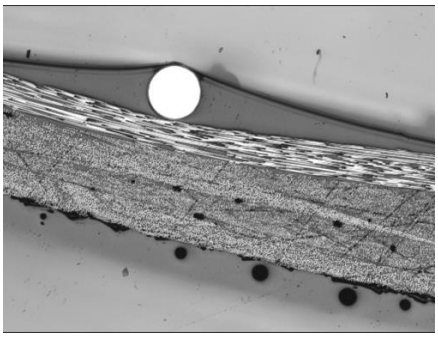

Fig. 110 Detail of copper wire placed on the surface of the filament wound specimen before curing.

The symmetrical convex octagon-shaped specimens were made using filament winding technology with Integrated Loop Technology (ILT) joints at the ends, produced in a single step. Potential applications for these components could include the constructing of robotic arms for automated processes. Two types of specimens were created – those with one ILT joint for flexural loading (refer to Fig. 111 (a)), and those with two ILT joints for torsional loading (refer to Fig. 111 (b)).

(a) (b)

Fig. 111 Configuration of the flexural loading (a); Configuration of the torsional loading (b). [A14]

6.2.1 Experimental procedure

6.2.1.1 Specimen preparation

The same procedure for specimen preparation was used as was described in Section 6.1.1.1.

6.2.1.2 Electrical contact preparation

A nickel coating was used for the preparation of an electrically conductive connection to the carbon fiber tows. Subsequently, copper wires were soldered to the ends of the carbon fiber tows. These were then wrapped around the spindle during the manufacturing process of the samples, as shown in Fig. 112. The carbon fibers with electrically conductive endings were integrated during manufacturing just before the first filament wound layer. The electrical connection to the CFRP specimens was achieved by using carbon fiber tows with soldered copper wires.

6.2.1.3 Experimental setup

The flexural tests were conducted using an IST Instron PL63N servo hydraulic actuator. The configuration of the flexural test is depicted in Fig. 111 (a). The test was carried out under displacement control at a loading speed of 8 mm/min.

The torsional test was performed using an INOVA AT 8-100-V1 servo-hydraulic torsional actuator. For the torsional test, the specimen was attached at one end to a rigid frame, while the torsional moment of the loading machine was applied to the other end through a pin inserted into the eyelet, as shown in Fig. 111 (b).

The change in electrical resistance was measured by 4-wire resistance measuring method using an Agilent 34401A multimeter. The same terminals were used for electrical voltage and current on the specimens, see Fig. 112.

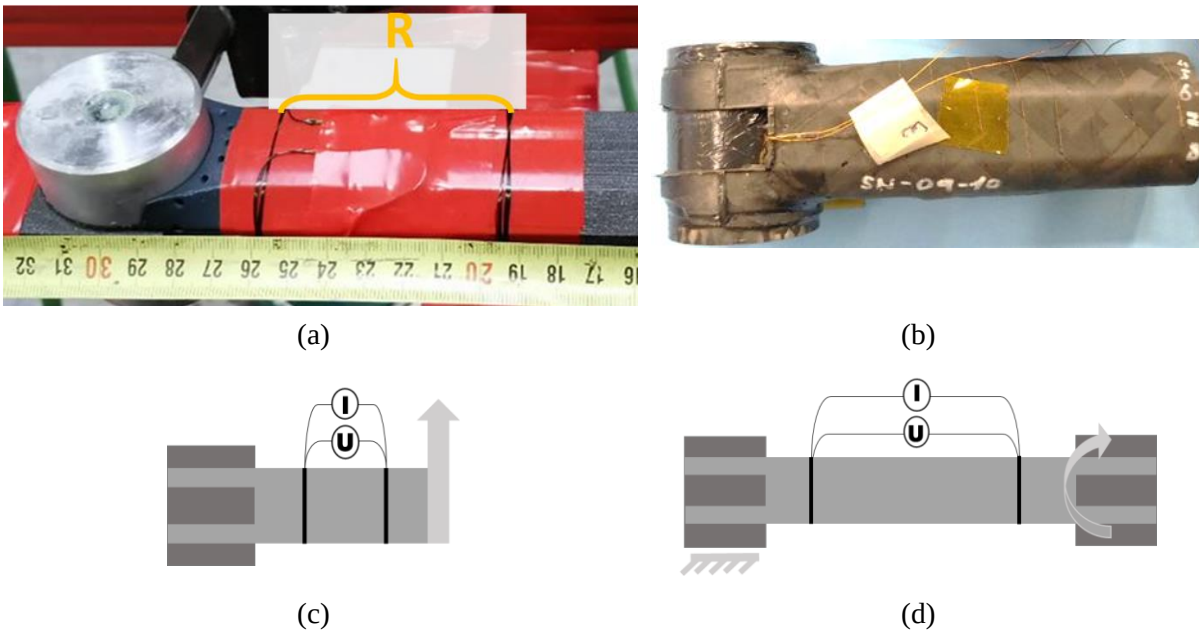

(a) (b)

(c) (d)

Fig. 112 2 (a) Integration of the carbon fiber tow as electrical contact before filament winding procedure; (b) Specimen for flexural loading after manufacturing; (c) Configuration of electrical resistance measurement during flexural test; (d) Configuration of electrical resistance measurement during torsional test. [A14]

The distance between terminals was set at 60 mm for the flexural specimens and 200 mm for the torsional specimens. Our objective was to explore a configuration that incorporates separate terminals for electrical current and voltage, as this configuration was anticipated to be more precise for measuring electrical resistance, due to the elimination of contact resistance. Unfortunately, the removal of the spindle after manufacturing resulted to damage of the second pair of electrodes.

6.2.2 Results and discussion

6.2.2.1 Flexural loading

For each specimen, the initial electrical resistance was measured before mechanical loading. The measured data are presented in Table 20. There is a variation in measured electrical resistance among the specimens, the highest value is more than 80 % greater than the lowest value. For better comparison among the measured data, the increase in measured electrical resistance for each specimen, ΔR, is given in the graphs. This increase, ΔR, was calculated by subtracting the initial electrical resistance before loading R_0 (given in Table 20) from the actual measured electrical resistance during loading. The relative bending moment Mo_{rel} was calculated according to the following formula:

$$Mo_{rel} = \frac{Mo}{Mo_{av}} \cdot 100[\%], \text{ where} \tag{27}$$

$$Mo_{av} = \frac{\sum Mo_{max}}{Number\ of\ specimens} \tag{28}$$

Results for three cycles of operational loading are shown in Fig. 113 which illustrates the measured electrical resistance change and relative resistance moment of cyclic flexural tests. A correlation between the applied load and measured electrical resistance change is evident for specimens SN-9 and SN-11. For specimen SN-8, a slight decrease in measured electrical resistance change is observed as the applied load is increases. On the other hand, opposite trend can be seen in electrical resistance change measured for specimen SN-10. We can observe a big increase of measured electrical resistance during first increase of bending moment and another slight increase for next two loading cycles. Considering the highest measured electrical resistance of the pristine specimen and the differing measurements for the specimen SN-10, we can assume, that this may be due to slightly damaged electrical contacts.

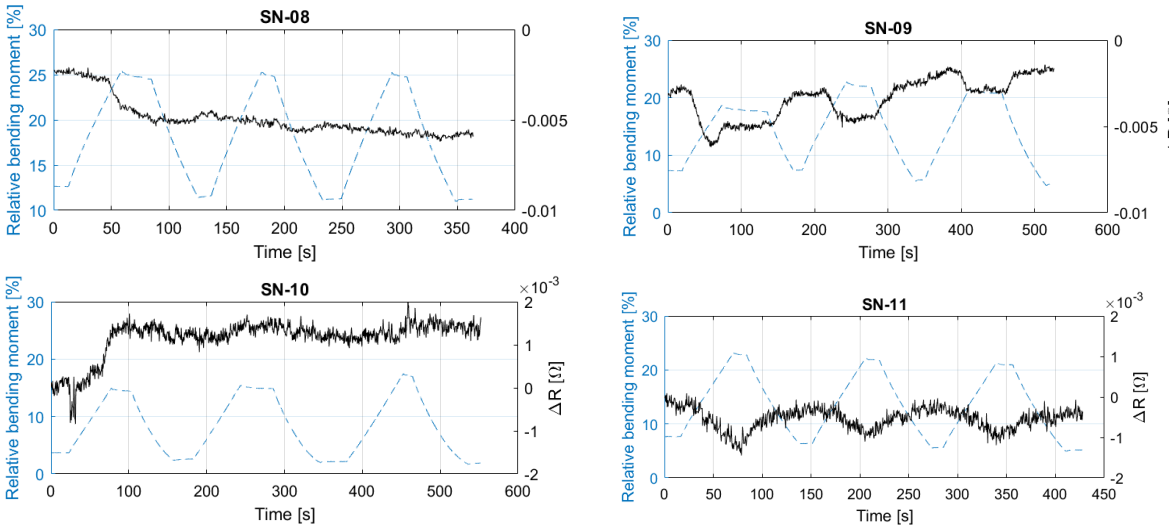

Fig. 113 Measured electrical resistance changes and relative resistance moment of cyclic flexural tests.

Differences in the curve of measured electrical resistance change during static loading are also observed for specimen SN-10 compared to other specimens, as seen in Fig. 114. For specimens SN-8, SN-9, and SN-11, a slight decrease in measured electrical resistance change is noted, which could be attributed to minor structural damage potentially increasing the specimen's electrical conductivity. For specimen SN-10, there is an increase in measured electrical resistance from the beginning of loading. A step change was observed during the fracture of all specimens, as shown in Fig. 114. Detailed information about the step change in measured electrical resistance is provided in Table 20 and Fig. 115. To identify the step change, three values are introduced: electrical resistance before fracture (*RBF*), peak electrical resistance during fracture (*RP*) and electrical resistance after fracture in loaded state (*RAF*).

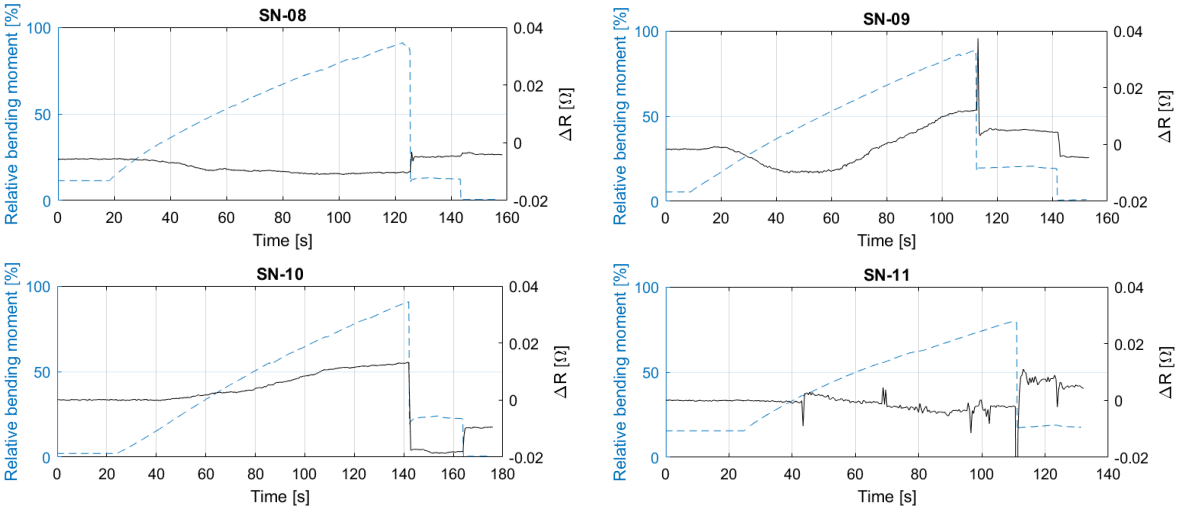

Fig. 114 Measured electrical resistance changes and relative resistance moment of quasi-static flexural tests.

It is evident that the step change in measured electrical resistance was more pronounced than the signal fluctuation observed for specimen SN-11. Based on this observation, we can suppose that fracture detection could be feasible under continual electrical resistance measurement of such constructions.

Table 20 Measured electrical resistance during flexural loading

Specimen Number	El. resistance of pristine specimen	El. resistance before fracture	Peak el. resistance during fracture	El. resistance after fracture (loaded)	Peak relative resistance change	After fracture relative resistance change	Signal fluctuation
	R_0 (Ω)	*RBF* (Ω)	*RP* (Ω)	*RAF* (Ω)	*(RP-RBF)/R0* (%)	*(RAF-RBF)/R0* (%)	(%)
8	0.135	0.125	0.132	0.130	5.2	3.8	0
9	0.117	0.129	0.154	0.120	21.5	-7.7	0
10	0.193	0.206	no peak	0.176	no peak	-15.8	0
11	0.107	0.101	0.015	0.109	-80.6	7.9	2.4

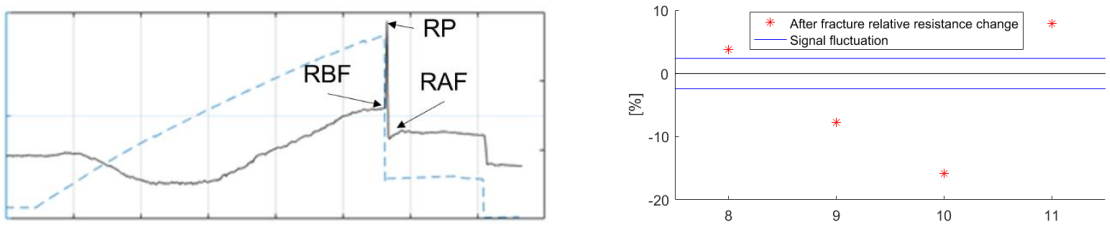

Fig. 115 Evaluation of the after fracture relative resistance change

6.2.2.2 *Torsional loading*

First, the initial electrical resistance of each sample was measured. Specimen SN-20 showed a resistance value of 3.96 Ω, while specimen SN-21 had a resistance value of 0.74 Ω. The relative torsional moment, Mt_{rel}, was calculated using the same method as for Mo_{rel} (refer to equations (27) and (28)). Fig. 116 demonstrates a clear correlation between the applied torsional loading and the resulting changes in electrical resistance.

Comparing flexural loading, where part of the specimen's cross section is subjected to tension and another part to compression with torsional loading, where the entire-cross section is uniformly loaded, the torsional loading is more suitable for monitoring of operational loading.

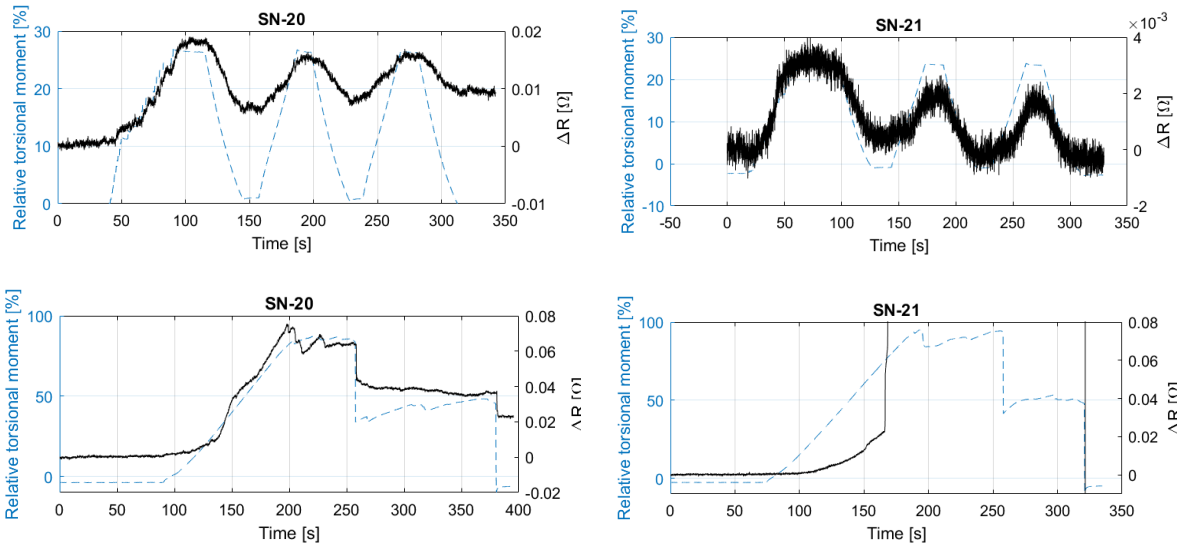

Fig. 116 Measured electrical resistance changes and relative resistance moment of cyclic and static torsional tests.

Our measurements indicate that continuous electrical resistance measurement can effectively identify fractures in specimens subjected to torsional loading, as illustrated in Fig. 116. We also observed a step change in the measured electrical resistance when the specimen's fracture occurred.

6.2.2.3 *Electrical contacts and its influence on the structure*

There were two basic requirements to the electrical contacts. First, they had to be placed on the inner surface of the sample. We also had to make sure that they didn't affect the strength of the specimens. To prove this, we measured the maximum strength values for both the samples with integrated electrical contacts and those without any. The results are shown in Fig. 117.

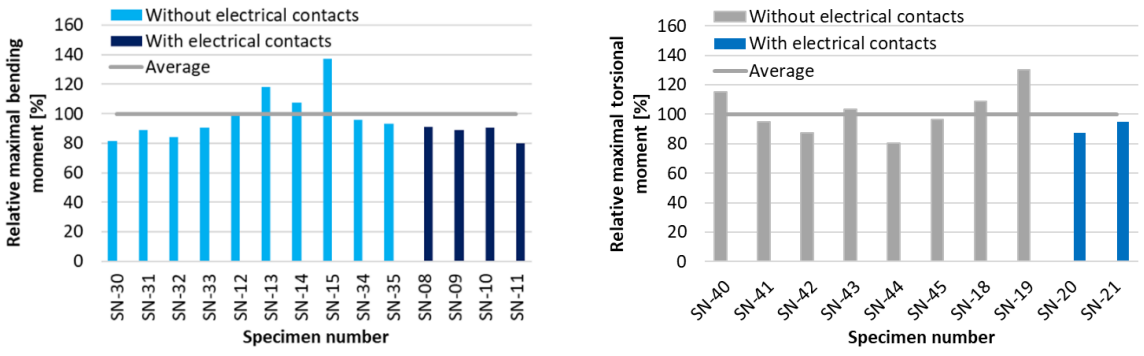

(a) (b)

Fig. 117 Comparison of relative maximal bending moments of specimens with and without electrical contacts (a), Comparison of relative maximal torsional moments of specimens with and without electrical contacts (b).

6.2.3 Conclusions and suggestions for further work

The ER measurement method was used for fracture monitoring of CFRP composite wound specimens with ILT joints. The novel approach to electrical contact preparation was tested. Further conclusions and suggestions can be drawn:

- Preparation of electrical contact on the inner surface of the profile manufactured using filament winding is feasible by the usage of carbon fiber tow with nickel coating at the ends, nevertheless improvement of the production technology is needed.
- Use better spindle separation for smoother extraction of the spindle after manufacturing.
- It was shown that 2-terminal continuous electrical resistance measurement can reveal fracture during flexural and torsional loading, but for further experimental campaigns 4-terminal measurement is suggested.
- When comparing the investigated types of loading, the presented measurement configuration appears to be more suitable for monitoring operational loading during torsional loading than during flexural loading.
- The effect of the integrated electrical contacts on the ultimate strength of the structure is lower than the average value of measured strengths, but comparable to the values of the relative strengths.

6.3 Further practical investigations - Electroplating deposition of copper on carbon fiber fabric

A process for electroplating of carbon fabric in a copper cyanide bath was also developed and published [A8] and [A9]. This process could be used for further experiments regarding ERCM on CFR composites.

Fig. 118 CF cloth with deposition of copper on several carbon fiber tow

7 Conclusions and future work

This thesis deals with the possibility of using carbon fiber sensors for condition monitoring of composite structures. A potential new area of application for these sensors has been proposed. This area is the detection of impact damage in composite structures. Although a number of SHM approaches and methods have addressed the detection of impact damage on composites, no universal approach has yet been found. The behavior of CF sensors made of several types of materials has been described. The operational effects were evaluated and a method for controlling CF sensors integrated into GFRP composites was proposed and validated. The second field of investigation was the possibility of detecting the growth of delamination of CFRP composite using the method of measuring the change in electrical resistance of the material. The influences on the possibility to detect delamination were evaluated. Furthermore, the methods of determining the electrical resistivity of the material for FE analysis were compared. Based on the experimental measurements, a suitable method for determining the electrical resistivity of the material was recommended.

In the last part of the study, the possibility of using CF sensors for monitoring the CFRP composite part was examined, and insights were gained regarding the possibility of integrating CF sensors during fabrication. A new method for producing electrical contacts during the filament winding procedure was also proposed and tested, which enables the production of electrical contacts on the part during the filament winding of composite profile. The use of such contacts was verified on a component loaded in bending and torsion.

7.1 Conclusions

The aims of the thesis were accomplished with the following comments:

7.1.1 Objective A: Impact detection using CF sensors

The possibility of impact damage detection was verified. It was found that CF sensors made of different carbon fiber tow show different sensitivity to impact damage. During two experimental campaigns, the response of CF sensors made of different material was investigated. The influence of temperature change on the measured signal of the CF sensor was quantified. The influence of short-term cycling was shown in two experimental campaigns. The carbon fiber tow which exhibits best properties was tested under long-term cycling in the third experimental campaign. It was shown that there is no evidence of damage to the CF sensor after 1000 cycles of mechanical loading. The behavior of CF sensor after BVID impact damage during 1000 cycles was described.

The influence of stacking sequence on the sensitivity of the sensor to the impact damage was quantified. It was revealed, that under the tested configuration the position of the sensor close to the opposite side of the specimen to the impact is the most convenient for the impact damage. The inspection of the CF sensor using thermal camera was suggested and tested. It was found that damage of the sensor during manufacturing of the GFRP composite can be revealed. The thermal camera imaging can be also used for localization of the impact along the CF sensor. It was shown that the length of the sensor has negligibly influence on the possibility of impact detection. The relationship between electrical resistance change measured via CF sensor after impact was and mechanical response of the structure to the impact was described. The relationship, which was found could be used for adjusting the loading of the structure after impact damage, so that the structure would not be overloaded.

The author's findings in this area are published in [A1], [A5], [A6], [A18].

7.1.2 Objective B: Delamination detection using electrical resistance change method on CFRP composite

The appropriate procedure for electrical resistivity measurement was determined. The results of several measurement configurations were compared, and results were used for FE analysis of delamination detection. It was shown that the results of FE analysis correspond to the experimental data when proper resistivity in the simulation is used. It was found that reporting of results of FE simulations in relative values of resistance is potentially misleading and can hide the error in electrical resistivity determination.

It was found that electrical resistivity values of the CF composite with PPS matrices show comparable values of electrical resistivities as was determined for CFRP composite. The influence of the temperature change, electrical resistivities and contact configuration on the delamination detection was determined.

The author's findings in this area are published in [A2], [A3], [A4], [A7], [A10], [A11], [A12].

7.1.3 Objective C: Experimental verification on experimental level

The CF sensors were used for monitoring of a CF filament wound profile, within this research objective. First CF sensors were attached to the surface. It was confirmed that thin layer of adhesive used for installing of strain gauge is a sufficient electrical insulation. Then CF fibers were integrated during manufacturing of the component. It was found that glass fiber layer is a sufficient electrical insulator between the CF sensor and CF filament wound layers. The strain measurement of such integrated CF sensor gives comparable results with integrated optical fiber for distributed fiber optic sensing.

A novel approach for electrical contact manufacturing on the inner side of carbon fiber filament wound profile was suggested and tested. Although several technological modifications need to be done. The proposed method enables to monitor electrical resistance change of the profile during loading. According to gathered data, it is possible to distinguish fatal fracture of the profile when compared to operational loading.

The author's findings in this area are published in [A8], [A9], [A13] to [A24].

7.2 Theoretical and practical outcomes

7.2.1 Theoretical outcomes

- The contribution is a systematic investigation and description of the influences that affect the experimental measurements using CF sensors. The effects of elongation and temperature change have been quantified for several types of carbon fibers.
- Another contribution is the original results of the experimental analysis of the effect of the impact on the CF sensor integrated into the composite laminate. The effect of the sensor position in the laminate lay-up was also evaluated.
- Furthermore, original experimental data regarding the behavior of CF sensors under cyclic loading were obtained.
- Another contribution is the development of technology of the copper deposition on a carbon fiber as an alternative to the commonly employed nickel-plating process used for the preparation of electrical contacts during the production of CF sensors.
- Beneficial is also determining the influence of the method of determining electrical resistivity of the examined material on the accuracy of delamination size prediction based on ERCM measurements and FE analysis.
- Based on FE analysis and experimental measurements, the influence of temperature variation, electrical resistivity, and contact configuration for the detection of delamination in the direction through the material thickness.

7.2.2 Practical outcomes

- Integration of the CF sensors were successfully accomplished during the autoclave manufacturing method from prepreg sheets.
- Integration of CF sensors was also successfully accomplished during winding manufacturing process.
- It was shown that active thermographic inspection can be successfully used for the inspection of the CF sensors integrated in the GFRP composite.
- It was revealed that the manufacturing of CF sensors from PITCH carbon fiber tows is feasible, but very difficult even for experienced operator.
- For practical applications it was shown that CF sensors can be used for real time impact damage detection using strain gage transducer.
- It was shown that CF tows integrated during winding processes can be used as an electrical contact.

7.3 Future work and outlook

The promising results in the ability to detect impact damage using CF sensors will be used to detect impacts and possibly collisions on larger structural units.

Efforts will be needed to address the technological issues of handling larger CF sensors and integrating network of CF sensors during production.

CF sensors could also be used in futuristic tasks such as tracking the shape of large structures. Composite wings, for example, are designed to have a high bending stiffness, but the wing also twists during flight, thus changing the angle of attack. If the shape of the wing could be tracked online, it would be possible to adjust flight parameters.

The delamination detection using ERCM method is effective. The application of the method in practical applications is needed to reveal and solve practical issues with cabling and electrical contact preparation.

8 References

[1] S. Klute, D. Metrey, N. Garg and N. Rahim, "IN-SITU STRUCTURAL HEALTH MONITORING OF COMPOSITE-OVERWRAPPED PRESSURE VESSELS", in *lunainc.com*, 2015.

[2] M. Dvořák, J. Neužil and M. Rastogi, "Analysis of applicability of selected SHM methods", 2015.

[3] A. Tabatabaeian, S. Liu, P. Harrison, E. Schlangen and M. Fotouhi, "A review on self-reporting mechanochromic composites: An emerging technology for structural health monitoring", *Composites Part A: Applied Science and Manufacturing*, vol. 163, 2022.

[4] G. Gardiner, "Structural health monitoring: NDT-integrated aerostructures", *Composites World*, 2015.

[5] Raju, "Interlaminar Progressive Failure Analysis of Composite Curved Aircraft structural components using MSC MARC", *documents.pub*. [Online]. Available: https://documents.pub/document/interlaminar-progressive-failure-analysis-of-composite-curved-aircraft-structural-components-using-msc-marc.html?page=1. [Accessed: 2023-12-09].

[6] S. Sanchez-Saez, E. Barbero, R. Zaera and C. Navarro, "Compression after impact of thin composite laminates", *Composites Science and Technology*, vol. 65, no. 13, pp. 1911-1919, 2005.

[7] A. Horoschenkoff and C. Christner, "Carbon Fibre Sensor: Theory and Application", in *Composites and Their Applications*, N. Hu, ed. InTech, 2012.

[8] K. Hoffmann, *An Introduction to Stress Analysis and Transducer Design using Strain Gauges*. .

[9] C. Christner, A. Horoschenkoff and H. Rapp, "Longitudinal and transverse strain sensitivity of embedded carbon fibre sensors", *Journal of Composite Materials*, vol. 47, no. 2, pp. 155-167, 2013.

[10] J. Park, T. Okabe, N. Takeda and W. Curtin, "Electromechanical modeling of unidirectional CFRP composites under tensile loading condition", *Composites Part A: Applied Science and Manufacturing*, vol. 33, no. 2, pp. 267-275, 2002.

[11] A. Todoroki, M. Tanaka and Y. Shimamura, "Measurement of orthotropic electric conductance of CFRP laminates and analysis of the effect on delamination monitoring with an electric resistance change method", *Composites Science and Technology*, vol. 62, no. 5, pp. 619-628, 2002.

[12] W. Lu, M. Zu, J. Byun, B. Kim and T. Chou, "State of the Art of Carbon Nanotube Fibers: Opportunities and Challenges", *Advanced Materials*, vol. 24, no. 14, pp. 1805-1833, 2012.

[13] L. Lin, X. Wang, B. Yang, L. Zhang, Z. Zhao, X. Qu, Y. Lu, X. Jiang and S. Lu, "Condition monitoring of composite overwrap pressure vessels based on buckypaper sensor and MXene sensor", *Composites Communications*, vol. 25, 2021.

[14] X. Wang and D. Chung, "Electromechanical behavior of carbon fiber", *Carbon*, vol. 35, no. 5, pp. 706-709, 1997.

[15] P. Scholle and M. Sinapius, "A Review on the Usage of Continuous Carbon Fibers for Piezoresistive Self Strain Sensing Fiber Reinforced Plastics", *Journal of Composites Science*, vol. 5, no. 4, 2021.

[16] S. Blazewicz, B. Patalita and P. Touzain, "Study of piezoresistance effect in carbon fibers", *Carbon*, vol. 35, no. 10-11, pp. 1613-1618, 1997.

[17] C. Owston, "Electrical properties of single carbon fibres", *Journal of Physics D: Applied Physics*, vol. 3, no. 11, pp. 1615-1626.

[18] A. Horoschenkoff, S. Selting and H. Rapp, "Einsatzpotential von Messfedern aus elektrisch kontaktierten Kohlenstofffasern mit hexagonaler Anordnung fuer Leichtbaustrukturen aus Faserverbundwekstoffen", in *Leichtbaukolloquium im Landshut*, 2007.

[19] N. Kalashnyk, E. Faulques, J. Schjødt-Thomsen, L. Jensen, J. Rauhe and R. Pyrz, "Strain sensing in single carbon fiber epoxy composites by simultaneous in-situ Raman and piezoresistance measurements", *Carbon*, vol. 109, pp. 124-130, 2016.

[20] H. Huang and Z. Wu, "Static and dynamic measurement of low-level strains with carbon fibers", *Sensors and Actuators A: Physical*, vol. 183, pp. 140-147, 2012.

[21] H. Huang, C. Yang and Z. Wu, "Electrical sensing properties of carbon fiber reinforced plastic strips for detecting low-level strains", *Smart Materials and Structures*, vol. 21, no. 3, 2012.

[22] C. Yang, X. Wang, Y. Jiao, Y. Ding, Y. Zhang and Z. Wu, "Linear strain sensing performance of continuous high strength carbon fibre reinforced polymer composites", *Composites Part B: Engineering*, vol. 102, pp. 86-93, 2016.

[23] K. Schulte and C. Baron, "Load and failure analyses of CFRP laminates by means of electrical resistivity measurements", *Composites Science and Technology*, vol. 36, no. 1, pp. 63-76, 1989.

[24] E. Häntzsche, A. Matthes, A. Nocke and C. Cherif, "Characteristics of carbon fiber based strain sensors for structural-health monitoring of textile-reinforced thermoplastic composites depending on the textile technological integration process", *Sensors and Actuators A: Physical*, vol. 203, pp. 189-203, 2013.

[25] N. Kalashnyk, E. Faulques, J. Schjødt-Thomsen, L. Jensen, J. Rauhe and R. Pyrz, "Monitoring self-sensing damage of multiple carbon fiber composites using piezoresistivity", *Synthetic Metals*, vol. 224, pp. 56-62, 2017.

[26] W. Gajda, "A Fundamental Study of the Electromagnetic Properties of Advanced Composite Materials", vol. 1978. 1978.

[27] A. Horoschenkoff, T. Muller and A. Kroell, "On the characterization of the piezoresistivity of embedded carbon fibres", in *ICCM International Conferences on Composite Materials*, 2009.

[28] A. Kunadt, E. Starke, G. Pfeifer and C. Cherif, "Messtechnische Eigenschaften von Dehnungssensoren aus Kohlenstoff-Filamentgarn in einem VerbundwerkstoffMeasuring Performance of Carbon Filament Yarn Strain Sensors Embedded in a Composite", *tm - Technisches Messen*, vol. 77, no. 2, pp. 113-120, 2010.

[29] T. Quadflieg, O. Stolyarov and T. Gries, "Carbon rovings as strain sensors for structural health monitoring of engineering materials and structures", *The Journal of Strain Analysis for Engineering Design*, vol. 51, no. 7, pp. 482-492, 2016.

[30] M. Saifeldeen, N. Fouad, H. Huang and Z. Wu, "Advancement of long-gauge carbon fiber line sensors for strain measurements in structures", *Journal of Intelligent Material Systems and Structures*, vol. 28, no. 7, pp. 878-887, 2017.

[31] C. Luan, X. Yao, H. Shen and J. Fu, "Self-Sensing of Position-Related Loads in Continuous Carbon Fibers-Embedded 3D-Printed Polymer Structures Using Electrical Resistance Measurement", *Sensors*, vol. 18, no. 4, 2018.

[32] A. Horoschenkoff, T. Mueller and A. Kroell, "On the charakterization of the piezoresistivity of embedded carbon fibres".

[33] T. Muller, A. Horoschenkoff and A. Rapp, "Carbon fibre sensor for crack monitoring of composite materials", in *ICCM-19 Proceedings*, 2013, pp. 4193-4204.

[34] A. Horoschenkoff, T. Müller, C. Strössner and K. Farmbauer, "Use of carbon-fibre sensors to determine the deflection of composite-beams", in *18th International Conference on Composite Materials: International Conference on Composite Materials*, 2011.

[35] T. Matzies, C. Christner, A. Horoschenkoff and H. Rapp, "Carbon fibre sensor meshes: Simulation and experiment", *Computational Materials Science*, vol. 64, pp. 122-125, 2012.

[36] C. Cherif, E. Haentzsche, R. Mueller, A. Nocke, M. Huebner and M. Hasan, "Carbon fibre sensors embedded in glass fibre-based composites for windmill blades", in *Smart Textiles and their Applications*, Elsevier, 2016, pp. 329-352.

[37] N. Forintos and T. Czigany, "Reinforcing carbon fibers as sensors: The effect of temperature and humidity", *Composites Part A: Applied Science and Manufacturing*, vol. 131, 2020.

[38] S. Mekid, H. Daraghma and S. Bashmal, "Electromechanical Assessment and Induced Temperature Measurement of Carbon Fiber Tows under Tensile Condition", *Materials*, vol. 13, no. 19, 2020.

[39] Y. Park, H. Roh, T. Yu and A. Gyekenyesi, "Electromechanical analysis of CFRP for real-time structural self-sensing and non-destructive evaluation", in *Nondestructive Characterization and Monitoring of Advanced Materials, Aerospace, Civil Infrastructure, and Transportation XV*, 2021, pp. 11-.

[40] A. Kunadt, A. Heinig, E. Starke, G. Pfeifer, C. Cherif and W. Fischer, "Design and properties of a sensor network embedded in thin fiber-reinforced composites", in *2010 IEEE Sensors*, 2010, pp. 673-677.

[41] J. Abry, "In situ detection of damage in CFRP laminates by electrical resistance measurements", *Composites Science and Technology*, vol. 59, no. 6, pp. 925-935.

[42] A. Todoroki, D. Haruyama, Y. Mizutani, Y. Suzuki and T. Yasuoka, "Electrical Resistance Change of Carbon/Epoxy Composite Laminates under Cyclic Loading under Damage Initiation Limit", *Open Journal of Composite Materials*, vol. 04, no. 01, pp. 22-31, 2014.

[43] A. TODOROKI, K. SUZUKI, Y. MIZUTANI and R. MATSUZAKI, "Electrical Resistance Change of CFRP under a Compression Load", *Journal of Solid Mechanics and Materials Engineering*, vol. 4, no. 7, pp. 864-874, 2010.

[44] S. Wang and D. Chung, "Mechanical damage in carbon fiber polymer-matrix composite, studied by electrical resistance measurement", *Composite Interfaces*, vol. 9, no. 1, pp. 51-60, 2012.

[45] N. Angelidis, "Damage Sensing in CFRP Composites Using Electrical Potential Techniques", Dissertation thesis, 2004.

[46] S. Wang and D. Chung, "Negative piezoresistivity in continuous carbon fiber epoxy-matrix composite", *Journal of Materials Science*, vol. 42, no. 13, pp. 4987-4995, 2007.

[47] D. Chung, "Pitfalls and Methods in the Measurement of the Electrical Resistance and Capacitance of Materials", *Journal of Electronic Materials*, vol. 50, no. 12, pp. 6567-6574, 2021.

[48] M. Ueda, T. Yamaguchi, T. Ohno, Y. Kato and T. Nishimura, "FEM-aided identification of gauge factors of unidirectional CFRP through multi-point potential measurements", *Advanced Composite Materials*, vol. 28, no. 1, pp. 37-55, 2018.

[49] D. Chung, "A review to elucidate the multi-faceted science of the electrical-resistance-based strain/temperature/damage self-sensing in continuous carbon fiber polymer-matrix structural composites", *Journal of Materials Science*, vol. 58, no. 2, pp. 483-526, 2023.

[50] A. Baltopoulos, N. Polydorides, L. Pambaguian, A. Vavouliotis and V. Kostopoulos, "Damage identification in carbon fiber reinforced polymer plates using electrical resistance tomography mapping", *Journal of Composite Materials*, vol. 47, no. 26, pp. 3285-3301, 2013.

[51] M. Ogawa, C. Huang and T. Nakamura, "Damage detection of CFRP laminates via self-sensing fibres and thermal-sprayed electrodes", *Nondestructive Testing and Evaluation*, vol. 28, no. 1, pp. 1-16, 2013.

[52] A. Todoroki, Y. Tanaka and Y. Shimamura, "Composite Materials. Electric Resistance Change Method for Identification of Embedded Delamination of CFRP Plates", *Journal of the Society of Materials Science, Japan*, vol. 50, no. 5, pp. 495-501, 2001.

[53] K. Almuhammadi, T. Bera and G. Lubineau, "Electrical impedance spectroscopy for measuring the impedance response of carbon-fiber-reinforced polymer composite laminates", *Composite Structures*, vol. 168, pp. 510-521, 2017.

[54] G. Slipher, R. Haynes and J. Riddick, "Electrical Impedance Spectroscopy for Structural Health Monitoring", in *Experimental and Applied Mechanics, Volume 6*, N. Sottos, R. Rowlands and K. Dannemann, eds. Cham: Springer International Publishing, 2015, pp. 1-11.

[55] P. Scholle, S. Rüther and M. Sinapius, "Comparison of Electrical Contacting Techniques to Carbon Fiber Reinforced Plastics for Self-Strain-Sensing Applications", *C*, vol. 7, no. 4, 2021.

[56] T. Yamane and A. Todoroki, "Analysis of electric current density in carbon fiber reinforced plastic laminated plates with angeled plies", no. 166. pp. 268-276, 2017.

[57] L. Shen, J. Li, B. Liaw, F. Delale and J. Chung, "Modeling and analysis of the electrical resistance measurement of carbon fiber polymer–matrix composites", *Composites Science and Technology*, vol. 67, no. 11-12, pp. 2513-2520, 2007.

[58] L. Selvakumaran, Q. Long, S. Prudhomme and G. Lubineau, "On the detectability of transverse cracks in laminated composites using electrical potential change measurements", *Composite Structures*, vol. 121, pp. 237-246, 2015.

[59] A. TODOROKI, M. UEDA and Y. HIRANO, "Strain and Damage Monitoring of CFRP Laminates by Means of Electrical Resistance Measurement", *Journal of Solid Mechanics and Materials Engineering*, vol. 1, no. 8, pp. 947-974, 2007.

[60] N. Angelidis, "PhD Thesis - Damage sensing in CFRP composites using electrical potential techniques". 2004.

[61] S. Wang and D. Chung, "Self-sensing of flexural strain and damage in carbon fiber polymer-matrix composite by electrical resistance measurement", *Carbon*, vol. 44, no. 13, pp. 2739-2751, 2006.

[62] X. Wang and D. Chung, "Sensing delamination in carbon fiber polymer-matrix composite during fatigue by electrical resistance measurement", *Polzmer Composites*, vol. 18, no. 6, 1997.

[63] M. Louis, S. Joshi and W. Brockmann, "An experimental investigation of through-thickness electrical resistivity of CFRP laminates", *Composites Science and Technology*, vol. 61, no. 6, pp. 911-919, 2001.

[64] I. De Baere, W. Van Paepegem and J. Degrieck, "Electrical resistance measurement for in situ monitoring of fatigue of carbon fabric composites", *International Journal of Fatigue*, vol. 32, no. 1, pp. 197-207, 2010.

[65] S. Wang, D. Chung and J. Chung, "Impact damage of carbon fiber polymer–matrix composites, studied by electrical resistance measurement", *Composites Part A: Applied Science and Manufacturing*, vol. 36, no. 12, pp. 1707-1715, 2005.

[66] A. Iwasaki and A. Todoroki, "Statistical Evaluation of Modified Electrical Resistance Change Method for Delamination Monitoring of CFRP Plate", *Structural Health Monitoring*, vol. 4, no. 2, pp. 119-136, 2005.

[67] D. Wang, S. Wang, D. Chung and J. Chung, "Sensitivity of the two-dimensional electric potential/resistance method for damage monitoring in carbon fiber polymer-matrix composite", *Journal of Materials Science*, vol. 41, no. 15, pp. 4839-4846, 2006.

[68] A. Liberson, B. Walsch and M. Roemer, "Damage Quantification in Electrically ConductiveComposite Laminate Structure", 2006.

[69] T. Swait, F. Jones and S. Hayes, "Damage detection and amelioration by electrical resistance for smart composites", in *ICCM18 Proceedings*, 2011.

[70] J. Cagáň, "Hardware implementation of electrical resistance tomography for damage detection of carbon fibre–reinforced polymer composites", *Structural Health Monitoring*, vol. 16, no. 2, pp. 129-141, 2017.

[71] A. Todoroki, "The effect of number of electrodes and diagnostic tool for monitoring the delamination of CFRP laminates by changes in electrical resistance", *Composites Science and Technology*, vol. 61, no. 13, pp. 1871-1880, 2001.

[72] M. Zappalorto, F. Panozzo, P. Carraro and M. Quaresimin, "Electrical response of a laminate with a delamination: modelling and experiments", *Composites Science and Technology*, vol. 143, pp. 31-45, 2017.

[73] T. Takeda and F. Narita, "Fracture behavior and crack sensing capability of bonded carbon fiber composite joints with carbon nanotube-based polymer adhesive layer under Mode I loading", *Composites Science and Technology*, vol. 146, pp. 26-33, 2017.

[74] T. Takeda and F. Narita, "Fracture behavior and crack sensing capability of bonded carbon fiber composite joints with carbon nanotube-based polymer adhesive layer under Mode I loading". pp. 26-33, 2017.

[75] H. Kim, G. DeFrancisi, Z. Chen, J. Rhymer, S. Funai, M. Delaney, S. Fung, J. Le and S. White, "Impact Damage Formation on Composite Aircraft Structures", 2010.

[76] "Aero Vodochody AEROSPACE a.s.", *aero.cz*, 2018. [Online]. Available: http://www.aero.cz/cz/o-nas/media/novinky/novy-velitel-vzdusnych-sil-cr-potvrdil-zajem-o-l-39ng/. [Accessed: 2018-08-31].

[77] R. Doubrava, J. Raška and M. Oberthor, "Bird strike zkoušky plochých kompozitních panelů pro ověření numerických analýz při vývoji vzduchovodu L-39NG", *Transfer*, vol. 13, no. 4, pp. 6-8, 2017.

[78] K. Hoffmann, *Anwendung der Wheatstoneschen Brückenschaltung*. Darmstadt, Germany: Hottinger Baldwin Messtechnik GmbH.

[79] M. Dvořák, J. Had, M. Růžička and Z. Pošvář, "Monitoring of 3D Composite Structures Using Fiber Optic Bragg Grating Sensors", *Structural Health Monitoring - an International Journal*, pp. 1159-1602, 2011.

[80] *Elektrická měření : návody k laboratorním cvičením: doplňkové skriptum : určeno pro stud. fak. elektrotechn*, 3. přeprac. vyd. Praha: Ediční středisko ČVUT, 1992.

[81] K. Takahashi and H. Hahn, "Investigation of temperature dependency of electrical resistance changes for structural management of graphite/polymer composite", *Journal of Composite Materials*, vol. 45, no. 25, pp. 2603-2611, 2011.

[82] K. Ogi and H. Inoue, "Temperature dependence of electrical resistance in carbon fibre and carbon fiber composites", in *Proceedings of 12th U.S. -Japan Conference on Composite Materials*, 2006, pp. 200-206.

[83] "Compotech", *Compotech.com*, 2023. [Online]. Available: https://compotech.com/what-we-do/machine-tool/automation-and-manipulation/. [Accessed: 2023-12-09].

[84] S. Wang, D. Chung and J. Chung, "Self-sensing of Damage in Carbon Fiber Polymer–Matrix Composite Cylinder by Electrical Resistance Measurement", *Journal of Intelligent Material Systems and Structures*, vol. 17, no. 1, pp. 57-62, 2006.

[85] D. Kwon, P. Shin, J. Kim, Z. Wang, K. DeVries and J. Park, "Detection of damage in cylindrical parts of carbon fiber/epoxy composites using electrical resistance (ER) measurements", *Composites Part B: Engineering*, vol. 99, pp. 528-532, 2016.

[86] M. Dresselhaus, G. Dresselhaus, K. Sugihara, I. Spain and H. Goldberg, *Graphite Fibers and Filaments*. Berlin: Springer-Verlag, 1988.

[87] M. Dvořák and N. Schmidová, "Experimentální ověřování vlastností snímačů". 2015.

9 Publications

9.1 Publications related to the topic

9.1.1 Reviewed papers

[A1] N. Schmidová, et al. "Impact Damage Detection of a Glass Fabric Composite Using Carbon Fiber Sensors with Regard to Mechanical Loading", *Applied Sciences*, 2022, 2022(12), ISSN 2076-3417. DOI 10.3390/app12031112

9.1.2 Conference contributions

[A2] N. Schmidová, M. Dvořák, and M. Růžička, "Structural Health Monitoring of CFRP Using Electrical Resistance Measurement", In: *21st Workshop of Applied Mechanics - Proceedings*, Praha, 2016-12-21. Praha: České vysoké učení technické v Praze, Fakulta strojní, 2016. p. 37-40. ISBN 978-80-01-06085-8.

[A3] N. Schmidová, and R. Fajtl, "Modeling of Electrical Resistance Measuring Method for Sensing Damage and Deformation in CFRP Composites", In: *Sborník konference TECHSOFT ENGINEERING ANSYS 2017 Setkání uživatelů a konference*. TECHSOFT ENGINEERING - ANSYS 2017 - Setkání uživatelů a konference, Orea Resort Devět Skal, 2017-05-24/2017-05-26. Praha 4: TechSoft Engineering, 2017. ISBN 978-80-905040-7-3.

[A4] N. Schmidová, M. Dvořák, and M. Růžička, "Sensing Damage in CFRP Composite Beam by Electrical Resistance Measurement", In: *Experimental Stress Analysis 2017. 55th International Scientific Conference Experimental Stress Analysis 2017*, Nový Smokovec, 2017-05-30/2017-06-01. Košice: Technical University of Kosice, 2017. p. 13-14. ISBN 978-80-553-3167-6.

[A5] N. Schmidová. and M. Růžička, "Carbon Fibers for Sensing and Damage Detection of Composite Materials", In: *Proceedings. 25th Workshop of Applied Mechanics*, Praha, 2018-12-07. Praha: České vysoké učení technické v Praze, Fakulta strojní, 2018. p. 46-49. ISBN 978-80-01-06536-5.

[A6] N. Schmidová, A. Horoschenkoff, and M. Růžička, "Investigation of The Electrical Resistivity of Damaged Carbon Fibers Sensors with Regard to SHM", In: Proceedings of the *18th European Conference on Composite Materials*, Athens, 2018-06-23/2018-06-28. University of Patras, 2018. Available from: http://www.eccm18.org

[A7] N. Schmidová, et al., "Monitoring of Delamination Growth on the MMB Specimens Using FBG Sensors and Electrical Resistance Measurement Method", In: *Conference Proceedings 56th conference on experimental stress analysis*, Harrachov, 2018-06-05/2018-06- 07. Praha: Česká společnost pro mechaniku, 2018. p. 367-373. ISBN 978-80-270-4062-9.

[A8] P. Szelag, and N. Schmidová, "Pokovení uhlíkové tkaniny", In: *Proceedings of 51. celostátní aktiv galvanizérů*, Jihlava: Česká společnost pro povrchové úpravy, 2018. ISBN 978-80-905648-4-8.

[A9] P. Szelag, and N. Schmidová, "Technologie galvanického mědění uhlíkových vláken", In: *Proceedings of 44. Projektování a provoz povrchových úprav*. Jelínková Zdenka - PPK, 2018. ISBN 978-80-906304-2-0.

[A10] N. Schmidová, et al., "Delamination detection using electrical resistance change method and its reliability". In: F.-K., Chang, A. Guemes, and F. Kopsaftopoulos, eds. Structural Health

Monitoring 2019, Enabling Intelligent Life-cycle Health Management for Industry Internet of Things (IIOT). 12th International Workshop on Structural Health Monitoring: Enabling Intelligent Life-Cycle Health Management for Industry Internet of Things (IIOT), Stanford, 2019-09-10/2020-03-12. Lancaster, Pennsylvania: DEStech Publications, Inc., 2019. p. 1582-1589. ISBN 9781605956015.

[A11] N. Schmidová, et al., "Delamination Detection Using Electrical Resistance Change Method and Its Reliability". In: *Proceedings of 36th Danubia Adria Symposium on Advances in Experimental Mechanics*. Plzeň, 2019-09-24/2019-09-27. Pilsen: University of West Bohemia, 2019. ISBN 978-80-261-0876-4.

[A12] N. Schmidová, M. Dvořák, and M. Růžička. "Comparison of the Published Contact Configurations for the Determination of Electrical Resistivity of CFRP Composite", In: *Proceedings of EAN 2019 57th conference on experimental stress analysis*, Luhačovice, 2019, Praha: Česká společnost pro mechaniku, 2019. p. 462-468. ISBN 9788021457669.

[A13] N. Schmidová, et al., "Monitoring of Integrated Loop Technology Joints under Flexural Loading", In: *60th annual international conference on Experimental Stress Analysis - Book of Extended Abstracts*, 2022, Praha: CTU FME. Department of Mechanics, Biomechanics and Mechatronics, 2022. ISBN 978-80-01-07010-9.

[A14] N. Schmidová, et al., "Damage Detection of CFRP Filament Wound Tubes Using Electrical Resistance Measurement", In: MOREIRA, P. and L.F. GALRAO DOS REIS, eds. Procedia Structural Integrity. European Structural Integrity Society, 2022. p. 1306-1313. ISSN 2452-3216. DOI 10.1016/j.prostr.2022.12.166

[A15] D. Blaha, et al., "Strain measurement using a distributed fiber optic method: Influence of fiber optic installation, strain measurement comparison methods", In: *60th annual international conference on Experimental Stress Analysis - Book of Extended Abstracts*, 2022, Praha: CTU FME. Department of Mechanics, Biomechanics and Mechatronics, 2022. p. 14-15. ISBN 978-80-01-07010-9.

[A16] D. Blaha, et al., "A Strain Measurement Using Distributed Fiber Optic Sensing System on a Composite Demonstrator". In: *23rd International Scientific Conference Applied Mechanics 2022 Book of Abstracts*, 2022, Liblice, Praha: CTU FME. Department of Mechanics, Biomechanics and Mechatronics, 2022. p. 13-16. ISBN 978-80-01-06974-5

[A17] V. Kulíšek, T. Ponížil, and N. Schmidová, "Návrh a optimalizace kompozitních rámů kol". In: *Sborník Konference a setkání uživatelů Ansys 2022*. Konference a setkání uživatelů Ansys 2022, Blansko, TechSoft Engineering, spol. s r.o., 2022. ISBN 978-80-907196-3-7.

[A18] N. Schmidová, et al., "Behavior of Carbon Fiber Sensors Under Cyclic Loading and Impact Damage", In: *Proceedings of 33th Workshop of Applied Mechanics*, Praha: České vysoké učení technické v Praze, Fakulta strojní, 2023. ISBN 978-80-01-07267-7.

9.1.3 Research reports

[A19] N. Schmidová, et. al. "SHM integrovaných spojů kompozitních profilů". [Research Report] 2020. Report no. ČVUT 12105/20/23

[A20] Ponížil, T., et al. "Odborná zpráva o postupu prací a dosažených výsledcích za rok 2020". [Research Report] 2020. Report no. ČVUT 12105/20/24.

[A21] Zámečníková, T., et al. "MKP modely zkušebního vzorku součásti s integrgovanými spoji s modely snímačů deformace zatížené ohybem a krutem". [Research Report] 2021. Report no. 12105/21/08.

[A22] Ponížil, T., et al. "Odborná zpráva o postupu prací a dosažených výsledcích za rok 2021". [Technical Report] 2021. Report no. 12105/21/02.

[A23] Uher, O., et al. "Odborná zpráva o postupu prací a dosažených výsledcích za rok 2022". [Research Report] 2022. Report no. 12105/22/14.

9.1.4 Other results

[A24] N. Schmidová, et al., "Funkční vzorek integrovaného spoje vybaveného snímači pro SHM". [Functional Sample] 2021.

9.2 Other publications of the author

9.2.1 Reviewed papers

[B1] Schmidová, N., et al. "Development of Adaptable CF RP Energy Absorbers for Car Crashes". *Materials Today: Proceedings.* 2018, 5(13), ISSN 2214-7853. DOI 10.1016/j.matpr.2018.08.152

[B2] Dvořák, M., et al. "Experimental Development of Composite Bicycle Frame". *Applied Sciences*. 2022, 12(16), ISSN 2076-3417. DOI 10.3390/app12168377

9.2.2 Conference contributions

[B3] Papuga, J., et al. "FinLiv concept and its effect on fatigue methods validation studies". In: *16th International Colloquium mechanical fatigue of materials - Conference Proceedings*. XVI International Colloquium "Mechanical Fatigue of Metals", Brno, 2012-09- 24/2012-09-26. Brno: Ústav fyziky materiálů AV ČR, 2012. p. 200-207. ISBN 978-80-87434-05-5.

[B4] Schmidová, N. and J. Papuga. "Fatigue prediction by multiaxial criteria in the region of limited lifetime". In: *Proceedings of 13th Youth Symposium on Experimental Solid Mechanics*. 13th Youth Symposium on Experimental Solid Mechanics, Děčín, 2014-06-29/2014-07-02. Praha: České vysoké učení technické v Praze, Fakulta dopravní, 2014. p. 104-107. ISBN 978-80-01-05556-4. Available from: http://www.itam.cas.cz/ysesm2014/proceedings/id_41_ysesm2014_proceedings.pdf

[B5] Dvořák, M., et al. "Development of Structural Health Monitoring System for Ultralight Aircraft". In: Experimental Stresss Analysis 2016. *54. konference Experimentální Analýza Napětí*, Srní, 2016-05-30/2016- 06-02. Plzeň: Západočeská universita, Fakulta aplikovaných věd, 2016. ISBN 978-80-261-0624-1.

[B6] Schmidová, N., et al. "Development of the Adaptable Energy Absorbers for Car Crashes". In: *21st Workshop of Applied Mechanics - Proceedings*. 21st Workshop of Applied Mechanics, Praha, 2016-12- 21. Praha: České vysoké učení technické v Praze, Fakulta strojní, 2016. p. 58-61. ISBN 978-80-01-06085-8.

[B7] Dvořák, M., et al. "Use of FBG Sensors for Delamination Growth Measurement under Mode I loading". In: *55th Conference on Experimental Stress Analysis 2017- Proceedings*. 55th International Scientific Conference on Experimental Stress Analysis 2017, Nový Smokovec, 2017-05-30/2017-06-01. Košice: Technical University of Kosice, 2017. p. 102-107. ISBN 978-80-553-3167-6.

[B8] Růžička, M., et al. "Health and usage monitoring system for the small aircraft composite structure". In: *AIP Conference Proceedings. 2nd international conference on smart materials technologies (ICSMT 2017)*, St. Petersburg, 2017-05-19/2017-05-21. American Institute of

Physics Inc., 2017. vol. 1858. ISSN 0094-243X. ISBN 978-0-7354-1532-4. DOI 10.1063/1.498994

[B9] Schmidová, N., et al. "Influence of the beam geometry on the course of force during impact". In: 23rd Workshop of Applied Mechanics - *Proceedings. 23rd Workshop of Applied Mechanics*, Praha, 2017-12-15. Praha: České vysoké učení technické v Praze, Fakulta strojní, 2017. p. 56-60. ISBN 978- 80-01-06372-9.

[B10] Schmidová, N., et al. "development of the adaptable energyabsorbers for car crashes". In: *DAS2017 proceedings*. 34th Danubia Adria Symposium on Advances in Experimental Mechanics, Trieste, 2017-09-19/2017-09-22. Trieste: University of Trieste, 2017. p. 192-194. ISBN 978-88- 8303-863-1.

[B11] Doubrava, K., et al. "Experimental Analysis of Composite Jet Engine Air Inlet". In: *36th Danubia Adria Symposium on Advances in Experimental Mechanics*. Plzeň, 2019-09-24/2019-09-27. Pilsen: University of West Bohemia, 2019. ISBN 978-80-261-0876-4.

[B12] Dvořák, M., et al. "Fiber optic strain sensor system for structural analysis of jet engine air intake". In: *EAN 2019 57th conference on experimental stress analysis conference proceedings*. 57th conference on experimental stress analysis EAN 2019, Luhačovice, 2019-06-03/2019-06-06. Praha: Česká společnost pro mechaniku, 2019. p. 77-80. ISBN 9788021457669.

[B13] Kropík, B., et al. "Detection and Monitoring of Failures in CFRP Specimens with Integrated Joints by Acoustic Emission Method". In: *27th Workshop of Applied Mechanics - Proceedings*. Praha: České vysoké učení technické v Praze, Fakulta strojní, 2019. p. 20-23. ISBN 978-80-01-06680-5.

[B14] Malá, A., et al. "Finite Element Analysis of Composite Tubes with Integrated Loop Connections". In: *proceedings of computational mechanics 2019*. 35th conference with international participation computational mechanics 2019, Srní, 2019-11-04/2019-11-06. Plzeň: Západočeská univerzita v Plzni. Fakulta aplikovaných věd, 2019. p. 114-116. ISBN 978-80-261-0889-4

[B15] Dvořák, M., et al. "Embedded fiber optic sensors for structural analysis of composite bicycle frame". In: *58th Conference on Experimental Stress Analysis - Book of Full Papers*. 58th Conference on Experimental Stress Analysis, Sobotín, 2020-10-19/2020-10-22. Brno: Czech Society for Mechanics, 2020. p. 51-54. ISBN 978-80- 248-4451-0. Available from: https://ean.vsb.cz/files/Book_of_Full_Papers.pdf

[B16] Kropík, B., et al. "Identification of MTB Enduro Bicycle Frame Behaviour". In: *58th Conference on Experimental Stress Analysis - Book of Full Papers*. 58th Conference on Experimental Stress Analysis, Sobotín, 2020-10- 19/2020-10-22. Brno: Czech Society for Mechanics, 2020. p. 252-262. ISBN 978-80-248-4451-0. Available from: https://ean.vsb.cz/files/Book_of_Full_Papers.pdf

[B17] Malá, A., et al. "Analýza tuhosti a pevnosti vinutých trubek s integrovanými spoji". In: *Mechanika kompozitních materiálů a konstrukcí 2020 - Proceedings*. Mechanika kompozitních materiálů a konstrukcí 2020, Kamenice, 2020-09-09/2020-09-10. Praha: ČVUT v Praze, Fakulta strojní, Ústav mechaniky, biomechaniky a mechatroniky, 2020. p. 15-19. ISBN 978-80-01-06767-3.

[B18] Dvořák, M., et al. "Experimental Investigation of Pull-Out Load Bearing Capacity of Threaded End Pieces for Composite Pull Rods". In: *Experimental Stress Analysis 2021 - Book of Extended Abstracts*. 59th conference on experimental stress analysis, Litomyšl, 2021-09-29/2021-11-01. Praha: CTU. Faculty of Civil Engineering, 2021. 1.. ISBN 978-80-01-06884-7

[B19] Malá, A., et al. "Finite element analysis of composite tubes with integrated loop technology joints". In: *Proceedings of computational mechanics 2021*. 36th Conference with international participation computational mechanics 2021, Srní, 2021-11-08/2021-11-10. Plzeň: University of West Bohemia, 2021. p. 146-148. ISBN 978-80-261-1059-0.

[B20] Kropík, B., et al. "Flexural and Torsional Loading of Integrated Loop Technology Joint". In: *60th annual international conference on Experimental Stress Analysis - Book of Extended Abstracts*. 60th annual international conference on Experimental Stress Analysis, Praha, 2022-06-06/2022-06-09. Praha: CTU FME. Department of Mechanics, Biomechanics and Mechatronics, 2022. ISBN 978-80-01-07010- 9.

[B21] Mendová, K., et al. "Tensile properties of primary coating materials for FBG sensors". In: *23rd International Scientific Conference Applied Mechanics 2022 Book of Abstracts*. AM 2022 - Applied Mechanics, Liblice, 2022-04-04/2022-04-06. Praha: CTU FME. Department of Mechanics, Biomechanics and Mechatronics, 2022. p. 129-132. ISBN 978-80-01- 06974-5.

[B22] Dvořák, M., et al. "Experimental Investigation of Pull-out Load Bearing Capacity of Threaded End Pieces for Composite Pull Rods". In: *EAN 2021 59th conference on experimental stress analysis*. Litomyšl, 2021-09-29/2021-10-01. Praha: CTU FCE. Department of Mechanics, 2022. p. 16- 19. ISBN 978-80-01-06885-4. Available from: https://mech.fsv.cvut.cz/ean2021/final-book-ean2021.pdf

[B23] Kropík, B., et al. "Tension and Compression Optimization of Integrated Loop Technology Joint". In: *EAN 2021 59th conference on experimental stress analysis - Proceedings*. Litomyšl, 2021-09-29/2021-10-01. Praha: CTU FCE. Department of Mechanics, 2022. p. 99-106. ISBN 978-80-01- 06885-4.

[B24] Blaha, D., et al. "Analysis of an axially loaded composite tube measured by distributed fiber optic sensors". In: *Mechanika kompozitních materiálů a konstrukcí 2023 - Proceedings*. Mechanika kompozitních materiálů a konstrukcí MK2, Dobříš, 2023-03-23/2023-03-24. Plzeň: Západočeská univerzita v Plzni. Fakulta aplikovaných věd, 2023. p. 11-16. ISBN 978-80-261-1150-4.

9.2.3 Research reports

[B25] Papuga, J., et al. "Evaluation of experimental data available for validating criteria intended for an estimation of the fatigue limit". [Research Report] Praha: ČVUT v Praze, FS, 2012. Report no. FAD/12/006

[B26] Dvořák, M. and N. Schmidová. "Experimentální ověřování vlastností snímačů". [Research Report] 2015. Report no. 12105/15/50.

[B27] Dvořák, M. and N. Schmidová. "Experimentální měření vzorků a konstrukčních uzlů". [Research Report] 2015. Report no. 12105/15/49.

[B28] Schmidová, N., M. Dvořák, and M. Vlček. "Výroba vzorků s optickými vlákny". [Research Report] 2015. Report no. 12105/15/48.

[B29] Schmidová, N., M. Dvořák, and J. Václavík. "Development of SHM Features Integration". [Research Report] 2016. Report no. 12105/16/29

[B30] Dvořák, M. and N. Schmidová. "Experimentální měření vzorků a konstrukčních uzlů". [Technical Report] 2016. Report no. 12105/16/32.

[B31] Schmidová, N., M. Dvořák, and M. Vlček. "Výroba vzorků s optickými vlákny". [Technical Report] 2016. Report no. ČVUT 12105/16/31.

[B32] Dvořák, M., N. Schmidová, and M. Kadlec. "DCB specimens tests". [Technical Report] 2017. Report no. 12105/17/24.

[B33] Schmidová, N. and M. Dvořák. "Simulace a výpočty uzlů". [Technical Report] 2017. no. 12105/17/40.
[B34] Dvořák, M. and N. Schmidová. "Experimentální měření vzorků a konstrukčních uzlů". [Technical Report] 2017. Report no. 12105/17/32.
[B35] Dvořák, M., N. Schmidová, and M. Štěpánek. "Kalibrace senzorického systému v letounu U-15". [Technical Report] 2017. Report no. 12105/17/31.
[B36] Šašek, L., et al. "Odborná zpráva o postupu prací a dosažených výsledcích za rok 2016". [Research Report] 2017. Report no. TA04031450-2016V001.
[B37] Dvořák, M. and N. Schmidová. "Development of algorithms for evaluation of FBG sensor signals". [Research Report] 2018. Report no. 12105/18/18.
[B38] Šašek, L., et al. "Závěrečná odborná zpráva o postupu prací a dosažených výsledcích za roky 2014-2017". [Research Report] 2018. Report no. TA04031450-2017V001.
[B39] Kropík, B. and N. Schmidová. "Experimentální program - integrované spoje". [Research Report] 2019. Report no. 12105/19/34.
[B40] Zámečníková, T., et al. "MKP analýza nosníku s integrovaným spojem". [Research Report] 2019. Report no. 12105/19/22.
[B41] Dvořák, M., et al. "Deformační odezva vzduchovodu určená pomocí FBG snímačů (motorová zkouška 12/2018) ". [Research Report] Praha: ČVUT v Praze, Fakulta strojní, Ústav mechaniky, biomechaniky a mechatroniky, 2019. Report no. 12105/19/30.
[B42] Dvořák, M., et al. "Deformační odezva vzduchovodu určená pomocí FBG snímačů (motorová zkouška 06/2019)". [Research Report] Praha: ČVUT v Praze, Fakulta strojní, Ústav mechaniky, biomechaniky a mechatroniky, 2019. Report no. 12105/19/06.
[B43] Doubrava, K., et al. "Deformační chování kompozitního vzduchovodu letounu L-39NG během pozemní motorové zkoušky". [Research Report] Praha: ČVUT v Praze, Fakulta strojní, Ústav mechaniky, biomechaniky a mechatroniky, 2019. Report no. 12105/19/05.
[B44] Schmidová, N., M. Dvořák, and H. Chlup. "Zkušební zařízení na optomechanická měřidla". [Technical Report] 2020. Report no. 12105/20/40.
[B45] Malá, A., et al. "MKP modely zkušebního vzorku součásti s integrovanými spoji a rámu jízdního kola se zadní stavbou". [Research Report] 2020. Report no. 12105/20/28.
[B46] Chlup, H., et al. "Experimentální zjišťování charakteristik opt. vláken, FBG snímačů, materiálů primárních a sekundárních ochran". [Research Report] 2020. Report no. 12105/20/33.
[B47] SChmidová, N., et al. "Odborná zpráva o postupu prací a dosažených výsledcích za rok 2020". [Research Report] 2020. Report no. 12105/20/34
[B48] Uher, O., et al. "Odborná zpráva o postupu prací a dosažených výsledcích za rok 2021". [Research Report] 2021. Report no. 12105/21/30.
[B49] Mendová, K., et al. "Mechanické vlastnosti lepených spojů s optickými vlákny". [Research Report] 2021. Report no. 12105/21/26.
[B50] Schmidová, N., et al. "Odborná zpráva o postupu prací a dosažených výsledcích za rok 2021". [Research Report] 2021. Report no. 12105/21/29.
[B51] Schmidová, N., et al. "Odborná zpráva o postupu prací a dosažených výsledcích za rok 2022". [Research Report] 2022. Report no. 12105/22/04.

9.2.4 Other results

[B52] Papuga, J., et al. "Summary of verified computation technologies". [Verified Technology] 2014.
[B53] Dvořák, M., et al. "Technologie implementace optických snímačů při výrobě kompozitní konstrukce". [Verified Technology] 2017.

[B54] Ponížil, T., et al. "Funkční vzorek - Rám jízdního kola z kompozitních profilů s integrovanými spoji". [Functional Sample] 2021.
[B55] Chromý, J., et al. "Funkční vzorek kompozitového táhla pro ovládací systémy v automotive". [Functional Sample] 2022
[B56] Chromý, J., et al. "Prototyp kompozitového táhla se závitovými koncovkami pro ovládací systémy v letectví". [Prototype] 2022.
[B57] Laznová, V., et al. "Upínací zařízení pro zatěžování vzorků s lepeným optickým vláknem". [Functional Sample] 2022.
[B58] Laznová, V., et al. "Funkční vzorek měřidla náklonu pro malé rozsahy". [Functional Sample] 2022
[B59] Schmidová, N., et al. "Zkušební zařízení pro testování optomechanických měřidel". [Functional Sample] 2022.
[B60] Laznová, V., et al. "Funkční vzorek měřidla posunutí s malou měřicí základnou". [Functional Sample] 2022.
[B61] Laznová, V., et al. "Funkční vzorek měřidla posunutí s velkou měřicí základnou". [Functional Sample] 2022.
[B62] České vysoké učení technické v Praze, Praha 6, Dejvice; Compo Tech PLUS, spol. s r. o., Sušice, Sušice II. "Kompozitové táhlo s koncovkami". Inventors: M. Dvořák, et al. Czechia. Utility Model CZ 36801. 2023-01-31. Available from: https://isdv.upv.cz/webapp/resdb.print_detail.det?pspis=PUV/40624

10 List of figures

11 List of tables